SCUOLA INTERNAZIONALE SUPERIORE STUDI AVANZATI (SISSA)
INTERNATIONAL SCHOOL FOR ADVANCED STUDIES
PhD COURSE IN FUNCTIONAL AND STRUCTURAL GENOMICS
Trieste, Itally

Foxg1 and *Emx2* control of cortico-cerebral astrogenesis and *Emx2* as a novel tool to suppress glioblastoma multiforme

THESIS SUBMITTED FOR THE DEGREE OF "DOCTOR PHILOSOPHIAE"
Academic Year 2015/2016

Candidate:
Carmen Falcone

Supervisor:
Prof. Antonello Mallamaci

ABSTRACT

Cortico-cerebral astrogenesis is a tightly regulated process. Astrocytic outputs mainly depend on two factors: progression of multipotent precursors towards the astroglial lineage and sizing of the astrogenic proliferating pool. Uncontrolled proliferation of astroglial cells in adult may give rise to severe pathologies, such as glioblastoma multiforme (GBM), for which no cure is presently available.

The aim of this study was to study the role of two transcription factors, *Foxg1* and *Emx2,* in the regulation of mouse corticocerebral astrogenesis and to employ *Emx2* as a possible therapeutical tool to counteract GBM. We addressed this issue by combined gain- and loss-of-function methods, in vivo as well as in primary cultures of cortico-cerebral precursors and of patients' GBM cell lines.

We found that *Foxg1* antagonizes the commitment of early neural stem cells toward glial fate, while *Emx2* suppress the proliferation of astrocyte-committed progenitors.

We showed that *Foxg1* inhibits the transcription of the well-known glial gene *Gfap,* possibly by impacting the regulation of the gliogenic transactive pathways. Then, we found that *Emx2* overexpression in cortico-cerebral stem cells shrunk the proliferating astrogenic pool, resulting in a severe reduction of the astroglial outcome. We showed that this was caused by *EgfR* and *Fgf9* downregulation and that both phenomena originated from exaggerated Bmp signaling and Sox2 repression. Furthermore, we provided evidence that in vivo temporal progression of Emx2 levels in cortico-cerebral multipotent precursors contributes to confine the bulk of astrogenesis to postnatal life.

Finally, we translated our findings on *Emx2* role in the normal astrogenesis to a possible gene therapy to suppress glioblastoma multiforme tumor. As for this last part of the study, we investigated the impact of *Emx2* overexpression on patient malignant cells in vitro as well as upon transplantation into mouse recipient brains. We discovered that *Emx2* overexpression induced the collapse of seven out of seven *in vitro* tested glioblastoma cell lines. Moreover, it suppressed four out of four of these lines *in vivo* in short-term approaches and it also increased the survival of GBM-

transplanted mice in a long-term experiment. As proven by dedicated rescue assays, the anti-oncogenic activity of *Emx2* originated from its impact on at least six metabolic nodes, which accounts for the robustness of its effect. Finally, in two out of two tested lines, the tumor culture collapse was also achieved when *Emx2* was driven by a neural stem cell-specific promoter, likely active within tumor-initiating cells. All that points to *Emx2* as a novel, promising tool for therapy of glioblastoma and prevention of its recurrencies.

INDEX

1. INTRODUCTION

1.1 Cortico-cerebral astrogenesis

1.1.1 Spatio-temporal articulation

Glia constitutes 10-20% of the cells in the Drosophila nervous system and at least 50% of the cells in the human brain (Herculano-Houzel, 2011; Rowitch and Kriegstein, 2010). This suggests that glial cells exhibit important roles in the increasing complexity of the nervous system. Glial cells can be very heterogeneous: some particular cells showing macrophage-like functions constitute the "microglia", while astrocytes and oligodendrocytes are part of what is called "macroglia".

In particular, astrocytes play a wide range of roles in the central nervous system. They provide structural support, modulate the chemical environment by influencing water balance and ion distribution, and participate in the blood-brain barrier maintainance. Astrocytes are also crucial for the development of neural circuits and provide support to the dynamic machinery underlying synapse formation, function and elimination. Indeed, they regulate calcium flux and also release and reuptake neuropeptides (Rowitch and Kriegstein, 2010; Sloan and Barres, 2014). It is not surprising that dysfunction of astrocyte development may lead to severe pathological states such as autism, schizophrenia and epilepsy.

In the developing embryo, neuroepithelial cells give origin to both neurons and glial cells. For long time, these two populations were considered to derive from distinct precursor pools diverging early during development. Conversely, the process is more complex and articulated with what previously thought. Studying the roles of astrocytes in development and disease will be crucial to clarify the relationship among neurons and glia in the maturing brain (Molofsky et al., 2012).

Numerous studies have shown that, even if committed progenitors may emerge very early during development, there is one single precursor population called *radial glia* (RG). This is now also considered as *neural stem cells* population (NSCs). Moreover, NSCs give rise to *transit amplifying intermediate progenitors* (IPCs) before generating one of the different, specific neural subtypes. Intermediate

progenitors are lineage restricted and coexist not only in the embryo but also in some germinal regions in the adult (Kriegstein and Alvarez-Buylla, 2009).

Everything begins in the *ventricular zone* (VZ), a defined region next to cerebral ventricles (*Fig. I.1*). As anticipated above, around E9-E10 in mouse, neuroepithelial cells start transforming themselves into RG cells, with contacts with both pial and ventricular surfaces, but cell bodies within the VZ. The lengthening of the pia-directed radial process is associated with the progressive thickening of the cortex throughout neurogenesis. RG cells retain the capability to undergo interkinetic nuclear migration (INM) (Del Bene, 2011). Such peculiar mitotic behaviour consists in nuclear movement at different the cell cycle phases. Analyzing step by step RG cells mitotic behaviour, nuclei going through the S-phase, lay on a layer quite distant from the ventricle, while nuclei in M phase, align themselves along the surface of the ventricle, and finally nuclei in G1 and G2 phases pass through the mid region of M and S phases. This behavioural pattern results in the formation of a pseudostratified layer of cells (Kriegstein and Alvarez-Buylla, 2009). RG cells also undergo some relevant cytoskeletal modifications and the conversion of tight junctional complexes to adherens junctions. Moreover, they start to express specific genetic markers (e.g.: GLAST, RC2, Pax6 and BLBP protein), which witnesses a common origin for neurons and glia. Firing of the Notch pathway takes place at high level close to the apical side in RG cells and seems fundamental to maintain RG cell identity and self-renewal (Zhang et al., 2008). In addition to proliferative activity, RG can directly give rise to neurons, or, more frequently, to different pools of *intermediate progenitors* (IPCs), which are characterized by a continual proliferative activity even though they are already addressed to one specific differentiated progeny. Most of these IPCs do not perform INM and place themselves in the *subventricular zone* (SVZ) with different regional distribution coherently with the different areas in the developing brain.

Taking into account the prenatal temporal window, around E11, early radial glial cells within dorsal telencephalon mainly generate *neuronal intermediate progenitors* (nIPCs) which in turn will originate the almost totality of cortico-cerebral *glutamatergic* neurons. (Cortico-cerebral *gabaergic* neurons are born in rodents by progenitors located in ventral telencephalon and rostral hypothalamus; however in primates a substantial fraction (circa 2/3) also originates from cortico-cerebral autochtonous progenitors).

A second output of dorsal telencephalic RG cells is represented by astrocytes, which are generated to a large extent after the neuronogenic process is completed. Most astrocytes, still divide locally before terminal differentiation (Ge et al., 2012). A peak in the production of astrocytes just after birth is strongly reported, then this phenomenon globally fades around the end of the second week of postnatal life. Nevertheless, the process of astrocytic proliferation may as well be detected in the postnatal murine cortex (Hajós et al., 1981; Ichikawa et al., 1983). As regards cortico-cerebral oligodendrocytes, the situation is more complex, as their progenitors (oIPCs) derive from different telencephalic regions. NSCs cells are then retained in some restricted regions of postnatal and adult brain, where they are able to produce not only glial cells but also neurons.

Of course, a fine regulation in time and space is required to modulate the commitment of NSCs towards one fate or another. Therefore, how combination of transcription and secreted factors in the embryonic and adult SVZ regulate the neuron-to-astrocyte switch is one of the most investigated question in the study of astrogenesis and more in general in the modern developmental genetics.

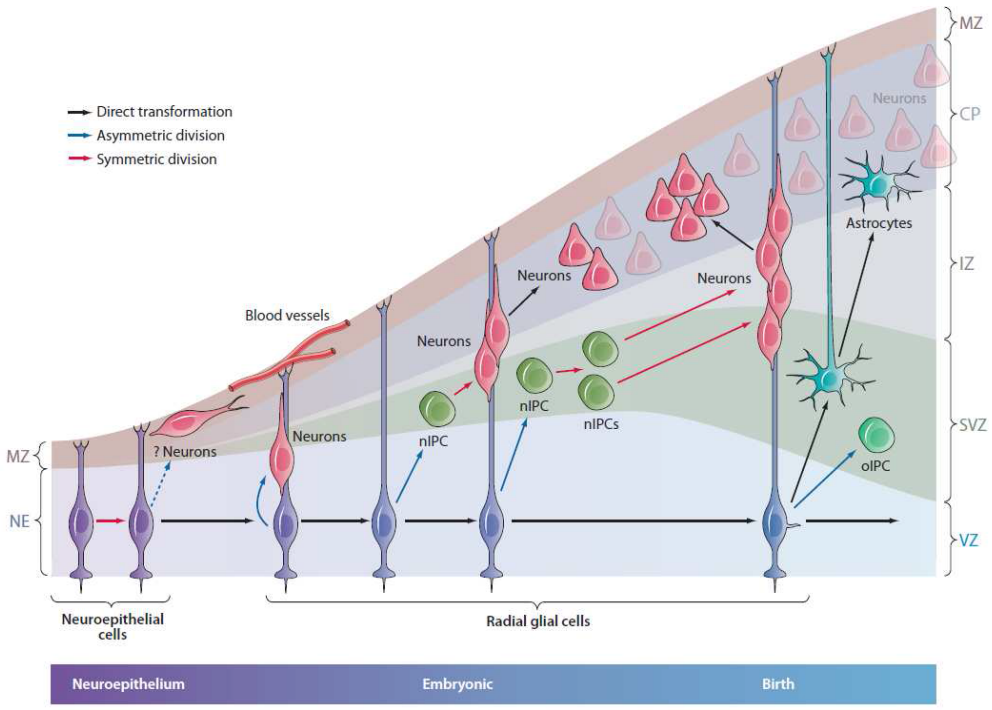

Figure I.1. Neurogenesis during cortical development (*adapted from Kriegstein and Alvarez-Buylla, 2009*)

1.1.2 Clonal articulation

As already mentioned above, at some point in the developing embryo, neural stem cells must face the option to remain in a pluripotent self-renewing cell state, enter neurogenesis and become new neurons, or shift into gliogenesis. Complex genetic mechanisms underlie such big decision. Indeed, one of the main goals of the studies in progress in the modern developmental genetics is to understand which specific molecular mechanisms (cell-autonomous or not), signaling molecules and effector pathways are involved in the regulation of this hard decision so finely restricted in time and space (*Fig. I.2*).

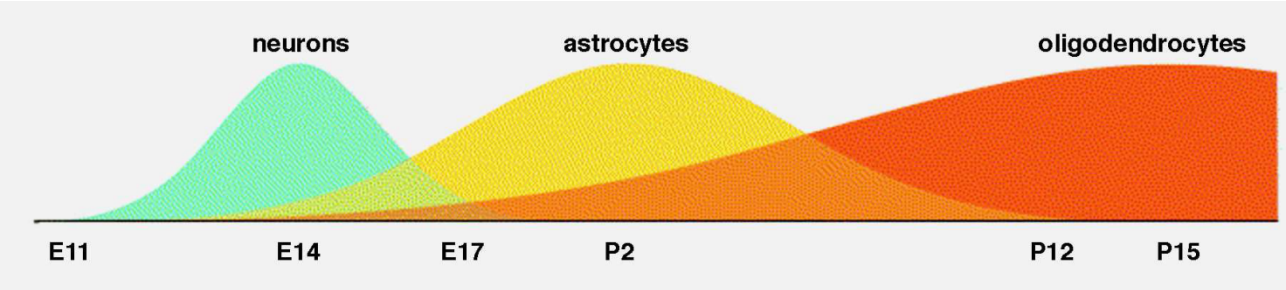

Figure I.2. Cortico-cerebral histogenesis

Astrocytes are no longer seen as a homogenous population of cells. Fibrous astrocytes with the classic ‘‘star-like’’ appearance are usually present in white matter where their dense glial filaments are stained with the intermediate filament marker GFAP. When they are in close proximity to capillaries they physically connect to capillary walls with their prolongations known as "vascular feet". The most numerous type of astrocytes are the protoplasmic glia, which are present in grey matter tissue and are mostly recognized with S100B labeling. It has been suggested that fibrous and protoplasmic astrocytes might be developmentally distinct (Nishiyama et al., 2009). In addition, there are at least two more subpopulations of astrocytes, known as specialized ‘‘radial’’ astroglia: Bergmann glia, which is found in the cerebellum, and Muller cells, which are the primary glial cell in the retina.

Astrocytes can be originated from RG cells directly. This is suggested by the fact that RG and astrocytes share the expression of the same markers (such as RC1)

(Misson et al., 1991) and that appearance of an increasing population of astrocytes is coincident with disappearance of RG population. Also, RG fluorescent label with DiI and retroviral label are retained in the newborn astrocytes (Noctor et al., 2008; Voigt, 1989). Astrocyte differentiation starts when RG cells lose their bipolar morphology to switch to an unipolar one, by retracting the pial process. Then, these cells gain multipolar morphology thanks to the appearance of radial processes, typical of astroglial cell types. Newly born, immature astrocytes migrate to their final locations, where they undergo local divisions before terminal differentiation (Ge et al., 2012). In fact, recent studies show that most of mouse cortical astrocytes are generated from clonal divisions of early differentiated astrocytes (Ge et al., 2012) and that such clones may arrange domains of distinct astrocyte classes (García-Marqués and López-Mascaraque, 2013). Also, there is still room for the presence of a yet-to-be identified astrocyte restricted progenitor population. It has been reported the evidence of a bipotent subpopulation which expresses A2B5 and is able to give rise to oligodendrocytes and astrocytes too. This subpopulation has been early described in the rhombo-spinal domain and then also reported in telencephalon. Some studies suggest the possible coexistence of both restricted and bipotential glial progenitors neonatally (Levison and Goldman, 1993; Luskin and McDermott, 1994).

The gliogenic switch happens around E16-18 in murine cerebral cortex, when there is the NSCs transition from neurogenesis to gliogenesis (Deneen et al., 2006; Ge et al., 2012; Molofsky and Deneen, 2015). During neuronogenesis, Dnmt1 is responsible for the methylation of glial genes, while Ngn1 sequesters p300/CBP complex which cannot bind pStat3 proteins. First, NSCs switch to gliogenic fate thanks to Nuclear factor I (NfIA) activation, which inhibits Dnmt1 and leads to demethylation of glial genes promoters. Additionally, bone morphogenetic proteins (BMPs), Notch signaling and other extrinsic factors activate Stat3:p300/CBP complex that initiate glial gene transcription.

These mechanisms will be explained more in detail in the following paragraphs. Once they have been specified, the intermediate astrocyte precursors express some specific markers, such as Glast, FABP7/BLBP and FGFR3. Then, astrocytes migrate to colonize their final destination. Although there are studies examining polarity and basic migratory mechanisms underlying such migration, these processes remain not well characterized in vivo.

After migration, astrocyte start their terminal differentiation and acquire the expression of the canonical markers Gfap (mainly in fibrous astrocytes), s100β (in protoplasmic astrocytes), Aldh1L1, AldoC, AScgb1, Glt1 and Acquaporin4. However, each of these markers show some limitations, as illustrated in *Table I.1* (adapted from (Molofsky et al., 2012)).

Marker	Expression onset	Advantages	Caveats
Glast	mE11.5, cE5	Early expression	Also expressed in some oligodendrocyte precursors
NFI A/B	mE11.5, cE5–cE6	Early expression	Also expressed in oligodendrocyte precursors and mature motor neurons
FABP7/BLBP	mE8–mE9, cE2	Early expression	Also expressed during neurogenic stages in radial glia
FGFR3	mE9.5, cE3	Early expression	Also expressed during neurogenic stages in radial glia and oligodendrocyte precursors
Sox9	mE9.5–E10, cE3–cE4	Early expression	As above
Reelin/slit	cE4	Early expression; subtype specificity	Also expressed by neurons; uncharacterized outside spinal cord
AldhlL1	mE9.5	Early expression that persists in mature astrocytes; labels both fibrous and protoplasmic astrocytes	Incompletely characterized; expressed early in radial glia, (unclear whether these are fated to become astrocytes only)
Id3	mE14.5	Early expression	Also expressed in some oligodendrocyte precursors
Aldolase C	mE15	Antibody detects fibrous and protoplasmic astrocytes	Also expressed in pial and purkinje cells
GFAP	mE17.5–mE18.5	Robust, well-characterized marker of mature fibrous astrocytes and reactive astrocytes	Poorly labels protoplasmic astrocytes; turned on relatively late in development
S100β	mE15.5–mE16.5	Robust, good antibodies available	Also labels oligodendrocytes; turned on late
Aquaporin-4	mE18	Subtype specific? (preferentially labels endfeet near blood vessels and pia)	Also in ependymal cells; white matter-restricted
CD44	E18.5–P0, cE10	Cell surface marker potentially useful for flow cytometry	Incompletely characterized
Glutamine synthetase	Embryonic to early postnatal	Expressed in fibrous and protoplasmic subtypes	Incompletely characterized

Note that onset of expression varies in different regions of the CNS, with marker detection generally sooner in spinal cord versus forebrain. See the text for details. (mE) Mouse embryonic day; (cE) chick embryonic day; (P) postnatal day.

Table I.1. Markers of astrocytes and their progenitors (*Adapted from* (Molofsky et al., 2012))

Interestingly, the same patterning factors that modulate neuronal type generation can play an instructive role also in generation of diverse astrocyte subtypes. For instance, canonical signaling factors like Sonic Hedgehog (SHH), Fibroblast growth factor (FGFs), WNTs and BMPs provide positional information to developing macroglial cells through morphogen gradients along the dorsal–ventral, anterior–posterior and medial– lateral axes.

Moreover, in spinal cord, different subtypes of astrocytes with different positional identities can be identified on the basis of their expression of different

transcription factors (Pax6, Nkx6.1) and cell surface markers (Reln and Slit1). In fact, it has been shown that astrocytes are allocated in mouse spinal cord and brain accordingly to their embryonic origin sites in the VZ. These specific domains implicates some limitations of the astroglial response to injury (Tsai et al., 2012). Finally, astrocytes take cortical positions that reflect the inside-out pattern of cortical neurons: later-born glia take superficial positions indeed (Ichikawa et al., 1983) (*Fig. I.3*). Nevertheless, the in vivo validation of the structure of gliogenic compartments and lineages is still fully in progress.

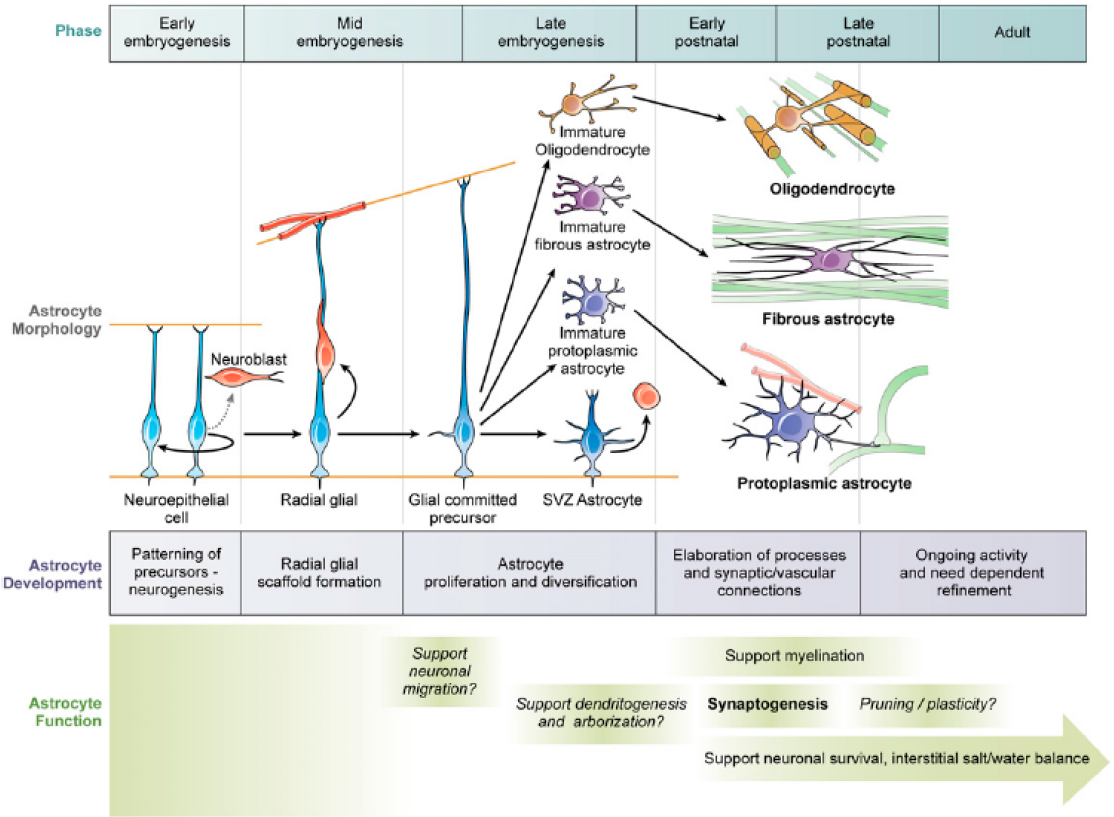

Figure I.3. Changes in astrocyte morphology and function across development. (*Adapted from* (Molofsky et al., 2012))

1.1.3 Molecular mechanisms

Several molecular mechanisms control the perfect timing of astrogenesis. Exhaustive studies have been made on the modulators of astroglial gene promoters (*Gfap*, *S100β*).

As already stated above, early neural stem cells (NSCs) are insensitive to cytokines triggering the main pro-astrogenic pathway, the Jak/Stat pathway. In particular, during the neuronogenic phase, proneural genes cooperate in order to promote neuronal differentiation and inhibit glial fate choice. For instance, Neurogenin 1 (Ngn1) binds the p300/CBP complex, so sequestering it from its interaction with Stat3, a well-known inducer of glial genes transcription. Moreover, prominent methylation of glial genes is reached thanks to the help of DNA methyltransferase I (DNMT1). These mechanisms both lead to the inhibition of the Jak/Stat axis.

Even when precursors face a heavy chromatin remodeling, which results in the demethylation of *Gfap* and *S100β* promoters, other independent brakes of astrogenesis are at work, such as the ErbB4-NCoR signaling.

Conversely, at the end of neuronogenic window, precursors are finally ready to initiate astrogenesis, thanks to the release of astrogenic brakes and to the action of multiple pro-active pathways. Among them, Notch signaling help the demethylation of *Gfap* promoter though its downstream effector NFIA, and act synergistically with Jak/Stat pathway to promote astrogenesis. Meanwhile, newborn neurons release the cytokines which trigger Jak/Stat activation too. Noticeably, Jak/Stat pathway itself is finely regulated by several plug-ins. Other signaling mechanisms help promoting astrogenesis initiation: Tgfβ, BMPs, PACAP/Dream pathway (summarized in *Fig. I.14* and *Fig. I.15*). Finally, specific mechanisms control the maintanance of astrocytic identity. All these mechanisms will be explained in detail below.

Inhibition of astrogenesis

The main brakes of astrogenesis are at work during neuronogenesis in order to prevent premature astrogenesis. They are mostly represented by a group of mechanisms that inhibit the main astrogenic pathway, the Jak/Stat pathway, and by an independent antiastrogenic system, the Nrg1/ErbB4/NCoR/RBPJk pathway.

- ***Inhibition of CT1/JAK/STAT3 pathway***

During neuronogenesis, the proneural factor Neurogenin 1(Ngn1) binds p300/CBP complex so sequestering it from a possible interaction with phospho-Stat3. At the same time, together with Ngn2, NeuroD1 and Mash1, it promotes neuronal differentiation (Cheng et al., 2011).

SHP2-Ras-Mek-Erk pathway is also implicated in the promotion of neurogenesis at the expenses of astrogenesis, by inhibiting the canonical Jak/Stat axis. In particular, Src homology phosphotyrosine phosphatase 2 (SHP2) is a phosphatase that dephosphorylates Stat3. It is also suggested that SHP2 could inhibit Stat3 transcription by methylation of astrocyte genes. To date, no specific activator of the SHP2-Ras-Mek-Erk pathway is identified which induces the inhibition of astrogenesis, although BDNF is a potential candidate (Barnabé-Heider and Miller, 2003).

Moreover Reelin, together with Disabled 1 (Dab1), suppress astroglial differentiation by affecting Jak/Stat pathway. In fact, when Dab1 is deleted in NSCs, NeuroD expression is decreased, which in turn results in augmented Stat3 phosphorylation (Kwon et al., 2009).

Another important role in silencing Stat3 activity is exerted by the suppressor of cytokine signaling 3 (Socs3), which also increases neurogenesis (Cao et al., 2006).
Finally, a crucial role is played by epigenetic regulation of Stat3- binding sites on glial gene promoters. This will be discussed more in detail in the dedicated section.

- ***Nrg1/ErbB4/NCoR/RBPJk antiastrogenic pathway***

This pathway represents a crucial brake to prevent premature astrogenesis. The ligand Neuregulin 1 (Nrg1), expressed by neural precursors and neurons, is involved in the "canonical" activation of ErbB receptors, which consists in their homo- or hetero- dimerization and the induction of their intracellular tyrosine kinases, which in turns activate the Raf/Mek/Erk and the phosphoinositide-3-kinase (PI3K) machineries (Mei and Xiong, 2008). Conversely, as for the inhibition of astrogenesis, Nrg1 exerts its role by binding the juxta-membrane α (jMα) isoform of ErbB4, so activating an alternative pathway, called the non-canonical pathway. In this case, upon its activation, ErbB4 undergoes two sequential cleavages, by TACE (TNF-α-converting enzyme) and presenilin-dependent γ secretase, respectively. This leads

to the release of an intracellular domain (ErbB4-ICD), which specifically bind the corepressor N-CoR thanks to Tgfβ-activated protein kinase 1 (Tak1)-associated binding protein 2 (Tab2) bridge. This trimeric ErbB4/Tab2/NCoR complex translocates to the nucleus and directly inhibits the transcription of astrocytic genes (*Fig. I.4*). Remarkably, mice knock-out for *ErbB4* exhibit a premature cortical astrogenesis, a phenotype which may be rescued by re-expression of this gene (Sardi et al., 2006). It was also suggested that this trimeric complex could further bind the recombination signal binding protein for immunoglobulin J region (RBPJk), with highly affinity to NCoR. In this way, the complex could bind to the Gfap promoter at the RBPJk binding site (Miller and Gauthier, 2007). Remarkably, robust Nrg1 signaling in early murine cortical precursors would physiologically prevent precocious activation of astrogenesis, even in the presence of early firing of the Jak/Stat axis. Subsequently, the fading of Nrg1 signaling, caused by the late ErbB4 downregulation (Fox and Kornblum, 2005; Kornblum et al., 2000), would result in the progressive release of this astrogenic brake, around E18 and later in mice.

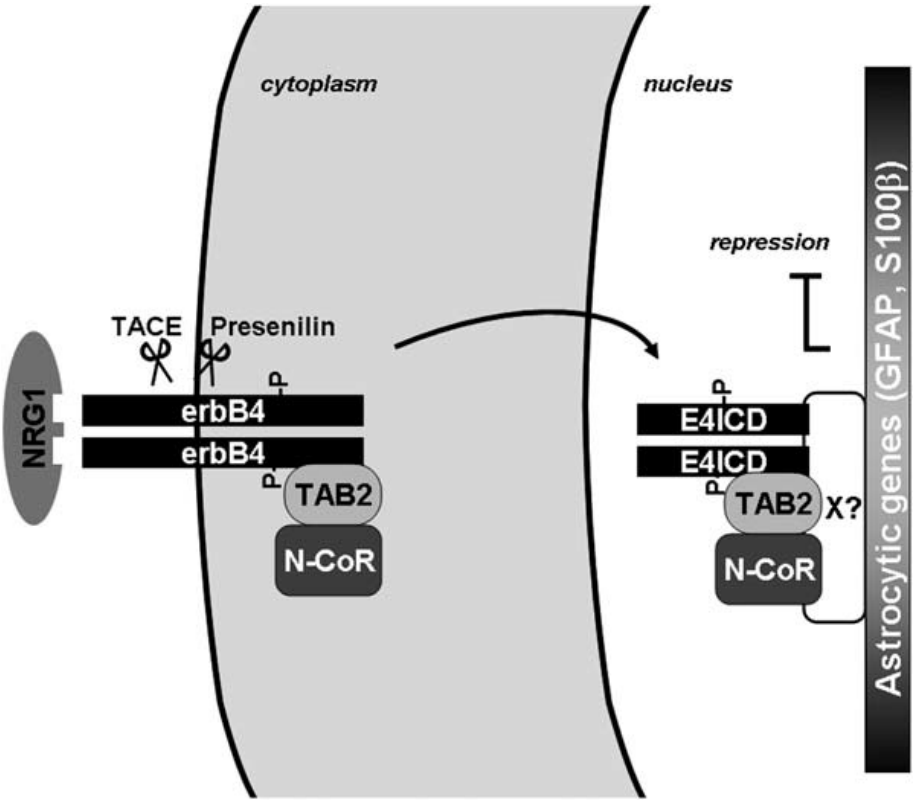

Figure I.4. ErbB4 intracellular pathway. (*Adapted from* (Sardi et al., 2006))

Spatio-temporal epigenetic regulation

Accessibility of chromatin to transcription is finely regulated during development. It has been demonstrated that the proper progression of cortico-cerebral neurogenesis, followed by astrogenesis, needs a precise temporal regulation of chromatin accessibility to transcription. During early neurogenesis, chromatin is condensed at the level of glial genes. Also, there are generalized changes in chromatin structure which guide NSCs choice towards neuronal or astrocytic fates. Afterwards, when astrogenesis is about to peak up, there are specific epigenetic changes at proneural genes in order to down-regulate their expression, as well as a progressive opening of astrocytic chromatin. These events will be better explained below.

- ***Chromatin closure at glial genes during early neuronogenesis***

Interestingly, endogenous S100β and GFAP levels are null in the early cortex even if some cytokine and pStat are available. Remarkably, this situation doesn't change even if early neuroblasts are transfected with a constitutively-active Stat. Upon exposure to Lif, pStat3 is upregulated but its binding with Gfap promoter is prevented. It is reasonable to ascribe this phenomenon to the low accessibility of Stat3 responsive elements (Stat3-RE) on glial genes promoters.

First, astrocytic chromatin closure depends on the augmented methylation of DNA at glial genes. *DNA methyltransferase* gene (Dnmt1) is a potential candidate for the methylation of CpG residues of DNA during neuronogenesis. In fact, deletion of such genes in NSCs promotes the switch from neurogenesis to astrogenesis (Fan et al., 2005). Such methylation recruits methyl CpG binding proteins such as methyl CpG binding protein 2 (MeCP2), which, together with Sin3 transcription regulator homolog A (Sin3A), further condense chromatin and hence inhibits gene expression ((Fan et al., 2005; Icardi et al., 2012; Jones et al., 1998; Namihira et al., 2004)). Moreover, the SHP2-Ras-Mek-Erk pathway may play an additional role in such promoter methylation, considering that it has been shown to induce DNA methylation by DNA methyltransferase 3 in non-neural cells (Pruitt et al., 2005).

In addition to DNA methylation, a second crucial mechanism controlling chromatin remodeling is represented by Histone 3 differential covalent modifications. The peculiar hallmarks of repressed chromatin state are di-methylation at histone3-lysine 9 (H3K9me2) and tri-methylation of histone3-lysine

27 (H3K27) and absence of acetylation at histone3-lysine 9(H3K9) and histone3-lysin 14(H3K14). This can be supported by the presence of Retinic acid receptors (RARs) and N-CoR. In absence of retinoic acid (RA), RARs form a repressor complex with N-CoR and induce deacetylation of glial gene promoters by recruitment of histone deacetylases (HDACs) (*Fig. I.5*).

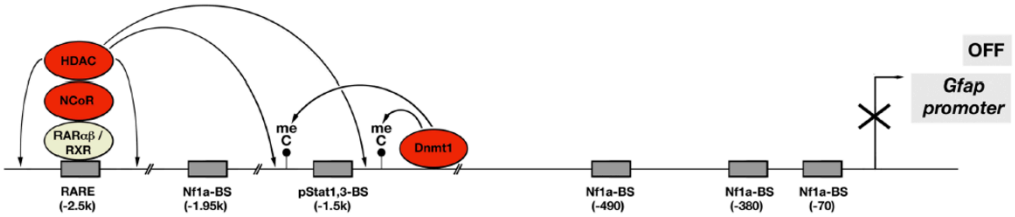

Figure I.5. Epigenetic regulation of the Gfap promoter by Nf1a and RA (OFF state) (*Adapted from* (Mallamaci, 2013))

- ***Large-scale changes of chromatin structure***

It has been shown that the young NSCs, prone to self-renewal or neuronal differentiation, preferentially show a chromatin open configuration in general. Subsequently, chromatin undergoes a progressive compaction which will channel neural precursors towards astrocytic fate (Kishi et al., 2012). The mechanism by which such generalyzed changes impact NSCs choice is still elusive. An hypothesis is that this could result in a reduction of proneural genes' transcription, which indirectly de-repress astrogenesis.

This epigenetic change is linked to two main groups of genes. The first one is High mobility group A (HmgA) proteins 1 and 2, which bind to histone H1, so preventing its interaction with internucleosomal DNA linkers. In this way, chromatin remains accessible during the neurogenic window. HmgA levels decrease at the end of neuronal differentiation, and this could be helpful for astrogenesis onset (Kishi et al., 2012). Besides HmgA, N-myc is also expressed at high level early in development, when it up regulates the histone acetyl-transferase gene *GCN5.* It supports the acetylation of histone H3 and H4, resulting in a more open state of chromatin (Knoepfler et al., 2006). N-myc effect is counteracted by p19Arf, which is conversely

highly expressed in late neural precursors and drive them to astroglial differentiation (Nagao et al., 2008).

- ***Epigenetic changes at pro neural genes***

A prominent change at proneural chromatin has been shown in the proximity of the Ngn1 transcriptional start site. Infact, there is a progressive increase of the repressive hallmark trimethyl-histone3-lysine27 (H3K27me3). This can explain the graduated downregulation of Ngn1 in vivo at the end of neuronogenesis. Polycomb group (PcG) proteins are responsible of reducing histone acetylation and increasing H3K27 methylation at Ngn1 promoter region (Hirabayashi et al., 2009). This mechanism precedes the onset of astrogenesis and is crucial for the neurono-to-astrogenic switch.

- ***Epigenetic remodeling of astroglial genes***

One of the main events involved in chromatin opening deals with Nf1A capability to mediate DNA demethylation, by inducing the dissociation of Dnmt1 from the Gfap promoter. At least four Nf1a binding sites have been mapped on Gfap promoter ((Cebolla and Vallejo, 2006; Piper et al., 2010)). It has been suggested that Dnmt1 release results in the passive loss of methylation of Gfap promoter (Namihira et al., 2009). Nf1A is induced by Notch signalling, one of the main promoters of astrogenesis (Grandbarbe et al., 2003), which will be further explained.

Although the vast majority of the studies have been done on Gfap gene, such demethylation have been described in many other cases (AldoC, ATP-sensitive inward rectifier potassium channel 10 gene(Kcnj10), sorption peptidase inhibitor b8 gene (Serpinb8) and SRY-box containing gene 8 (Sox8) among them) (Hatada et al., 2008).

Another key signal for opening the chromatin structure at Gfap promoter is fibroblast growth factor 2 (Fgf2). Ff2 is able to suppress H3K9 methylation in favor to H3K4 hypermethylation at the Stat3 binding site. This can induce Gfap expression in the presence of CNTF (Irmady 2011). Fgf2 signaling might stimulate H3K9→H3K4me switch thanks to methyltransferase SET7/9 ((Nishioka et al., 2002; Song and Ghosh, 2004)).

Additionally, retinoid acid (RA) changes the conformational state of its receptor bound to RARE site at the Gfap promoter region. This leads to the replacement of NCoR-HDAC by histone acetyl transferase p300/CBP, which in turn increase histone acetylation at surrounding sites ((Asano et al., 2009; Jepsen et al., 2007)). Remarkably, p300/CBP complex had been previously made available thanks to the downregulation of Ngn1, which no longer binds to it.

Among further agents inducing astroglial chromatin opening, there are also Coup-tf1 and 2. Since these agents are not sufficient to anticipate astrogenesis' onset, they might play only a permissive role. H3K9me2→H3K4me2 switch, H3 acetylation and DNA demethylation are evoked, even if indirectly, by Coup-tf1 and 2 (Naka et al., 2008).

All these mechanisms are summarized in *Fig. I.6* and *Fig I.7*.

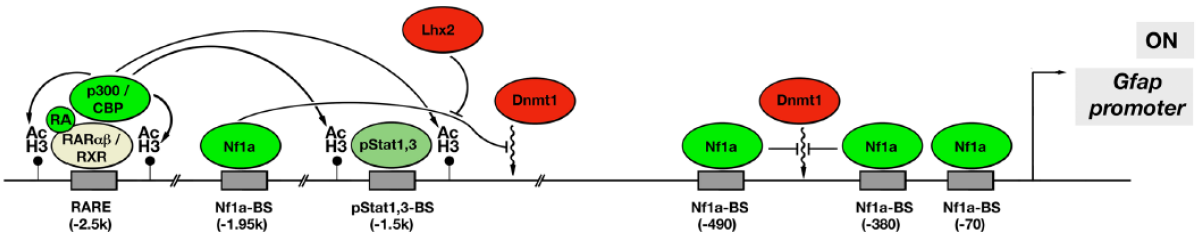

Figure I.6. Epigenetic regulation of the Gfap promoter by Nf1a and RA (ON state) *(Adapted from* (Mallamaci, 2013)*)*

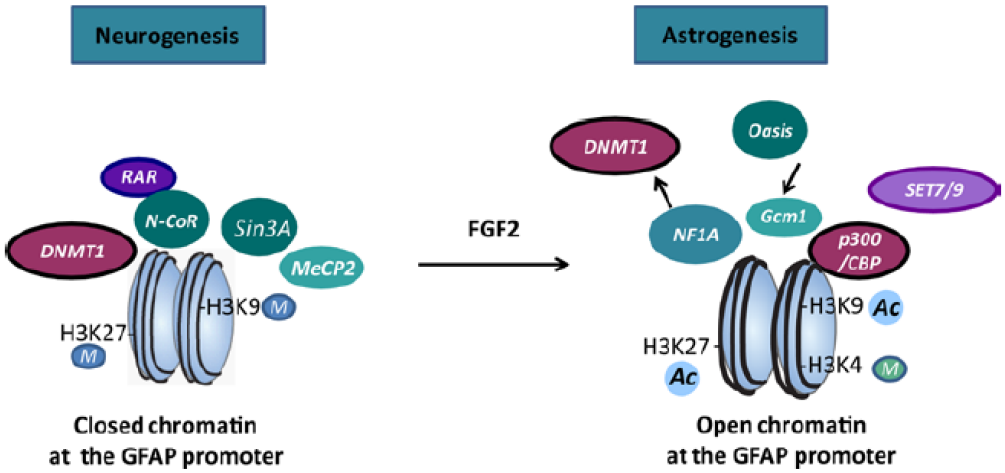

Figure I.7. Summary of epigenetic remodeling of the *Gfap* promoter. *(Adapted from* (Kanski et al., 2014)*)*

Stimulation of astrogenesis

- ***Ct1/Jak/Stat3 pathway***

Within cerebral cortex, as well as many other regions in the CNS, a key role in the trigger of astrocytogenesis is exerted by the Interleukin-6 (IL-6) family of gliogenic cytokines, including ciliary neurotrophic factor (CNTF), leukemia inhibiting factor (LIF), cardiotrophin-1 (CT-1), neuropoietin and CT-like factor. Neurons could be the main promoter of gliogenesis. Indeed, several studies report that these factors are secreted by newborn neurons, once they have been generated. These secreted factors bind to their α-coreceptors, such as Ciliary neurotrophic factor receptor α, CntfRα, and elicit the heterodimerization of the two β-subunits of glycoprotein 130 (gp130) and Lif-receptor β (LifRβ). This heterodimerization activates the gp130/Jak/Stat pathway in neural cortical precursors, therefore specifying the onset of astrogliogenesis (Rowitch and Kriegstein, 2010). Specifically, such heterodimerization is followed by the phosphorylation of Janus tyrosine kinase 1 and 2 (Jak1,2), constitutively bound to gp130/LifRβ. Jak1,2 in turn phosphorylate two key proteins: the suppressor of high-copy PP 1 protein 2 (Shp2) and Signal transducer and activator of transcription 1 and 3 (Stat1/3), both associated to specific binding sites on internal sites of the same receptors. Once phosphorylated, Stat1/3, they bind to the p300/CBP complex and translocate into the nucleus, where they bind specific pStat-responsive elements located on *Gfap*-, *S100β*- and *Aquaporin*-promoters and activate the transcription of the respective genes (He et al., 2005). Shp2, instead, triggers the mitogen-activated Erk kinase (Mek)/extracellular signal-regulated kinase (Erk) and the Akt cascades (Ernst and Jenkins, 2004). It doesn't directly transactivate astroglial genes, but it is crucial to the self-inhibition of this main astrogenic axis.

Interestingly, production of Gfap+ astrocytes is completely abolished in LIFRβ$^{-/-}$ and gp130$^{-/-}$, strongly affected in Ct-1$^{-/-}$ and only slightly reduced in CNTF and LIF mutants (Barnabé-Heider et al., 2005; Bonni et al., 1997; Koblar et al., 1998; Ochiai et al., 2001). These data not only point to Jak/Stat axis as the main inducer of astrogenesis, but also suggest that the real ligands involved in the initiation of the in vivo cascade probably is Ct1, specifically expressed by cortical neurons (Barnabé-Heider et al., 2005), possibly with the early help of Lif in some regions and the

subsequent support by Cntf, released by astrocytes, later in development (Derouet et al., 2004; Lillien et al., 1988).

Numerous modulatoy plugins act on this axis. First of all, two autocatalytic loops upregulate the process. pStat1 and 3 themselves upregulate directly the transcription of gp130, Jak1, Stat1 and Stat3, therefore enhancing the responsiveness of the system (He et al., 2005) (*Fig. I.8*). Also, as stated before, Cntf is produced from newborn astrocytes and mimics the effect of Ct1, by synergyzing with it.

Moreover, as the proper balance between astrogenesis and neuronogenesis needs to be mantained, negative modulators act on Jak/Stat axis. In details, Jak2 phosphorylation is limited thanks to the negative feedback provided by *Suppressor of cytokine signaling gene 3* (Socs3) and Shp2. Socs3 binds to the receptors and triggers the degradation of the ligand-receptor complex as well as the inhibition of Jak2 phosphorylation (Krebs and Hilton, 2001). Shp2 also binds to the same receptors phospho-tyrosine residues which interacts with Socs3 (Schmitz et al., 2000) and dephosphorylates Jak2, so dampening the firing of the pathway (Lehmann et al., 2003) (*Fig I.8*).

Furthermore, a prominent heteroregulation is crucial to finely tune Jak/Stat axis. Apart from competing with pStat1/pStat3 for the binding to the CBP/p300-pSmad1/pSmad4 complex, pro neural genes Neurog1 and 2 are able to downregulate the transcription levels of gp130, Jak1 and Stat1/3 (He et al., 2005). On the other hand, Neurofibrin 1 (Nf1) is able to convert RasGTP in its inactive form RasGDP (Scheffzek et al., 1997), so inhibiting Raf/Mek/Erk pathway during neuronogenesis (Wang et al., 2012). In the absence of Nf1, RasGTP can activate the cascade of Raf/Mek/Erk, which results in the stimulation of gp130 transcription through the final effectors Etv5/Erm proteins (*Fig. I.9*).

Among the various pathways interfering with the IL-6/Jak/Stat transduction machinery, the EGFR one plays a master role as a positive regulator. Lillien et al. performed an elegant experiment in which they demonstrate that EGFR (induced by Fgf2) is necessary and sufficient to promote cortical progenitors' differentiation to astrocytes, under high Lif (Viti et al., 2003). This EGF receptor has been shown to increase Stat3 levels and, remarkably, to render Stat3 more easily phosphorylable under high Lif, probably by scaffolding Jak2 and Stat3 together. The transfection of a constitutively-activated, phospho-mimetic variant of Stat3 into *EgfR*$^{-/-}$ progenitors

was however not able to rescue GFAP expression. This suggests that the full astrocytogenic activity of EgfR requires a wider range of still unknown effect which are independent of Stat3 activation (*Fig. I.9*). EgfR regulation of astrogenesis will be the subject of a dedicated paragraph.

Finally, different pathways modulate Stat3 phosphorylation. Delta/Notch/Hes axis is one of the major pathway involved. Hes1 and Hes5 act as bridges between jak2 and pStat3. In this way, they facilitate the phosphorylation of the former to the latter (Kamakura et al., 2004).

Neural myelocymatosis prooncogene (N-myc) and *INK4ap19 protein/alternate reading frame of the INK4a/ARF locus* (p19Arf) inhibit reciprocally. The first one is involved in the promotion of neurogenesis, by promoting NSCs self-renewal. The second one sustain astrogenesis; it is stimulated by pStat3 and facilitates with a positive feedback mechanism Stat3 phosphorylation via p53 (Nagao et al., 2008) .

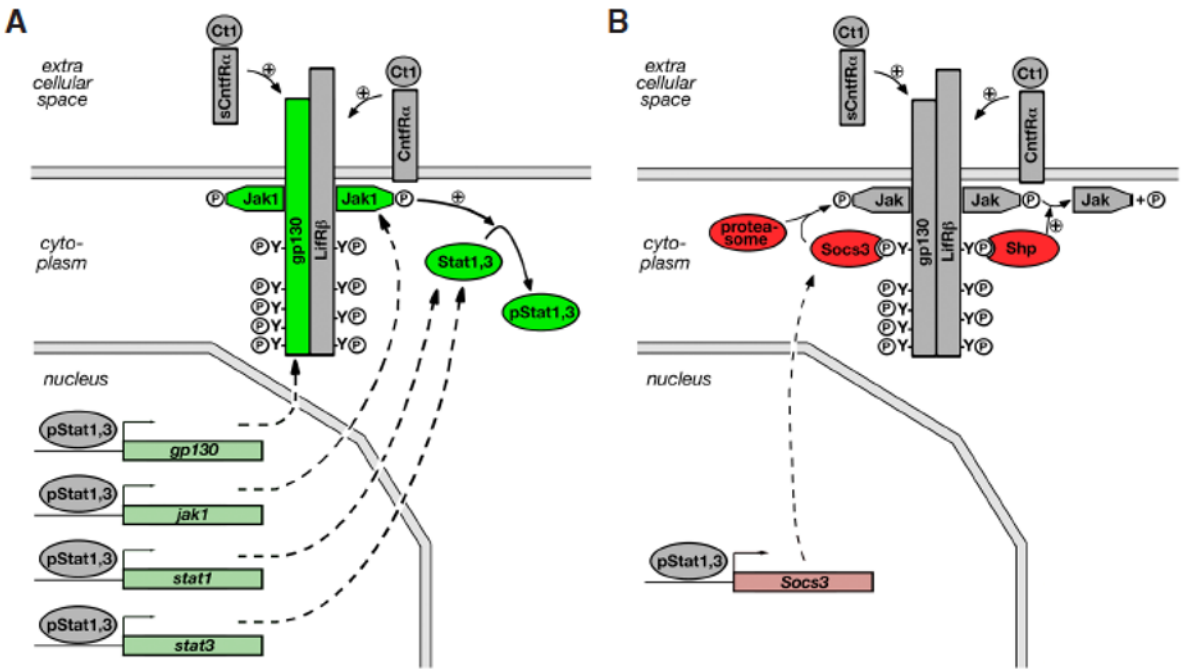

Figure I.8. Autologous regulatory loops modulating the Jak/Stat axis. *(Adapted from* (Mallamaci, 2013)*)*

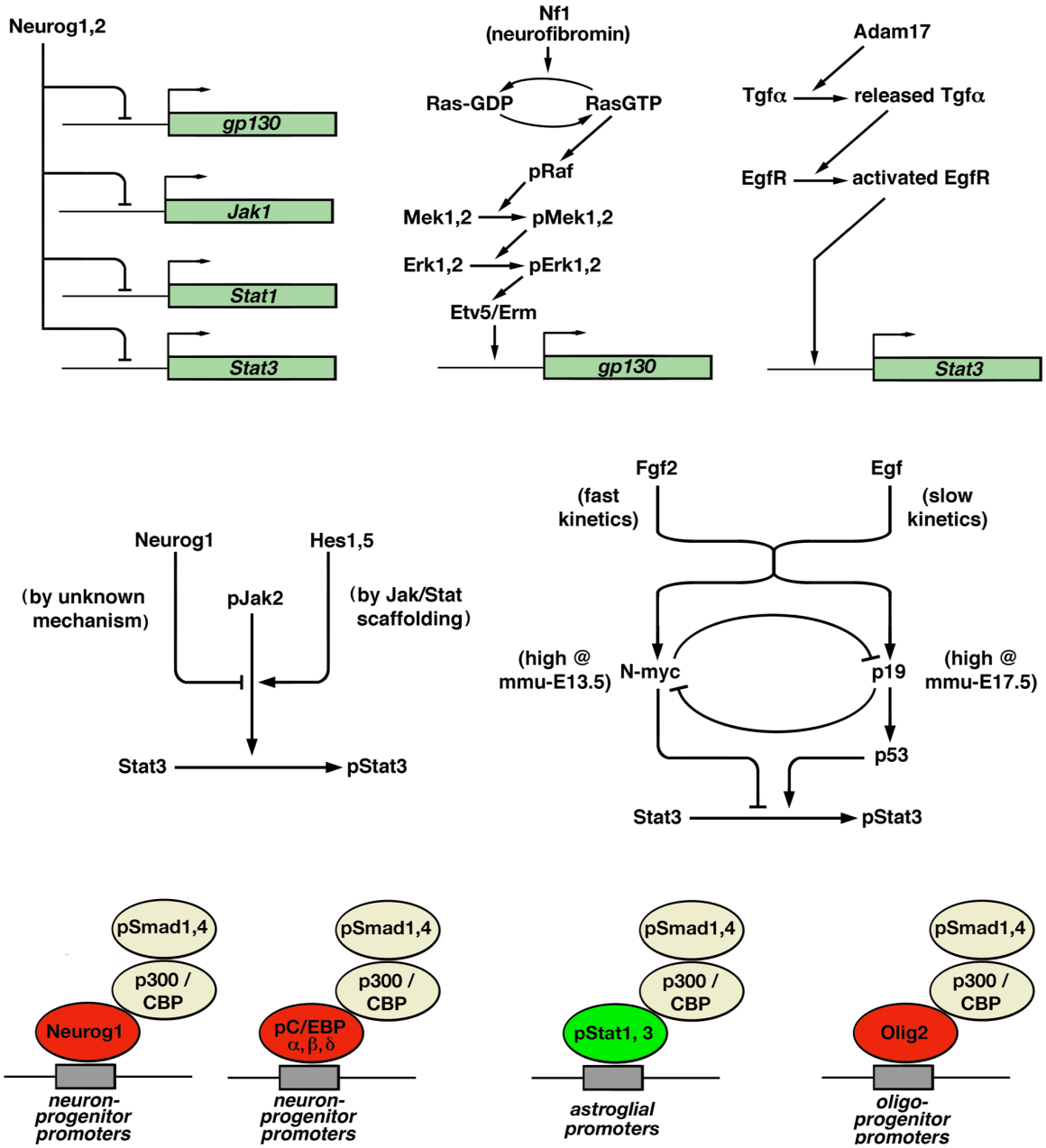

Figure I.9. Heterologous regulatory plugins modulating Jak/Stat axis. *(Adapted from* (Mallamaci, 2013)*)*

- ***Notch signaling***

Notch signaling is a notoriously highly conserved cell signaling system present in most multicellular organisms. This pathway performs different roles during development. It is essential for the maintainance of NSCs and it is endowed with an instructive role to directly promote the differentiation of several glial cell subtypes (Louvi and Artavanis-Tsakonas, 2006) (*Fig. I.10*).

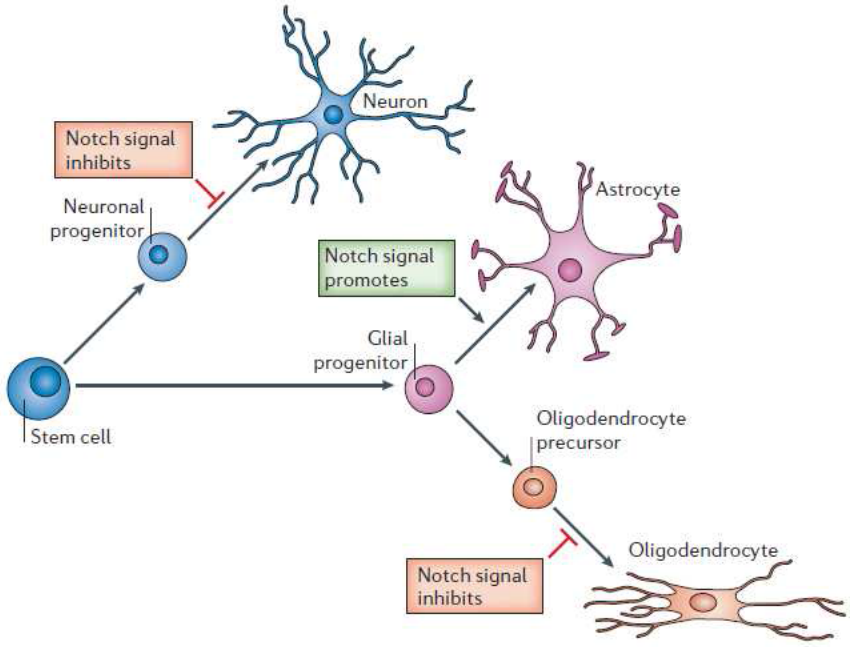

Figure I.10. Notch signaling throughout glial differentiation. *(Adapted from* (Louvi and Artavanis-Tsakonas, 2006)*)*

The well-known canonical signaling pathway is activated by the Notch ligands: Jagged and Delta-like proteins. When ligands are bound, Notch is cleaved by γ-secretase complex, containing presenilin1, Notch intracellular domain (NICD) is then released. It follows that NICD translocates into the nucleus where it interacts with DNA binding protein (such as c-promoter binding factor 1, CSL, aka Rbpjk) and stimulates transcription of Notch target genes, such as hairy enhancer of split (Hes), Hes1 and Hes5 (Guruharsha et al., 2012). During the neurogenic window, Hes1 and Hes5 inhibit neural genes transcription (Kageyama et al., 2005), while stimulating

NSCs self-renewal (Kopan and Ilagan, 2009). When development proceeds, newborn neurons keep stimulating Notch, by expressing its ligands. Thus, at late developmental stages, Notch signaling promotes the epigenetic remodeling of *Gfap* promoter through its target Nf1A, which promotes Dnmt1 released, as discussed above. The mechanisms that regulate this switch in the Notch response, from self-renewing to astrogenic, still remain unclear.

Noticeably, Notch signalling acts synergistically with Jak/Stat axis to promote astrogenesis (*Fig. I.11*). Stat3 itself induces the Notch ligand DLL1, which activates Notch signaling. Moreover, Socs3, the Stat3 inhibitor, also suppresses Hes5 expression (Cao et al., 2006). On the other hand, Hes1 induces Stat3 phosphorylation physically connecting Jak2 to it. Notch and Jak/Stat cross talk establishes a positive feedback loop that promotes the astrogenesis initiation (Kamakura et al., 2004). However, the astrogenic activity of Notch signalling requires Jak/Stat signalling, but not viceversa (Ge et al., 2012).

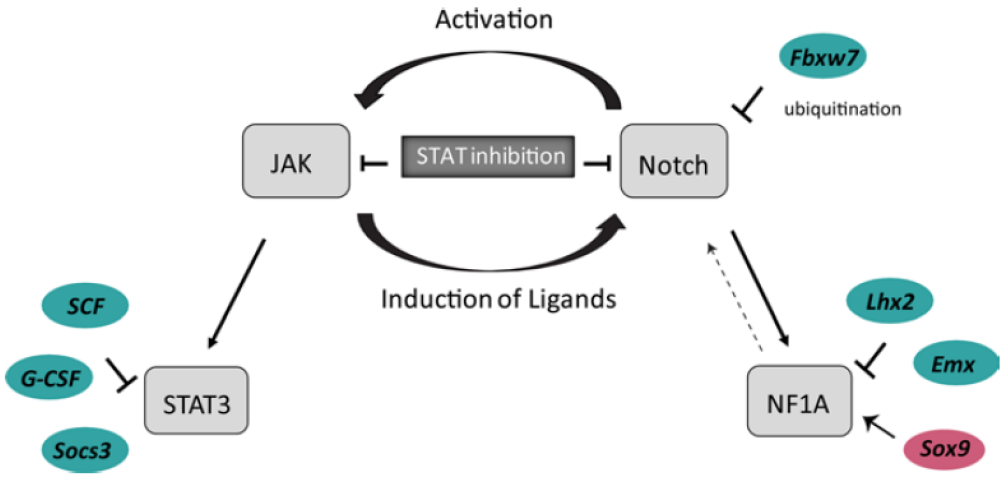

Figure I.11. Sinergic effect of Jak/Stat and Notch signaling at the onset of astrogenesis. *(Adapted from* (Kanski et al., 2014)*)*

Furthermore, Notch effector RBPJk, CSL-family factor, directly binds to an element within the GFAP promoter, at about 180bp with respect to the TSS, stimulating directly transcription (Ge et al., 2012). Intriguingly, RBPJk is able to bind NCoR (Kao et al., 1998). This complex could potentially silence astroglial genes

during neuronogenesis. Starting from E15.5, when Jak/Stat axis leads to progressive translocation of NCoR to the cytoplasm (Sardi et al., 2006), RBPJk would be free to bind NICD and stimulate gliogenesis (Miller and Gauthier, 2007).

- ***Bmp signaling***

It has been shown that combined Lif/Bmp2 stimulation activates *Gfap* in 2 days in E14.5 mouse embryos (Nakashima et al., 1999). Thus, Lif and bone morphogenetic factor 2 (Bmp2) cooperate in order to promote astrogenesis (Adachi et al., 2005).

However, no direct interaction has been observed between the two key transducers of the two pathways, Stat3 and Smad1. In fact, they are bridged by the p300/CBP complex, which interacts with Stat3 at its amino terminus and with Smad1 at its carboxyl terminus. This so-formed complex pStat3-p300/CBP- pSmad1 ternary complex, binds Gfap promoter and mediates a synergistic activation of its transcription by Lif and Bmp2 (Nakashima et al., 1999). Moreover,Bmp and pSmads might directly transactivate Gfap promoter, independently from pStat3, because addition of Bmp2 alone to culture insensitive to Lif induces a slight activation of such promoter (Nakashima et al., 1999).

Intriguingly, during neurogenesis in rat, p300/CBP complex is associated with both pSmad1 and Ngn1, but not with Stat3, which is however expressed at high levels. Later in development, at P3, when cortex is rich in astroglial precursors and is not expressing Ngn1 anymore, Stat3 is associated to p300/CBP (Sun et al., 2001). Given these data, p300/CBP-pSmad1 heterodimer may potentiate both neuronal and astrocytic programs, by complexing first Ngn1 and, then, pStat3. Remarkably, its function is dictated by a competition among its interactors for binding it. This competition is generally won by Ngn1. Therefore, until proneural factors are abundant, neuronal transcription is promoted. When neuronogenesis has been completed and pro neural genes are no longer expressed, p300/CBP-pSmad1 can bind pStat3 and finally allow astrocyte-specific transcription to rise (Sun et al., 2001) (*Fig. I.12*).

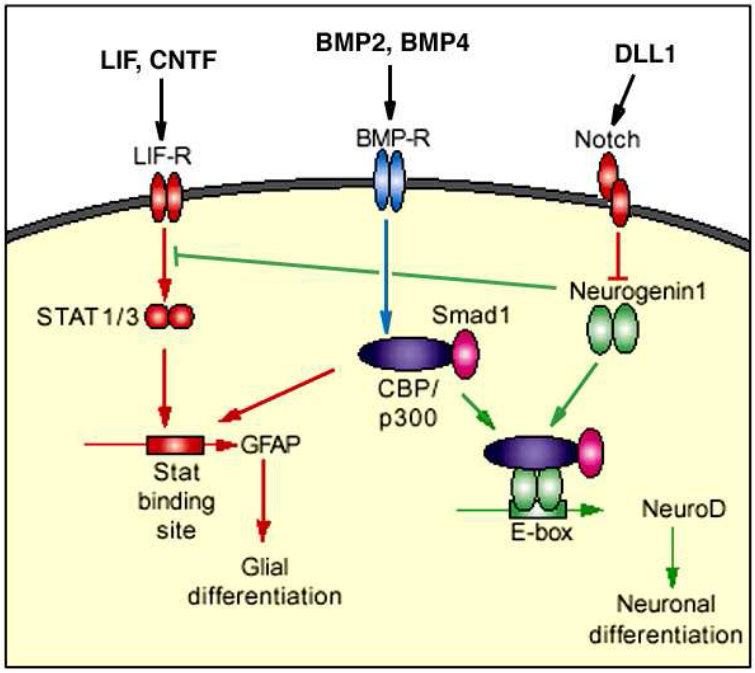

Figure I.12. BMP signaling in neuronogenesis and gliogenesis.

- ***Tgf-β signaling***

Transforming factors beta (TGF-βs) are multifunctional growth factors which act in key events of development and cell repair (Shi and Massagué, 2003). Tgf-β1 involves mainly 2 threonine kinase receptor, TgfRI and TgfRII, highly expressed in early development, which in turn activate Smad2/3 and Smad4 transcription factors. These proteins are phosphorylated and then complexed in Smad2/3-4 complexes, which translocate to the nucleus and regulate transcription (Shi and Massagué, 2003).

Tgf-β is not only implicated in late advancement of astrocyte differentiation, but it also has got a role in the commitment of pluripotent precursors to astroglial fates. In fact, cortical neurons may modulate the differentiation from radial glia cells to astrocytes, by secreting Tgf-β1 (de Sampaio e Spohr et al., 2002; Stipursky and Gomes, 2007). If conditioned medium derived from pure neuronal culture or astrocyte-neuronal co-culture is added to E14 cortical cultures in mouse, it is able to activate *Gfap* transcription and down regulate RG markers, such as Nestin and Blbp (Stipursky and Gomes, 2007).

Tgf-β can exert its pro-astrogenic function through diverse mechanisms. First, Smad2/3 proteins cooperate with Stat3 in order to increase Jak/Stat pathway-

mediated astrogenesis. Second, Tgf-β may induce a non-canonical MAPK/PI3K signaling in order to stimulate astrocytic differentiation (Stipursky et al., 2012).

Intriguingly, a key mediator of Tgf-β could be TAB2 (Yamaguchi et al., 1995). A model in which Tgf-β activation might sequester Tab2 from the inhibitor complex with ErbB4-NCoR, via Tak2 has been proposed. This could indirectly induce glial genes transcription (Stipursky and Gomes, 2007). The cross- talk between ErbB4-NCoR and Tgf-β1 signaling may be crucial to finely tune the neuronogenic-to-gliogenic switch.

- ***Pacap/Pac/Dream pathway***

Vallejo's team has discovered and characterized this pathway (Cebolla et al., 2008) and represents a fundamental biphasic regulation of astrocytic promoters (*Fig. I.13*). In the absence of the secreted factor called PACAP, Dream transcription factor sits on the *Gfap* promoter and acts as a trans-repressor. When PACAP binds to the PAC1 receptor, cytoplasmic cAMP is upregulated and calcium massively dashes into the cell. Dream is sensitive to the Ca^{2+} and is converted into a trans-activator. The PACAP/PAC1/cAMP/Dream pathway works in parallel to theCT1/IL6R/Jak/Stat pathway illustrated above. That is the reason why, if Jak/Stat axis is efficient, Dream-KO only determines a transient shrinkage of the astrocytic compartment between E17 and P7, associated to an enlargement of the neuronal one (Cebolla et al., 2008).

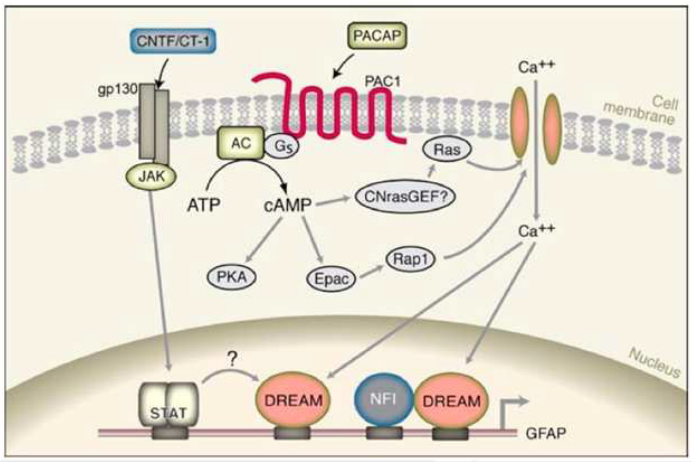

Figure I.13. PACAP/../Dream pathway. *(Adapted from*(Cebolla et al., 2008)*)*

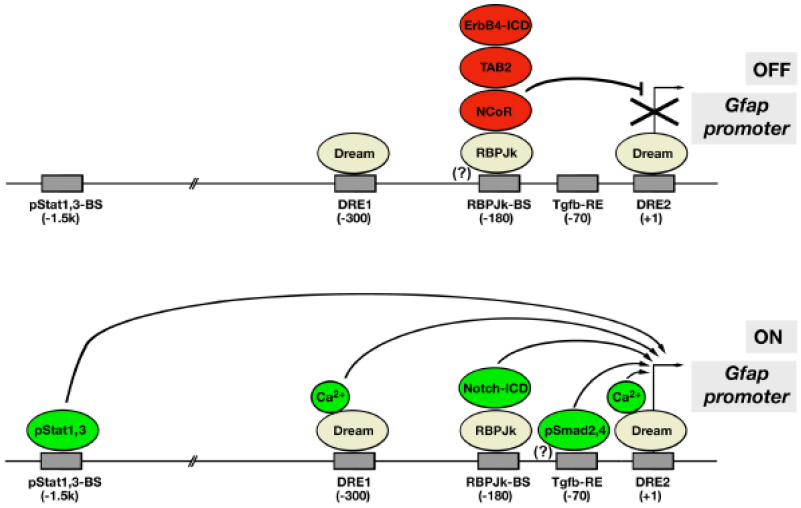

Figure I.14. Summary of transmodulators interacting with the *Gfap* promoter. *(Adapted from*(Mallamaci, 2013)*)*

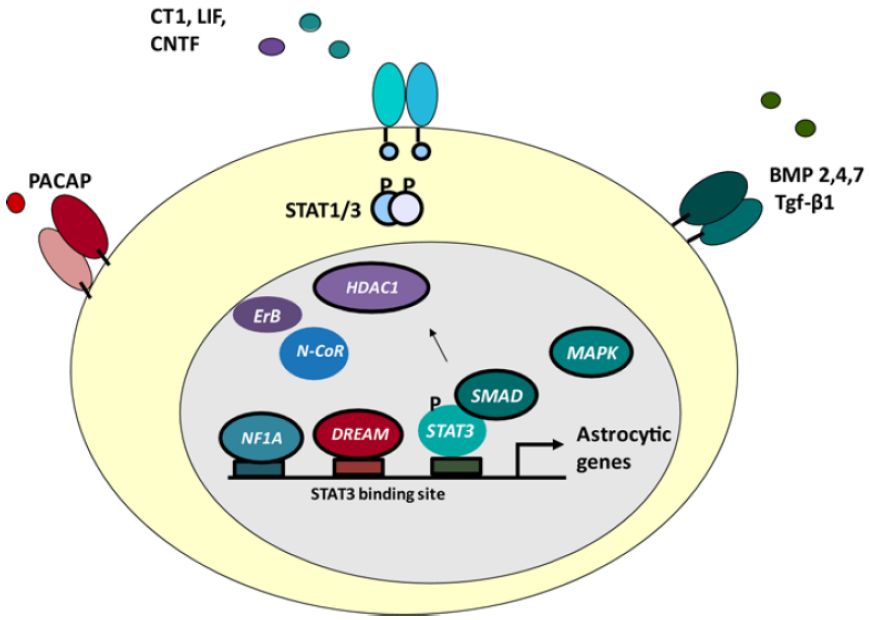

Figure I.15. Summary of the integrated network of stimuli converging to initiate astrogenesis. *(Adapted from* (Kanski et al., 2014)*)*

Modulation of astroblasts population kinetics

This regulation is still poorly understood and few genes have been found to be implicated in it. Two of them are here explained, the same genes were also studied in my work.

- ***Epidermal growth factor receptor (EgfR) signaling***

EgfR is a cell-surface receptor, member of the ErbB family of receptors. It is expressed at low level in the ventricular zone of the neuronogenic pallium and, at progressively higher levels in basal proliferative layers during development in cerebral cortex (Caric et al., 2001).

EgfR is an important regulator of astrogenesis. First, it is involved in the commitment of precursors to astroglial fates. For instance, mice lacking EgfR show a delayed astrocyte development (Kornblum et al., 1998; Sibilia et al., 1998). Also, overexpression of EgfR in rat cortex during neuronogenesis upregulates astrocytic output. Administration of the two main EgfR ligands EgF and Tgfa does not elicit the same results, thus suggesting that EgfR levels, rather than ligand levels, are crucial for the firing of EgfR pathway and in turn for astrogenesis. When EgfR levels become sufficiently high at the end of neuronogenesis, astrogenesis can be induced. The molecular mechanism could possibly be explained by the fact that EgfR facilitate transmission of Ct1 signal through Jak/Stat axis, via *Stat3* upregulation, as already mentioned above (Burrows et al., 1997; Viti et al., 2003). Remarkably, the upregulation of Stat3 induced by EgfR sensitizes embryonic neural precursors to the astrogenic cytokines, such as Lif, sufficiently to promote astrogenesis, even in front of low levels of these ligands (Viti et al., 2003).

A further role of Egf/EgfR signaling is the promotion of proliferation of astrocyte-commuted precursors. To appreciate this effect on proliferation, simple delivery of exogenous ligand (Egf) is sufficient, when EgfR levels are already increased (Viti et al., 2003). Interestingly, experimental overexpression of EgfR in early cortical precursors (E11-E13 in mice) upregulates frequencies of both S100$\underline{\beta}^+$ and Gfap$^+$ astrocytes, whereas Stat3 overexpression in the same cells increases S100$\underline{\beta}^+$ cells only. On the one hand, this suggests that there must be a Egf-dependent mechanism different from Stat3 upregulation, in order to selectively induce Gfap expression. On the other hand, such expansion of Gfap$^+$ compartment couldd be due

to the increased proliferation rate of astroglial-committed progenitors (Garrett et al., 2002).

- ***Fibroblast growth factor 9 (Fgf9) signaling***

This protein is a member of the huge fibroblast growth factors (FGF) family. In general, members of this family hold plenty of mitogenic and cell survival properties and are involved in various biological processes, including embryonic development, cell growth, morphogenesis, tissue repair, tumor growth and invasion.

In particular, Fgf9 is a secreted factor that shows its main effect as a growth-stimulating effect on cultured glial cells. In the nervous system it has been shown to be produced mainly by neurons and may be fundamental for glial cell induction and development (Santos-Ocampo et al., 1996). In particular, it promotes a huge expansion of the perinatal astrogenic proliferating pool (Seuntjens et al., 2009) and also delays terminal differentiation of mature astrocytes (Lum et al., 2009). It has been thought to be produced by neurons, as neurogenesis is termined, in order to induce the onset of production of glial cells. Mad interacting protein 1 (Sip1) transcription factor slows down astroblasts proliferation, probably via Fgf9 inhibition (Seuntjens et al., 2009).

1.2 Glioblastoma Multiforme

1.2.1 Generalities

Glioblastoma multiforme (GBM) is the one of the deadliest human cancers and the most common primary brain tumors' subtype. Glioma tumors are aggressive and highly invasive central nervous system tumors. GBM is characterized as a glioma subtype, among other different gliomas, with diverse origin and features typified up to now. Gliomas are pathologically defined as tumors displaying histological and immunohistochemical evidence of glial differentiation. According to the World Health Organization (WHO) classification gliomas are characterised and graded. Firstly, they are distinguished on their hypothesized line of differentiation, which can be astrocytic, oligodendroglial or ependymal one. Then, they are graded on a malignancy scale of I to IV. Grade I tumors are benign and can be surgically removed if accessible for the resection. Grade II tumors are low-grade malignant and are not surgically curable. Grade III tumors are malignant, leading to death within few years; grade IV tumors are highly malignant and lethal within 9-12 months on average. Gliomas do not often metastasize outside the CNS, thus, tumor grade characterization is the main determinant of the patient's clinical outcome.

The common gliomas which affect the cerebral hemispheres of adult brains are also called diffuse gliomas because of their highly infiltrative nature. Infiltration is the main feature of malignancy. A highly infiltrative tumor renders surgical resection technically demanding and mostly ineffective. As anticipated above, diffuse gliomas are classified histologically as astrocytomas, oligodendrogliomas, or tumors with miscellaneous morphological features, such as oligoastrocytomas. To go further in detail, WHO classification distinguishes astrocytic tumors as pilocytic astrocytoma, grade I; astrocytoma, grade II; anaplaestic astrocytoma, grade III; finally glioblastoma multiforme (GBM), grade IV. GBM is the most malignant, it accounts for approximately 12-15% of all brain tumors, and in particular 60-70% of astrocytic tumors. GBM patients mean survival may go up to 18 months if tumor is treated by surgical resection, combined with radiotherapy and chemotherapy, unfortunately the mean survival time is less in the vast majority of cases.

GBM presents histological features of high malignancy, such as high cellularity, cellular pleiomorphism, rapid proliferation, microvascular proliferation, diffused

invasion and necrosis. These characteristics are the main criterion for the diagnosis of GBM (Steck et al., 1997).

GBM incidence increases with age. In fact, primary GBM tumors affect 62-years people on average while they are very rare in children. GBM occurs both in men and women, although primary GBM occurs more in men and secondary GBM more in women (Schwartzbaum et al., 2006).

1.2.2 Clonal origin

There are two GBM subtypes: primary and secondary GBM. Primary GBM occurs de novo, mainly in older patients, usually with no prior clinical evidence. Secondary GBM affect younger patients and has got a distinct clinical history. It is initially present as a low-grade astrocytoma, which subsequently transforms into GBM within 5-10 year as a recurrency, regardless of treatments received. Primary and secondary GBM subtypes show different frequency of specific genetic mutations associated with GBM. On the basis of the diverse frequencies of the associated genetic mutation, they have been proposed to represent two different clinical entities, developing along diverse pathways of origin. However, they behave in a clinical indistinguishable fashion and the median survival upon their establishment is mostly the same, as well as resistance to all the therapies.

In general, the origin of GBM is still not well understood. The presence of different glioma variants depending on diverse histological hallmarks, such as astrocytic, oligodendrocytic or mesenchymal, suggest that independent transformation events may occur in various terminally differentiated cells. More likely, the malignant transformation may occur in a progenitor cell, that is able to differentiate in different cell types.

Additionally, adult neural stem cells or early glial progenitors could initiate gliomagenesis. Although such cells are localized in precise areas of the brain, which are not often affected by GBM, they display both proliferative and migratory potentials, so that they could transform into tumor anywhere in the brain. Also, a tumor-associated mutation may activate the migratory property of these cells, as it has been shown in embryogenesis or in response to exogenous EGF stimulus in adult mice (Craig et al., 1996; Fricker-Gates et al., 2000).

Another possible source of GBM could be the mature astrocytes which dedifferentiate in response to a genetic mutation. There are already cells in the adult brain that are able to dedifferentiate in response to specific stimuli. Mature astrocytes are able to dedifferentiate into an earlier radial glia-like phenotype and acquire proliferative and migratory abilities. This could be the basis of gliomagenesis.

1.2.3 Standard therapy

The current standard of care for GBM tumor is based on a combined approach. A surgical resection of the mass, if feasible, is performed first. This might lead to a rapid improvement of the neurological symptoms and, in turn, dictate the possibility to intervene with the subsequent therapy options. These are needed in order to improve survival. A combination of radiotherapy and chemotherapy follows. In particular, chemotherapy for GBM involves alkylating agents, such as Temozolomide (TMZ). Its therapeutic benefit depends on its capability to alkylate/methylate DNA, mostly at the N-7 or O-6 position of guanine residues. In this way, TMZ damages DNA and triggers tumor cell death. However, some GBMs are able to repair this kind of DNA damage, thanks to the expression of O-6-methylguanine-DNA methyltransferase (MGMT) gene (Jacinto and Esteller, 2007). These cells become resistant to TMZ therapy. Conversely, in some tumors epigenetic silencing of the MGMT gene inhibits the synthesis of this enzyme and facilitate the sensitiveness to the therapy. This is why TMZ is effective for treating patients positive to methylated promoter of MGMT. The presence of MGMT protein in brain tumors, instead, predict poor response to TMZ (Hegi et al., 2009).

Although the standard of therapy for GBM has evolved into multimodal approaches, several patients still suffer the tumor progression due to the high infiltration of malignant cells into the brain tissues. Moreover, given the high heterogeneity of GBM, new therapies are aimed at finding specific personalized treatments.

1.2.4 Heterogeneity of molecular mechanisms undelying GBM

Glioblastoma multiforme is a highly heterogeneous tumor. It was the first cancer to be systematically studied by the Cancer Genome Atlas Research Network (TCGA). From the first genomic and transcriptomic analysis of two hundreds GBMs

already showed that a systematic analysis in a huge cohort of samples can help to distinguish the core biological pathways, relevant to tumor malignancy.

The first three core pathways reported in the initial TCGA publication were p53, Rb and receptor tyrosine kinase (RTK)/Ras/Phosphoinositide 3-kinase (PI3K) signaling (TCGA 2008). It was then showed that different combination of such alterations were found in different molecular subtypes of glioblastoma, resulting in high interpersonal variability. This may influence clinical outcome and specific individual response to therapy (Noushmehr 2010, Verhaak 2010). It is now clear that GBM growth and adaptation to targeted molecular treatments are driven by a signaling network with functional redundancy. Therefore, a deep comprehension of molecular alterations becomes more and more important to understand GBM pathogenesis, to infer tumor biology and finally to develop effective therapies. A wider variety of somatic genomic alterations have been described in recent years and a complex landscape was provided (Brennan et al., 2013) (*Fig. I.17*).

Among molecular mechanisms underlying it, there are pathways involved in the regulation of cell cycle, apoptosis, cell growth and survival, migration. Understanding the function of such mechanisms in normal brain development helps the investigation of how dysregulation may drive gliomagenesis. Here, the major genetic alterations associated with GBM and their relative pathways will be explained.

- **Growth factors pathways**

PDGF ligand and EGF receptor have been found prominently overexpressed in low-grade gliomas and in GBMs, respectively. This suggests they could have a possible role in gliomagenesis. Receptor tyrosine kinases act through several effector arms, such as Ras/MAP K (MAP kinase), PI3-K (phosphoinositide 3-kinase), PLC-γ (Phospholipase C), and JAK-STAT, in order to regulate cell proliferation, cell scatter and migration and cytokine stimulation.

PDGF is one of the main regulators of oligodendrocyte development. During embryogenesis, it is expressed by neurons and astrocytes, whereas its receptor (PDGFR-α) is restricted to glial progenitors and neurons (Yeh et al., 1993). After birth, PDGFR-α is down-regulated as glial progenitors differentiate into oligodendrocytes. Consistently, in the adult brain, PDGFR-α expression is high in the

ventricular and sub ventricular zone of the lateral ventricles, mainly restricted to neural stem cells, while PDGF is largely expressed by neurons and astrocytes (Oumesmar et al., 1997). Intriguingly, PDGFR-α positive cells show a morphology and immunohistochemistry typical of glial progenitors. A subpopulation of these cells also express NG2 (An integral membrane chondroitin sulfate proteoglycan) and are partiularly dynamic cells, able to respond to changes in environment. For instance, they can proliferate in response to stimuli such as demyelination and inflammation.

Tumors often overexpress both PDGF ligands and receptors, so establishing a stimulatory loop. Interestingly, robust expression of PDGF and PDGFR-α is often associated with p53 mutations in low grade gliomas (Hermanson et al., 1996). Given this link, it was suggested that the proliferative stimulus by PDGF signaling could promote the reentry into cell cycle, which cannot be antagonized by p53, as it is mutated. However, even if in combination with bFGF PDGF promote proliferation of glial progenitors in vitro (McKinnon et al., 1990), overexpression of PDGF is associated with low proliferative rate in low grade gliomas in vivo. Therefore, it was suggested that PDGF signaling may exert its role through pathway different from Ras/MAPK. For instance, it is possible for PDGF to induce in tumor cell migration through activation of PI3-K and PLC-γ.

EGFR gene amplification has been found in the majority of high grade astrocytomas (in 57.4% of GBM studied in (Brennan et al., 2013)). This is why EGFR activation is thought to be one of the main responsible of malignant transformation process towards GBM. EGFR is critical to regulate astrocyte and oligodendrocyte development too. As explained before, EGFR is crucial to sustain proliferation and survival of the neural stem cell compartment. This role in normal development provides a clue of its role in GBM. High levels of Ras-GTP effector have been found in high grade astrocytoma (Guha et al., 1997), thus suggesting that it can be activated by RTK activation driven by EGFR signaling. Approximately 40% of GBM with EGFR amplification also commonly express a variant form called EGFRvIII or del2-7EGFR, where genomic deletions eliminate exons 2-7 in the EGFR mRNA. This mutation results in a truncated EGFR, which does not have the extracellular ligand-binding domain and is constitutively activated, never down-regulated. This of course enhances tumorigenic properties of cells, by increasing proliferation and reducing apoptosis (Nagane et al., 1996; Nishikawa et al., 1994).

- **The p53 pathway**

The p53 pathway is the most commonly mutated pathway in tumorigenesis in general. The well-known tumor suppressor p53 is in charge to respond to DNA damage and numerous genotoxic and cytotoxic events by inducing cell cycle arrest and apoptosis. Also, it is an important transcription factor regulating thousands of genes, most of which involved in tumorigenesis and tumor invasion.

Allelic loss of chromosome 17p and p53 mutations are equally frequent in low-grade gliomas, anaplastic astrocytomas and secondary glioblastomas (Louis, 1994). This suggests that p53 inefficacy might be an early event in gliomagenesis. It seems it has got a prominent role in the development of secondary GBMs. Nevertheless, less frequent mutations are also found in primary GBMs, possibly as a secondary event due to genomic instability (Ohgaki and Kleihues, 2007; Ohgaki et al., 2004; St Louis et al., 1999). The fact that brain radiation during childhood is a risk factor for the onset of gliomas (Neglia et al., 1991) is possibly provoked by the deactivation of p53-dependent DNA damage checkpoint response, in order to allow cell survival following irradiation. In addition to increase proliferation, the p53 loss can induce the accumulation of other genetic mutations that then result in the secondary GBMs.

One of the most important modulators of p53 is the downstream gene target, *MDM2,* which has been found amplified in about 10 % of GBMs. MDM2 binds to p53 N-terminal transactivation domain and inhibits p53 transcriptional activity. Moreover, it serves as E3 ubiquitin ligase, thus orchestrating ubiquitination and proteosomal degradation of p53 (Huang et al., 1999; Kubbutat et al., 1997; Momand et al., 1992). MDM2 transcription is induced by p53 itself, so establishing a negative feedback loop. Interestingly MDM2 amplification has been exclusively found in tumors that did not display p53 mutations, suggesting that MDM2 overexertion could represent an alternative way to knock-down p53 pathway (Reifenberger et al., 1996).

ARF (p14ARF) is an upstream regulator of the p53 pathway. It directly inhibits MDM2 E3 ubiquitin ligase activity (Kamijo et al., 1998; Zhang et al., 2008). Inactivation or mutation of ARF have been found in both low grade and high grade gliomas. Together with INK4a (p16INK4a), an important regulator of pRB pathway, ARF is encoded by CDK2A locus. Deletion of such locus are frequent in GBMs. Moreover, co-deletion of ARF and INK4a promote the transformation from low- to

high-grade gliomas (Labuhn et al., 2001). This suggest this deletion could represent a key event in gliomagenesis.

- **The Rb pathway**

The tumor suppressor retinoblastoma (RB) is a crucial inhibitor of cell cycle progression, via direct inhibition of trascription factors of the E2F family. Loss of RB gene has been shown in GBM (Tortosa et al., 2000). Normally, during G1 phase, pRB is inactivated by Cyclin D/CDK4/CDK6- induced phosphorylation. When pRB needs to stay active, CDKN2B inhibits CDKs activation, thus preventing cell growth and cell cycle progression. CDKN2B is commonly inactivated in GBMs, while CDK4,6 are amplified (Lam et al., 2000) (*Fig. I.16*). This all results in a depletion of RB signaling and an augmented uncontrolled proliferation of GBM cells.

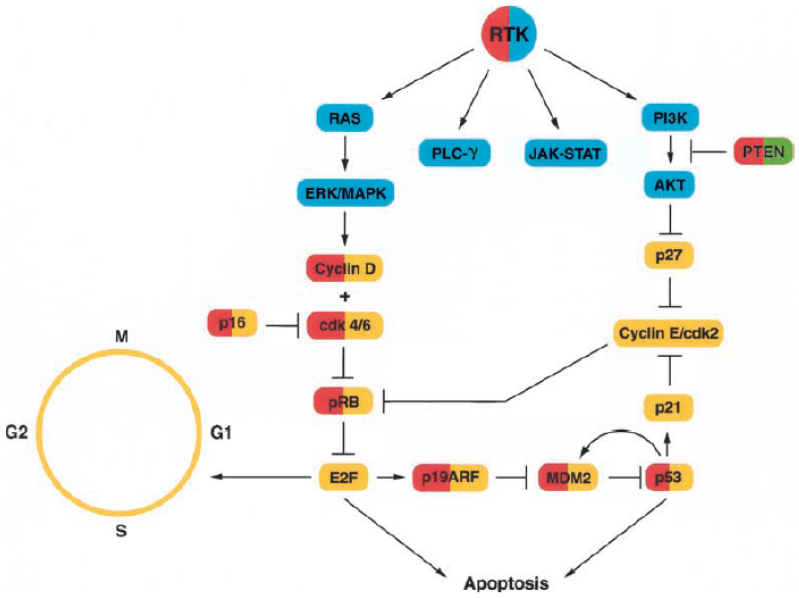

Figure I.16. Integration between RTK pathways and the cell cycle. *(Adapted from* (Maher et al., 2001)*)*

- **Chromosome 10q tumor suppressors (PTEN, Mxi1, DMBT1)**

Loss of heterozygosity on chromosome 10 is commonly found in high-grade gliomas. PTEN (phosphatase and tensin homology) is a tumor suppressor gene located on such chromosome. Mutations in PTEN gene locus have been identified in a wide variety of tumors, including both primary and secondary GBMs. PTEN negatively regulates PI3K/AKT/PKB pathway by inhibiting Akt signaling via

reduction of intracellular levels of phosphatidylinositol-3,4,5-triphosphate (Stambolic et al., 1998). Normally Akt activates the downstream effector mTOR, composed by mTORC1 and mTORC2, which integrates several upstream signals and regulate cell growth and division. Conversely, PI3K/AKT/mTOR pathway is stimulated by growth factors and their receptors, such as EGFR and PDGFR.

Thus, mutation or deletions of PTEN and amplification of EGFR/PDGFR result in over activation of PI3K signaling in GBM, which may clearly play an important role in glioma development and malignancy.

Summarizing the landscape of somatic alterations in GBM

So far, the palette of somatic alterations affecting major cancer pathways in GBM has been extended, thanks to the whole-exome and transcriptional sequencing data.

In particular, *Fig. I.17* and *Fig. I.18* (Adapted from (Brennan et al., 2013)), sum up the main alterations found in GBM patients, such as alterations in the PI3K/MAPK, p53 and Rb regulatory pathways.

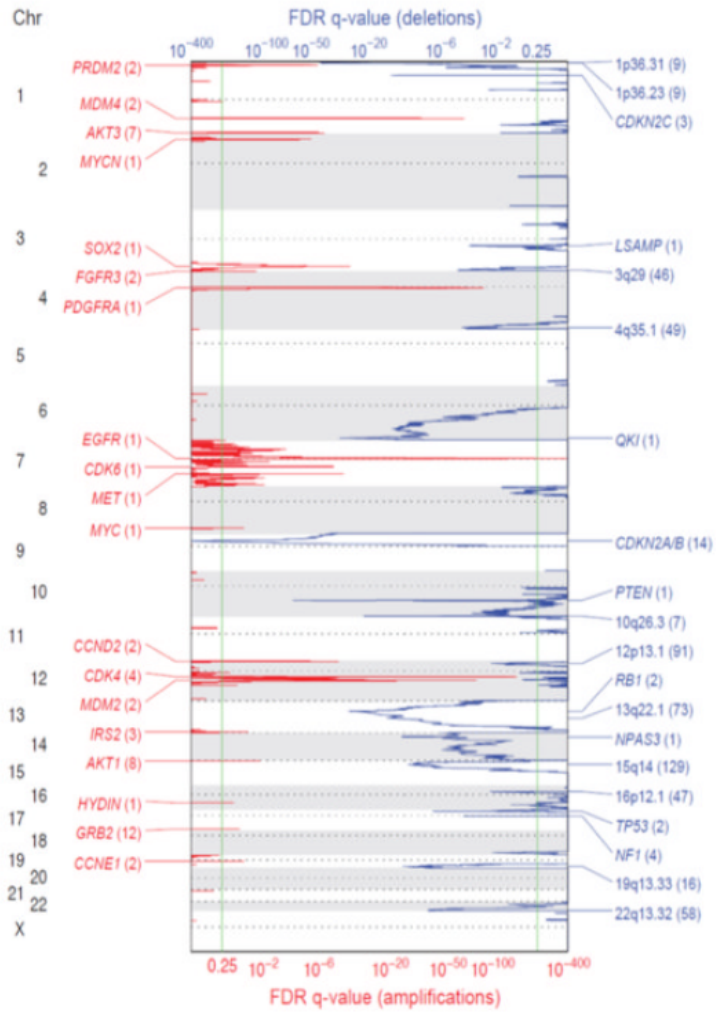

Figure I.17. Recurrent sites of DNA copy number aberration. *(Adapted from* (Brennan et al., 2013)*)*

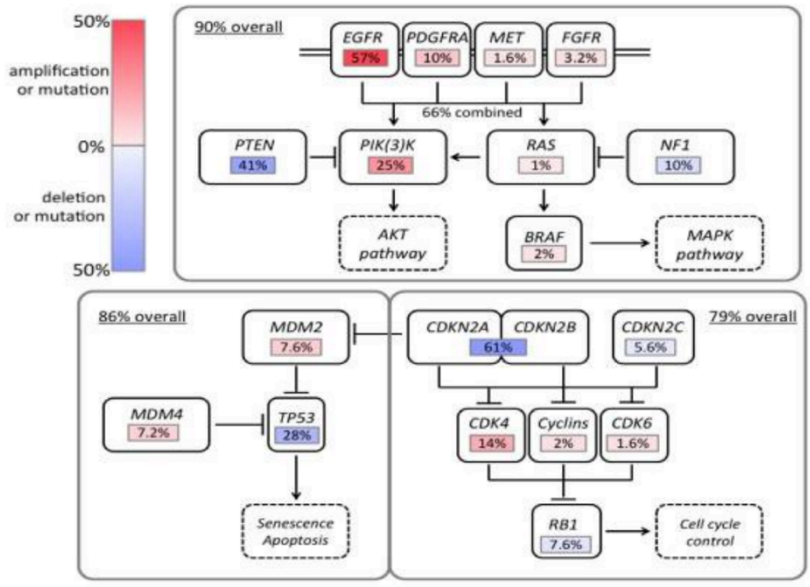

Figure I.18. Summary of overall alteration rate for canonical PI3K/MAPK, p53 and Rb regulatory pathways. *(Adapted from* (Brennan et al., 2013)*)*

1.3 *Emx2* gene

1.3.1 *Emx2* phylogenesis and structure

Emx2 is an homeobox regulatory gene encoding for a transcription factor. It shares an evolutionary common origin with the Drosophila melanogaster *empty spiracles (ems)*, showing 82% of homology in its homeobox domain. *Ems* regulates the formation of pre-antennal, antennal and intercalary segments of the embryo (Cohen and Jürgens, 1990; Dalton et al., 1989).

Emx2 is expressed early in the cerebral cortex. Indeed, it is activated in the mouse embryonic central nervous system at around E8.0-E8.5 (Gulisano et al., 1996). From this stage, it becomes more and more expressed in anterior dorsal neuroectodermal regions of the embryo. At E9.5, its expression domain includes the overlapping region of expression of *Emx1* (anterior boundary) and part of presumptive diencephalon. At this stage, *Emx2* mRNA is found also in the olfactory placodes and the coelomic epithelium which will generate the urogenital system..
From E10 *Emx2* expression is confined to the neuroepithelium while is absent in most postmitotic neurons of the transitional field and cortical plate (Gulisano et al., 1996). At E12.5 *Emx2* mRNA becomes restricted to the ventricular zone (*vz*), following a posterior/medial^{high}-anterior/lateral^{low} gradient. This pattern of expression becomes more pronounced from E14.5 onwards ((Gulisano et al., 1996; Simeone et al., 1992)). Furthermore, the distribution of the Emx2 protein displays the same anterior-posterior and medio-lateral gradient. Until E17.0, *Emx2* domain of expression remains confined to the proliferative layers of the cortex plus the pioneer neurons of Cajal-Retzius (Mallamaci et al., 1998).

The peculiar pattern of expression of *Emx2* mRNA and protein strongly suggested a role in cortical polarity, cell identity and patterning in the initial phases of arealization of cerebral cortex. Also, the presence of Emx2 in the proliferative layers pointed out a suitable role in the regulation of proliferation, as well as in the migration of cortical neuroblasts to their final destination in the mature cortex (McConnell, 1995). Finally, as *Emx2* mRNA is prevalently present in neuroepithelium, where neuroblasts divide giving rise to all the populations of the later mature cortex, *Emx2* was hypothesized to play an important role in fate decision. Consistently with

these predictions, *Emx2*$^{-/-}$ mutant mice display deep damages in central nervous system. The cerebral hemispheres, olfactory bulbs and hippocampus are roughly shrunken and the dentate gyrus is absent (Pellegrini et al., 1996; Yoshida et al., 1997). These brains also show disruption of migration, differentiation and innervation in specific neuronal populations (Mallamaci et al., 2000a, 2000b; Muzio and Mallamaci, 2005). The importance of *Emx2* is confirmed by the fact that *Emx2* $^{-/-}$ mutant die soon after birth because of the absence of urogenital system. Apart from CNS damages, they suffer specific skeletal defects, including the absence of scapulae and ilia (Pellegrini et al., 2001).

In the mouse, *Emx2* is located on chromosome 19. Its mRNA includes three exons, is 2598 bp long and encodes for a homeodomain transcription factor of 253 aminoacids. Interestingly, a transcript encoded by *Emx2* opposite strand was found both in human and in mouse. This antisense transcript overlaps with the *Emx2* mRNA gene head-to-head and has been called *Emx2*OS (Noonan et al., 2003). It has been demonstrated (Spigoni et al., 2010) that this non-coding RNA is involved in the regulation of *Emx2* pattern of expression. In fact, the two transcripts are both expressed in periventricular neural precurors of the cortical primordium, but show a mutually exclusive pattern in post-mitotic progenies of these precursors (Mallamaci et al., 1998; Simeone et al., 1992). While *Emx2*OS-ncRNA is expressed in newborn neurons belonging to the cortical plate, *Emx2* is highly expressed in Cajal-Retzius neurons residing within the marginal zone (Mallamaci et al., 1998). This mutual distribution proposes a possible negative cross-regulation between the two. Remarkably, *Emx2* antisense transcript seems to have a role in the shutting down of the expression of *Emx2* in the post-mitotic cells of the cortical plate (Spigoni et al., 2010).

1.3.2 *Emx2* role in R/C and D/V neural specification

Emx2 is primarily involved in large scale patterning of the rostral CNS, along the rostro-caudal and the dorso-ventral axis. Furthermore, it contributes to regulation of different aspects of cortico-cerebral development.

As for rostrocaudal specification of CNS, *Emx2* is firstly expressed in the territory rostral to the *zona limitans intratalamica* (ZLI) and contributes to its specification as telencephalic prethalamic field, in combination with *Otx2* and *Pax6*.

Relevant rostrocaudal patterning errors occurs indeed in Emx2$^{-/-}$, Otx2$^{-/+}$ mutants, where there is a shrinkage of the anterior prosencephalon and an enlargement of the tectum and the rombencephalon (Kimura et al., 2005). Emx2$^{-/-}$ Pax6$^{-/-}$ mouse embryos conversely show a duplication of the tectum and the collapse of prosomers anterior to the zona limitans intra-thalamica (ZLI) after E10.5 (Kimura et al., 2005).

As for dorso-ventral patterning, Emx2 cooperates with Pax6 in specifying the dorsal telencephalon as pallium. When both *Emx2* or *Pax6* are not present, the whole cortical development is disrupted and the cortex evolves to a striatum-like structure (Muzio et al., 2002). Later, at E14.5, the striatum itself of these Emx2/Pax6 double mutants further acquires features peculiar to the globus pallidus (Muzio et al., 2002).

1.3.3 *Emx2* roles in neural precursors kinetics: early and late activity

Emx2 controls proliferation and migration of cortical neuroblasts, it establishes cell role and identity within the proliferative layers and it maintains a position-dependent signal within the developing cortex. However, the influence of this transcription factor on cortical precursor kinetics and histogenesis is amazingly complex.

In early, neural precursors, it promotes cell cycle progression and it inhibits premature neuronal differentiation (Muzio et al., 2005). In this respect, *Emx2*$^{-/-}$ mutants show an elongation in neuroblasts cycling time due to lengthening of DNA synthesis phase. In addition, cortical progenitors leave cell cycle more frequently. These phenomena are associated with an increase in pro-neural/anti-neural gene expression ratio, a downregulation of the lateral inhibition machinery and a depression of the canonical Wnt signalling (Muzio et al., 2005). All these phenomena are more pronounced in the caudomedial than in rostral pallium.

On the contrary, in more advanced neural stem cells, Emx2 expression leads to the stop of proliferation and the decision to undergo neuronal differentiation (Galli et al., 2002; Gangemi et al., 2006).

Brancaccio et al (Brancaccio et al., 2010) confirmed the bimodal impact of Emx2 on NSC proliferation/differentiation kinetics. Moreover, they reported some new roles for this transcription factor. As shown by these authors, Emx2 promotes the transition from NSCs to early bipotent glial progenitors, inhibits further

expansion of these progenitors and ultimately decrease their final astroglial output. Moreover, it protects NPs from cell death and accelerates their neuronal differentiation (Brancaccio et al., 2010).

1.3.4 *Emx2* role in cortical regionalization, arealization and neocortical lamination

Emx2 is expressed early in the cortical primary proliferative layers, following a caudomedial^{high}-rostrolateral^{low} gradient. Thus it is more expressed in presumptive V1 area and less in presumptive frontal/motor areas. As such, it has a prominent role in cortical regionalization and arealization, as an inducer of caudomedial fates (Bishop et al., 2000; Gulisano et al., 1996; Mallamaci et al., 2000a; O'Leary, 1989; Simeone et al., 1992). In absence of Emx2, the neo/paleocortex is enlarged whereas the archicortical areas are strongly reduced: the dentate gyrus disappears and the hippocampus is shrunken. Along the antero-posterior axis the caudomedial areas (such as V1) are almost completely shrunken in favour of the rostrolateral ones, which are enlarged (Mallamaci et al., 2000a) . Opposite distorsions of the areal profile are displayed by gain-of-function mutants (Hamasaki et al., 2004).

Furthermore, *Emx2*$^{-/-}$ mutants display an an abnormal radial migration of cortical plate neurons which is quite similar to that of *Reeler* mutant mice. Early cortical plate neurons do not infiltrate the preplate, which is not split in marginal zone and subplate and forms a structure called super-plate. On the other side, late born neurons do not follow the classical inside-out rules. All that likely emerges as a consequence of impaired generation/differentiation of pioneer layer I neurons in charge of orchestrating neocortical lamination In fact, these mutants, from E13.5 on *Reln*-mRNA expression is reduced until it completely disappears at E15.5 (Mallamaci et al., 2000a). This reflects the fact that Cajal-Retzius cells, normally originating from the cortical hem and populating cortex along a caudomedial^{high}-rostrolateral^{low} gradient, are almost absent in *Emx2*$^{-/-}$ in the caudomedial region, possibly due to a reduction of the corresponding neuronogenic pool.

1.3.5 *Emx2* extraneural expression

Apart from being expressed in CNS, Emx2 shows various patterns of expression which underlie its importance in multiple tissues. At E12.5 for instance it

is expressed in the developing olfactory epithelium, the kidneys and the gonads. Indeed, knocked-down mutants die soon after birth because they defects of development of the urogenital system.

Interestingly, in Emx2-/- mice the early stages of gonad development are disrupted, with a dramatic enlargement of the surface of epithelial cells hosting tight junctions and migration of the epithelial cells significantly affected (Kusaka et al., 2010).

Microarray analysis of the epithelial cells of the embryonic gonad displays a dramatic upregulation of EGFR in Emx2 KO mice. Based on previous demonstration of an Egfr involvement in regulation of tight junctions assembly, such ectopic expression of EGFR was strongly suggested to act as a link between Emx2 ablation and junctional anomalies of Emx2-LOF mutants.

1.4 *Foxg1* gene

1.4.1 *Foxg1* phylogenesis and structure

Forkhead box G1 (*Foxg1*), formerly known as brain factor-1 (Bf-1) is a regulatory gene of the forkhead family encoding for a winged-helix transcription factor (TF).

The Forkhead family is characterized by a conserved DNA-binding domain called the 'Forkhead box', or FOX. The name 'Forkhead' takes its origin from a study in Drosophila where a mutation in a paralog of this gene caused the formation of an ectopic head structure that resembles a fork. Sometimes the forkhead proteins can be referred to as 'winged helix' proteins because of the three α-helices flanked by two loops resembling butterfly wings, which have been revealed thanks to X-ray crystallography. Such family is composed by more than 100 different transcription factors, displaying the most disparate functions.

The human *FOXG1* gene is located on chromosome 14 in position 13 on the long (q) arm. Foxg1 protein usually acts as a transcriptional repressor either in a direct or indirect manner. It plays a central role in the developing telencephalon. Indeed, *Foxg1*, among many other cortico-cerebral patterning genes, is a crucial TF for many aspects of cerebral cortex development. It is involved in cerebral cortex morphogenesis, including early distinction between pallial and subpallial fields, in dorsoventral patterning of the pallium, cell cycle control, lineage fate choices induction, regulation of neocortical cell differentiation and migration, tuning of astrogenesis rates. Most of these roles are elucidated below.

Remarkably, a proper dosage allele of this gene seems to be crucial. Even subtle alterations in its expression can lead to defects in the brain development or pathological conditions such as Rett Syndrome or West Syndrome.

1.4.2 *Foxg1* in telencephalic patterning and cortical arealization

Starting from E7 in mice, the primitive node or organizer and the anterior visceral endoderm (AVE) send signals for neural induction and maintenance in order to organize the early rostro-caudal patterning (Thomas and Beddington, 1996). In particular, the AVE secretes molecules called cerberus and dickkopf, which antagonize the posteriorizing effect of molecules expressed by the neural plate, such

as Wnt, Fgfs family members and retinoic acid (RA) (Altmann and Brivanlou, 2001; Sasai and De Robertis, 1997). Then, after the anterior neural induction, the secondary organizer, the Anterior Neural Ridge (ANR), is in charge to promote telencephalic development. ANR triggers the expression of Foxg1 via Fgf8 secretion (Houart et al., 1998; Shimamura and Rubenstein, 1997). In fact, when ANR is ablated in mice, the expression of the telencephalic markers Foxg1 and Emx1 is prevented (Shimamura and Rubenstein, 1997).

Furthermore, Hedgehog signaling induces *Foxg1* expression (Danesin et al., 2009). Thus, the coordinated stimulation by Fgf8 from ANR and Shh from the prechordal plate, allow a graded Foxg1 expression:high ventral/anterior to low dorsal/posterior.

As for the dorso/ventral specification of telencephalon, there is a balance of Gli3 and Shh expression, which show dorsalizing and ventralizing effects, respectively (Grove et al., 1998; Kuschel et al., 2003). In this scenario, Foxg1 cooperates with Fgf as ventralizing signal, downstream to Shh, in order to generate ventral cell types (Rallu et al., 2002). This is confirmed by the evidence that in *Foxg1*$^{-/-}$ the formation of the subpallium is strongly impaired (Xuan et al., 1995). Telencephalon is completely lost in Foxg1/Gli3 double mutants, suggesting that these two factors are essential to generate and maintain telencephalic dorsal and ventral subdivision, respectively (Hanashima et al., 2007). Noticeably, Fgf signaling is also crucial for the generation of the ventral cell types (Gutin et al., 2006). In this respect, Foxg1 is required for Fgf8 expression from ANR (Martynoga et al., 2005) and conversely, Foxg1 expression is itself regulated by Fgf signaling forming a positive feedback loop ((Shimamura and Rubenstein, 1997; Storm et al., 2006)). Beside its key centralizing role, Foxg1 is also required to restrict dorsal fates by limiting Wnt expression. Indeed, Foxg1 represses Wnt8b transcription, by directly binding to its promoter (Danesin et al., 2009).

In summary, Foxg1 takes part to a complex network of signaling pathways: it promotes ventral identity downstream of Shh and concomitantly controls the extension of the dorsal territory via a direct Wnt ligands' repression.

Moreover, Foxg1 plays a key task in the process of cortical arealization: it has an extremely important function during the subdivision of the cerebral cortex in distinct

anatomical and functional areas. Patterning centres imimplicated in cortical arealization are listed below:

(1) rostrally, the commissural plate (CoP) secretes Fgfs (Fgf3,8,17 and 18);

(2) dorsocaudally, the cortical hem secretes the class of bone morphogenetic proteins (Bmp2,4,5,6,7) and Wnts (Wnt2b, 3a, 5a, tb 8b);

(3) lateroventrally, the cortical antihem secretes the Epidermal growth factor family members (Tgfα, Nrg1 and Nrg3), Fgf7, and the Wnt signaling inhibitor, Sfrp2.

As stated before, Foxg1 is expressed in progenitor cells along a caudo/medial(low) to rostro/lateral(high) gradient. In *Foxg1*$^{-/-}$ mutants, cortical field is abnormally specified as a hippocampal anlage and the neocortical as well as the paleocortical programs are fully aborted (Muzio et al., 2005). Furthermore, there is a dramatic excess of Cajal Retzius neurons production(Hanashima et al., 2004; Muzio et al., 2005).

1.4.3 *Foxg1* in neural precursors kinetics

Foxg1 is implicated in the intricate regulation of the balance between proliferation and differentiation of neural precursors. At this level, the control of cell cycle progression and governing is crucial. In fact, during the neurogenesis, cell cycle duration is progressively prolonged, thanks to the lengthening of the G1 phase. In addition, an increasing number of cells exit from cell cycle (Takahashi et al., 1995) and cells start undergoing asymmetrical differentiate divisions, instead of self-renewing symmetrical ones (Calegari and Huttner, 2003; Götz and Huttner, 2005). These processes are finely regulated by Cdk-Cyclin complex inhibitors of the Kip/Cip family, as shown in Fig. I.19.

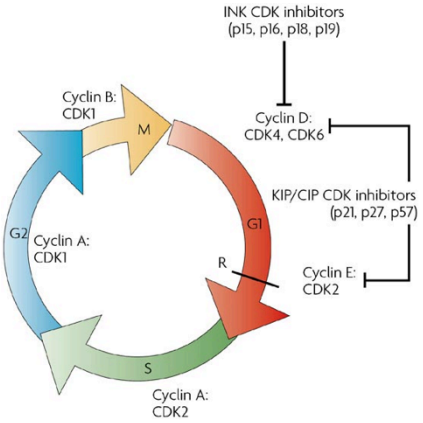

Figure I.19. Structure and regulation of the cell cycle. (*Adapted from* (Dehay and Kennedy, 2007))

Foxg1 mantains a telencephalic progenitor status and ensures that such progenitors maintain appropriate cell cycle kinetics. *Foxg1* expression is high in the proliferating cells of the neuroepithelium during neocortical development, while it declines in the postmitotic cells. *Foxg1*$^{-/-}$ mice show a reduced hemispheres size and a severely affected ventral telencephalic development. Overall, they exhibit reduced proliferation and increased differentiation (Hanashima et al., 2002; Martynoga et al., 2005; Xuan et al., 1995).

Foxg1 pro-proliferative activity depends on its capability to bind and inhibit the FoxO-Smad transcriptional complex, and in thus to obstruct p21 (Cip1) induction by Tgfb. In this way, p21 cannot mediate the cell cycle arrest at G1 phase (Dou et al., 1999; Seoane et al., 2004).

Furthermore, *Foxg1* acts together with Polycomb factor Bmi-1, repressor of the cell cycle inhibitors p16, p19 and p21. Bmi-1 overexpression in turn upregulates *Foxg1*, which is crucial to mediate promotion of neural progenitor cells self-renewal (Fasano et al., 2009).

Finally, *Foxg1* overexpression in neural stem cells induces the expansion of their compartment, perhaps by increasing NSCs self-renewal, promoting progenitor survival and delaying neurogenesis (Brancaccio et al., 2010).

1.4.4 *Foxg1* in neuronal differentiation and migration

Early during development, pyramidal neurons are born within the proliferative layers of the cerebral cortex and then migrate to their appropriate laminar position. This is performed thanks to both radial (through radial glial fibers) and tangential migration (Götz and Huttner, 2005). When pyramidal neuron precursors lie within the intermediate zone, they transiently acquire a multipolar morphology, then they detach from the radial glia and initiate axonal outgrowth, before entering the cortical plate ((Barnes et al., 2007; Noctor et al., 2004)). During these migratory phases, Foxg1 is expressed in a dynamic fashion. It is transiently down regulated in nascent pyramidal neuron precursors, allowing NeuroD1 and Unc5d expression, critical for the transition to the late multipolar phase. Subsequently, Foxg1 is specifically unregulated in order to induce the cells' exit from the multipolar phase and ingress into the cortical plate.

Foxg1 is also crucial for the proper lamination of cortical progenitor cells. The process of neocortico-genesis needs the early specification of Cajal-Retziuspioneer neurons, then the subsequent differentiation of deep layer neurons first and upper layer neurons after, as shown in figure *(Fig. I.20*).

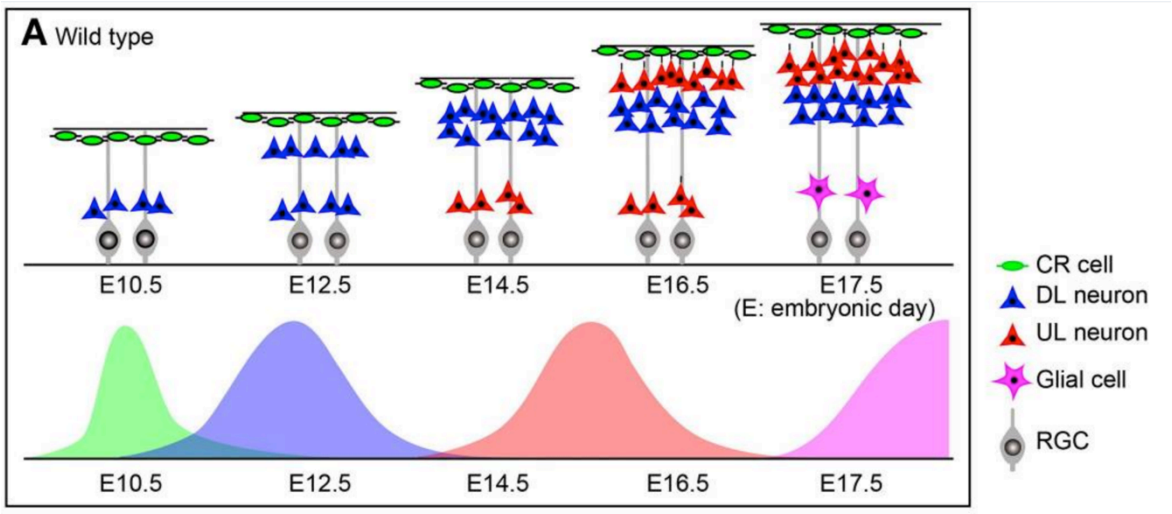

Figure I.20. Mechanisms of neuronal subtype transitions and integration in the cerebral cortex. *(Adapted from* (Toma et al., 2014)*)*

First, *Foxg1* and *Lhx2* instruct the cessation of the Cajal-Retzius cells' production, thus inducing progenitors to give rise to deep layer neurons (Hanashima et al., 2007; Kumamoto et al., 2013). As stated before, *Foxg1* is induced by Fgf8 expressed in the anterior neural ridge (Shimamura and Rubenstein, 1997) and subsequently expands caudally. Therefore, the onset of *Foxg1* expression represses several transcription factors in an opposing rostral-to-caudal gradient and regulates the transition from CR cell to DL neuron identity in a spatio-temporaldependent manner (Kumamoto et al., 2013).

Moreover, Foxg1 is responsible for *Tbr1* repression, which preceeds the onset of *Ctip2* and *Fezf2*, which mostly regulate deep layer specification. This suggest that *Tbr1* repression by *Foxg1* regulate the correct sequence of deep layer and upper layer neurons generation, by establishing the initial bias to deep layer identity (Toma et al., 2014).

Intriguingly, Foxg1 is present in both the nucleus and the cytoplasm: it is predominantly confined in the nucleus in areas of active neurogenesis, while it is translocated to the cytoplasm in early neuronal differentiation areas (Seoane et al., 2004). Recently, a Foxg1 fraction localized in mitochondria has been illustrated, suggesting a possible mechanisms for mitochondria in neuronal differentiation (Pancrazi et al., 2015).

Foxg1 is still expressed in post-mitotic neurons, suggesting that it could have an essential role in that compartment too.

1.4.5 *Foxg1* in astrogenesis control

In vitro studies by Brancaccio et al. (Brancaccio et al., 2010), showed that overexertion of FOxg1 in neural stem cells (NSCs) enlarged this compartment and reduced their astroglial output. Results of this study led to hypothesize that this phenotype might stem from defective defective commitment of neural stem cells to glial fates. In vertebrates, there is no evidence for *Foxg1* anti-gliogenic activity. However, two Drosophila *Foxg1* orthologs, Sloppy paired-1 and -2 (*Slp1* and *Slp2*), have been shown to promote neurogenesis at the expenses of gliogenesis (Bhat et al., 2000) and Foxg1 is able to rescue *Slp1&2-null* phenotype (Mondal et al., 2007).

2. AIM OF THE WORK

Aim of my study was to investigate the role of *Foxg1* and *Emx2* in the regulation of corticocerebral astrogenesis. In detail, I studied the involvement of *Foxg1* and *Emx2* in the early commitment of cortical precursor cells towards glial fates and in the proper astroblasts proliferation, respectively.

Furthermore, I investigated whether the modulation of *Emx2* expression levels could be exploited for therapeutical applications, in particular in the suppression of glioblastoma tumors.

3. MATERIALS AND METHODS

3.1 Lentiviral Vectors Packaging and Titration

Third generation self-inactivating (SIN) lentiviral vectors (LVs) were generated as previously described (Follenzi and Naldini, 2002) with some adjustments. In brief, HEK293T cells were co-transfected with the transfer vector plasmid plus three auxiliary plasmids (pMD2 VSV.G;
pMDLg/pRRE; pRSV-REV), in the presence of LipoD293TM (SigmaGen). The conditioned medium was collected after 24 and 48 hours, filtered and ultracentrifuged at 50000 RCF on a fixed angle rotor (JA25.50 Beckmann Coulter) for 150 min at 4°C. Lentiviral pellets were then resuspended in PBS 1X without BSA (Gibco).

LVs were titrated by Real Time quantitative PCR after infection of HEK293T cells, as previously reported (Sastry et al., 2002). One end point fluorescence titrated LV was included in each PCR titration session and PCR-titers were adjusted to fluorescence-equivalent titers throughout the study.

Where necessary, specific lentiviral plasmids were constructed with basic cloning techniques. DNA manipulations (extraction, purification and ligation), bacterial cultures and transformations were performed according to standard methods. Restriction and modification enzymes were obtained from New England Biolabs and Promega; DNA fragments were purified from agarose gel by QIAquick Gel Extraction Kit (Qiagen); plasmid preparations were done by DN PLASMID PURIFICATION KIT (Qiagen). Plasmids were grown in E. Coli, Xl1-blue or ElectroMAX™ Stbl4™ Competent Cells (Invitrogen).

LVs used for this study were referred to throughout the thesis according to the standard nomenclature: LV:pX-GOI, where pX is the promoter and GOI is the gene of interest.

They were:
LV_pPgk1-rtTA2S-M2-WPRE (Spigoni et al., 2010),
LV_Pgk1p-tTA-WPRE, obtained by transferring the BamHI/XhoI-cut tTA-cds fragment from LV:pTYF-1xSYN-tTA (Addgene #19980) [12] into the BamHI/SalI-cut LV_pPgk1-EGFP-WPRE, in place of EGFP.

LV_Nesp-rtTA-M2-WPRE, aka pNes/hsp68- rtTA2S-M2 (Brancaccio et al., 2010).
LV_Tre-Foxg1-EGFP (Brancaccio et al., 2010),
LV_TREt-Foxg1 (Raciti et al., 2013)
LV_TREt-Emx2-IRES2-EGFP (Brancaccio et al., 2010);
LV_TREt-*Emx2*-WPRE, aka LV:TREt-Emx2 [Furuta 1997];
LV:pTa1-mCherry (Brancaccio et al., 2010);
LV_Pgk1p-EGFP-WPRE, aka pCCLsin.PPT. hPGK.EGFP.Wpre [11];
LV_Pgk1p-mCherry-WPRE, constructed by transferring the mCherry module form LV_pTa1- mCherry [3] into LV_pPgk1-EGFP-WPRE (see below), in place of EGFP;
LV_TREt-IRES2-EGFP (derived from LV:TREt-luc- IRES2-EGFP, via deletion of the luc and the IRES2-EGFP cassettes,respectively);
LV_pCCLsin.PPT.hPGK.EGFR.pre (Mazzoleni et al., 2010);
LV_TREt-Sox2, aka TetO-FUW-sox2 (Brambrink et al., 2008), corresponding to plasmid #20326 of the Addgene collection;
LV_TREt-Brn2 aka Tet-O-FUW-Brn2 (Vierbuchen et al., 2010), corresponding to plasmid #27151 of the Addgene collection.
LV_TREt-IRES-PLAP-WPRE, obtained by replacing the XhoI/SalI fragment of LV_Pgk1p- EGFP-WPRE (see below) by an XhoI-compatible/ SalI-compatible element, including the XbaI-AgeI 0.35kb TREt fragment of P199 [4] and the EcoRI/ SalI 2.2kb IRES-PLAP fragment from pCLE [5];
LV_Pgk1p-FLAG-Hes6-BlaR [9];
LV_CMVp-FLAG-Eif4E (Addgene #38239) [10];
LV_pLenti6V5D(TOPO) [9];
LV_U6p-ctr-shRNA, obtained by cleaving the NotI-EcoRI fragment from LV_ctr-shRNA-EGFP, aka pll3.7 (Addgene #11795).
LV_U6p-antiFoxg1-shRNA (Sigma # SHCLND-NM_008241)
LV_U6p-antiTab2-shRNA, obtained by cloning oligonucleotides targeting Tab2 into the HpaI/XhoI sites of pll3.7 (Addgene #11795) (gift of Corfas Lab);

All lentiviruses were generated and titrated as previously described (Brancaccioet al., 2010).

3.2 Animal handling and embryo dissection

Animal handling and subsequent procedures were done according to European laws [European Communities Council Directive of November 24, 1986 (86/609/EEC)] and with National Institutes of Health guidelines. Wild type mice (strain CD1, purchased from Harlan-Italy), Emx2+/-mutants (Pellegrini et al., 1996) moved to a CD1 background, *Foxg1*$^{+/-}$ mutants (Hébert and McConnell, 2000), were maintained at the SISSA animal house facility. All embryos and pups were staged by timed breeding and vaginal plug inspection. Were necessary, embryos were genotyped by PCR, as previously described (Brancaccio et al., 2010). Pregnant females were killed by cervical dislocation. Embryonic cortices were dissected out in cold PBS, under sterile conditions.

3.3 Cortico-cerebral primary cultures

Cortical primordium was dissected from E12.5 or E14.5 mouse embryos and mechanically dissociated to single cells by gentle pipetting. The number of dissociated cells was quantified in a Burker chamber and neural precursors were then plated in 24-multiwell plates (Falcon) at the density of 1000 cells/μL. When required, they were infected with a mix of LTVs with molteplicity of infection (number of viruses per cell, m.o.i.) 8. As previously described (Brancaccio et al., 2010), this m.o.i. is sufficient to infect the almost totality of neural cells in these conditions. The dissection/infection day was referred to as "day in vitro 1" (DIV1). As for Emx2 or Foxg1 loss of function mice, the cell cultures were not infected. Precursor cells were cultured under pro-proliferative [1:1 DMEM-F12, 1X Glutamax(Gibco), 1X N2 supplement (Invitrogen), 1mg/ml BSA, 0.6% Glucose, 2 μg/ml mouse heparin (Stemcell technologies), 1X Pen/strept (Gibco), 10pg/ml Fungizone (Gibco), 20 ng/ml bFGF (invitrogen), 20 ng/mL EGF (Invitrogen)]. Where necessary, cells were then transferred to pro-differentiative conditions, according to various protocols, in order to finally perform immunofluorescence analysis, extract RNA for mRNA expression profiling or extract proteins for western blot analysis. As for *Foxg1* set of experiments, prodifflrentiative medium was composed by: Neurobasal A, 1X Glutamax, 1X B27, 1X Pen/strept (LifeTech). As for Emx2 study, prodifflrentiative medium was made up by: 1:1 DMEM-F12, 1X Glutamax(Gibco), 1X N2 supplement

(Invitrogen), 1mg/ml BSA, 0.6% Glucose, 2 µg/ml mouse heparin (Stemcell technologies), 1X Pen/strept (Gibco), 10pg/ml Fungizone (Gibco), 1mM N-acetylcysteine (sigma), 5% FBS (Clontech).

In particular, cells were cultured as floating neurospheres under pro-proliferative conditions or were attached to 200µg/ml poly-L-lysin coated coverslips in the pro-differentiative conditions at appropriate timing.

If an inducible TetON system was used to obtain the expression of the transgene, doxycyclin (Clontech) was added to the medium at the final concentration of 2µg/ml in due time.

In specific cases, medium was supplemented by 0.7 mM LDN193189 (Stemgent #130-096-226), or 20ng/mL Fgf9 (Sigma#SRP4057-10UG), or 30ng/mL Lif (Millipore), or 50ng/mL BMP4. In all differentiative mediums, FBS was tetracyclin-free.

3.4 Glioblastoma cell culture

Human U87MG GBM cell line and T98G GBM cell line were purchased from SIGMA (#89081402 and #92090213, respectively). Low passage criopreserved samples of them were employed to run this analysis. They were kept as adherent cultures in DMEM/Glutamax medium (ThermoFisher, #31966), supplemented with 10% FBS and 1X Pencillin/Streptomycin. Cells were cultured at 500 cells/µl and passaged by trypsin on days of counting or, at most, every 4 days.

GbmA-E cells originate from GBM surgical samples collected at IRCCS A.O.U. San Martino-IST, Dept of Neuroscience and Sense organs, Unit of Neurosurgery and Neurotraumatology, with patients' informed consent and in compliance with pertinent Italian law.

They were derived in Antonio Daga laboratory. Low passage criopreserved samples of them were employed to run this analysis. GbmA cells were cultured in "DMEM / F12 / glutamax / NeurobasalA" (ThermoFisher #10888- 022). GbmB-E were cultured as spheres in NeuroCult™ NS-A Proliferation Kit (Human) (StemCell Technologies, Vancouver - Canada, #05751). In both cases, mediums were supplemented with 1X Penicillin/Streptomycin, 2 µg/ml human heparin (StemCell Technologies #07980), 20 ng/ml recombinant human EGF (ThermoFisher #PHG0311), 20 ng/ml recombinant human FGF2 (ThermoFisher #PHG0261). All the

cells were cultured under normoxic conditions (5% CO2, 21% O2, 74% N2). Cells were cultured at 500 cells/µl and passaged by Accutase (Sigma, Milan - Italy, #A6964) on days of counting or, at most, every 4 days.

When required, cells were acutely infected, at a concentration of 500 cells/µl, by a mix containing lentiviral vectors, each one at a multiplicity of infection (m.o.i) = 6. This moi is sufficient to infect the almost totality of GBM cells in such conditions. Where required, they were subsequently transferred to polylysinated coverslips. In specific cases, medium was supplemented by 0.7 µM LDN193189 (Stemgent, Lexington - MA, #130-096-226), 20 ng/ml Fgf9 (Sigma #SRP4057- 10UG), or 10µg/ml BrdU. TetON-controlled transgenes were switched on by 2 µg/ml doxycyclin (Sigma #D9891- 10G).

3.5 GBM cell growth curves

After sphere dissociation, $2x10^5$ GBM cells/well were seeded in a 24-well plate and infected with LV_ Pgk1p-rtTA-M2-WPRE and LV_TREt-IRES-EGFP-WPRE or LV_TREt-Emx2-IRES-EGFP-WPRE, each at m.o.i. 6. Viable cells (trypan blue-excluding) were counted at fixed days on a hemocytometer. After every cell count, differently engineered cells were plated at the same concentration (2 . 105 GBM cells/well). Cell counting was performed on 1/200 of each biological sample (in case of Figure 1, 3 and 5 data, at *t*=0, each sample included 200,000 cells). Growth curves were interrupted when *Emx2*-GOF cell cultures had collapsed.

3.6 In vivo electroporation

P0 pups were anaesthetized on ice for 40–60 s. 2.0 mL of a solution containing 5.0 mg of DNA plasmid, mixed with 0.02% fast-green dye in phosphate buffered saline (PBS), was injected through the skull into the lateral ventricle, using a sharp pulled micropipette (hole external diameter about 30 mm) with the help of light fibers. Platinum tweezer-style electrodes (7 mm diameter) were placed on the lateral sides of the head and five pulses of 100 V were applied (each 50 ms long, interval between consecutive pulses 950 ms), sweeping the electrodes from lateral-lateral to dorsal-ventral by 25 angle intervals. For this purpose, a BTX ECM830 square wave pulse generator (Genetronics) was used. Animals were left to recover in a warm clean cage, they were transferred to their mother and were finally sacrificed 4 days later.

3.7 Neural precursor cell transplantation

As for *Foxg1*-GOF and- LOF in vivo experiments, P0 pups were anaesthetized on ice for 40-60s. 2.0 µl of a solution containing 400,000 cells (200,000 *Foxg1*-GOF-Egfp+ and 200,000 control-mCherry+ cells; or 200,000 *Foxg1*-GOF-mCherry+ and 200,000 control-Egfp+cells; or 200,000 α*Foxg1-shRNA*/Egfp+ and 200,000 control-*shRNA*/mCherry+ cells, pre-engineered by lentiviral transduction 7 days and 4 days before, respectively), mixed with 0.02% fast-green dye in DMEMF12/Glutamax Proliferation medium, were injected through the skull into the corticocerebral parenchyma, by free hands, using a sharp pulled micropipette (hole external diameter about 40 µm) with the help of light fibers. Animals were left to recover in a warm clean cage. Then they were transferred to their mother and were finally sacrificed 4 days later.

3.8 GBM short term in vivo experiments

P4 pups were anaesthetized on ice for 40-60s. 2.0 µl of a solution containing 200,000 cells (100,000 *Emx2*- GOF-Egfp+ and 100,000 control-mCherry+ cells, pre-engineered by lentiviral transduction 1 week before at MOI=6), mixed with 0.02% fast-green dye in NeuroCult™ NS-A Proliferation (Human) medium (StemCell Technologies #05751), were injected through the skull into the corticocerebral parenchyma, by free hands, using a sharp pulled micropipette (hole external diameter about 40 µm) with the help of light fibers. Animals were left to recover in a warm clean cage. Then they were transferred to their mother and were finally sacrificed 7 days later.

3.9 GBM survival experiments

For this study, nude (strain: Hsd:AthymicNude-Foxn1nu) mice were used. 6-weeks-old females were anaesthetized with Ketamine-Xylazine solution. 5.0 µl of a solution containing 300,000 cells (300,000 *Emx2*-GOF-Egfp+ cells in some mice, and 300,000 control-Egfp+ cells in the others; cells pre-engineered with lentiviral transaction 1 week before, at MOI=16), in DMEM-Glutamax medium, were injected through the skull into the striatum, by Hamilton syringe (Hamilton #7105KH), following the stereotaxic coordinates: AP +0.5; L -1.8; V -2.8.

Animals were left to recover in a warm clean cage. Then, they were checked each day and sacrificed when they showed clear symptoms of suffering. Survival curves were drawn.

3.10 Immunofluorescence sample preparation

Brains were fixed by immersion in 4% PFA overnight at 4C, washed by 1XPBS three times, equilibrated in 30%sucrose-1XPBS at 4°C, included into OCT (Killik), and frozen at 280C. Finally they were coronally sliced at 16 μm, by a Microm cryostat.

As for Emx2 protein quantification, neocortices collected from 10 E12.5 embryos and 5 P0 neonates were pooled by age, mechanically dissociated to single cells, allowed to acutely attach on polilysin-coated SuperFrost N1 slides and fixed for 15 min in 4% PFA at RT.

As for immunofluorescence on in vitro experiments, cells were blocked at due time and fixed for 15 min in 4% PFA at RT.

3.11 Immunofluorescence

Immunocytofluorescence was performed as previously described (Puzzolo and Mallamaci, 2010; Brancaccio et al., 2010). As for BrdU, its unmasking was performed by 0.2 M HCl for 150 at RT. In case of immunos with polyclonal anti-Aldolase C, anti-Emx2, and anti-Ki67 and monoclonal anti-S100b antibodies, antigen retrieval was performed by baking samples in 10 mM citrate buffer (pH56.0), at 700 W for 5, 5, 3, and 5 min, respectively. The following antibodies were used: anti-Aldolase C, rabbit polyclonal (Abcam #ab87122), at 1:50; anti-BrdU, mouse monoclonal, B44 antibody (Becton-Dickinson #347580), at 1:50; anti-CNPase, mouse monoclonal, clone 11-5B antibody (Abcam #ab6319), at 1:200; anti-Emx2 mouse monoclonal M06-4F7 antibody (Abnova#H00002018-M06), at 1:200 ; anti-p(Tyr1284)ErbB4 rabbit polyclonal (Abcam #61059), at 1:200; anti-Emx2, rabbit polyclonal (Mallamaci et al., 1998), at 1:700; anti-GFAP rabbit polyclonal (DAKO#Z0334), at 1:600; anti-GFP chicken polyclonal (Abcam #13970), at 1:400; anti-Ki67, mouse monoclonal (BD Pharmingen #550609), at 1:50;; anti-NCoR, rabbit polyclonal (Abcam #3482) at 1:200; anti-Pax6, rabbit polyclonal (Covance #PRB-278P), at 1:150; anti-RFP rat monoclonal 5F8 (Chromotek #5f8-20), at 1:500; antiS100b, mouse monoclonal, clone 4C4.9 (Abcam #ab4066), at 1:50; anti-S100b,

rabbit polyclonal (DAKO #Z0311), at 1:800–1:300; anti-Sox2 rabbit polyclonal (Abcam #97959), 1:1,000; anti-Tubb3 (TUJ1), mouse monoclonal(Biolegend #MMS-435P), at 1:1000. The following secondary antibodies were used: Alexa408 Goat Anti-Rabbit; Alexa594 Goat Anti-Rabbit; Alexa594 Goat Anti-Mouse, Alexa408 Goat Anti-Mouse, Alexa488 Goat Anti-Chicken, Alexa594 Donkey Anti-Rat.

Immunos were photographed on a Nikon Eclipse TI microscope equipped with a 20X objective and a Hamamatsu camera.

Images were imported and analyzed by Photoshop CS2 (Adobe) and ImageI softwares. In case of Emx2 immunodetection in vivo (by an Alexa 594 secondary antibody), tissue autofluorescence was assayed by inspecting emission at 520 nm, where no specific signal was expected.

Where not otherwise stated, each experiment was performed at least in biological triplicate. For each experimental condition and each biological replicate, >200 cells and 2,000–6,000 cells (from 20 randomly assorted photographic fields) were scored, as for in vivo and in vitro assays, respectively. Cell countings were performed by being blind of sample identity. Frequencies of immunoreactive cells were averaged and s.e.m.'s were calculated. Results were normalized against controls. Their statistical significance was evaluated by the t test (one-tail; unpaired). "n5x,y" refers to the number of samples scored for each genotype.

In the case of Emx2 protein quantification (*Fig. R.10 D,E*), photos were taken from 4 slides per age. Sox2+cell-containing fields were selected by an operator blind of Emx2-fluorescence and sample age. 30–40 randomly picked Sox2+ cells per slide were analyzed. Emx2-levels were evaluated by Photoshop-Histogram plugin, per each single cell. Data were analyzed by Excel and their significance was evaluated by the t test (one-tail; unpaired). "*n*" is the number of samples. In the case of Sox2 (*Fig. R.9 B,C*), immunofluorescence quantification was made similarly to Emx2, but on batches of about 300 cells per experimental condition and biological replicate.

3.12 Cytofluorometry

To prepare fluorescence activated cell sorting (FACS) analysis, cells were labeled as follows. Dissociated cortico-cerebral precursors, obtained as described above, were acutely infected with the following lentiviruses: LV:pNes/hsp68-rtTA2S-M2; LV:TREt-Emx2-IRES2-EGFP (or, alternatively, LV:TREt-Luc-IRES2-EGFP, as a

control); LV:pTa1-mCherry. 96 hr prior to analysis, transgenes were activated by doxycyclin addition. Moreover, 72 hr prior to analysis, standard Egf was replaced by biotinylated, Alexa Fluor 555 streptavidin-complexed Egf (equally concentrated), which was refreshed 48 hr later. Finally, just prior to fluorimetric profiling, cells were mechanically dissociated and further labeled with anti-A2B5 mouse monoclonal antibody, APC conjugated (MACS Miltenyi), at 1:10 concentration, according to manufacturer instructions.

Labeled cells were analyzed on a Cyan ADP flow cytometer (Dakocytomation, Denmark). Forward scatter (FSC) and side scatter (SSC) were used to exclude debris and cell aggregates (live gate). Cells belonging to the live gate were evaluated for their EGFP6/ mCherry6/Egf-Alexa5556/A2B5-APC6 fluorescence profile. Data analysis was performed by FlowjoTM software (Tree Star, Ashland). This experiment was performed in biological septuplicate. For each experimental condition, samples of 80,000 cells were scored. Frequencies of immunoreactive cells were averaged and s.e.m.'s were calculated. Statistical significance of results was evaluated by the t test (one-tail; unpaired). "*n*=x,y" refers to the number of samples scored for each genotype.

3.13 mRNA profiling

Total RNA was extracted from cells using Trizol™ (ThermoFisher #15596-026), according to Manufacturer's instructions and resuspended in sterile deionized water. Agarose gel electrophoresis and spectrophotometric measurements (NanoDrop ND-1000) were employed to estimate quantity, quality and purity of the resulting RNA. Prior to analysis, samples were processed by the TurboDNAfree kit (Ambion™), for 1 hour at 37°C. At least 1.0 μg RNA from each sample was retrotranscribed by SuperScriptIII™ (ThermoFisher #18080044) in the presence of random hexamers, according to manufacturer's instructions. RT-minus samples were scored as controls, in the case of intronless transcripts.

1/50 of the resulting cDNA was used as substrate of any subsequent qPCR reaction. PCR reactions were performed by the SsoAdvanced SybrGreen™ Supermix platform (Biorad), according to manufacturer's instructions. Each biological replicate was scored at least in technical triplicate and data were normalized against *Gapdh* and *GAPDH* for murine and human cell samples, respectively. Results were averaged

and further normalized on their controls. Averages ± s.e.m.'s were reported in Table 1. Statistical significance of results was evaluated by the t-test (one-tail; unpaired). "*n*" is the number of samples.

Oligo were as follows:

Murine oligos:

- *Brn2*, mBrn2/F1, 5' CAA CAA CAG CGA CCG CCA CATCTG GTG 3', and mBrn2/R1, 5' GTG AAG CTC GGC TGC GAA TAG AGC AAA C 3';
- *EgfR*, EgfR/F, 5' AGA CCC ACA GCG CTA CCT TGT TATCCA 3', and EgfR/R, 5' CAA CTA CAT CCT CCA TGT CCT CTT CAT CCA 3';
- *Emx2*, E2S/N2F, 5' GGA AAG GAA GCA GCT GGC TCACAG TCT CAG TCT TAC 3', and E2S/N2R, 5' GTG GTG TGT CCC TTT TTT CTT CTG TTG AGA ATC TGA GCCTTC 3';
- *Fgf9*, Fgf9/F4, 5' CGA GAA GGG GGA GCT GTA TGG ATCAGA A 3', and Fgf9/R4, 5' AGA GGT TGG AAG AGT AGG TGT TGT ACC AGT 3';
- *Gapdh*, Gapdh5/F, 5' ATC TTC TTG TGC AGT GCC AGCCTC GTC 3', and Gapdh5/R, 5' GAA CAT GTA GAC CAT GTA GTT GAG GTC AAT GAA GG 3';
- *Gfap,* Gfap/F, 5' GCA GAT GAA GCC ACC CTG GCT C 3', and Gfap/R, 5' CCA GAT CGC AGG TCA AGG CCT GCA G 3';
- *Hes5*, Hes5/F, 5' GCT CAG TCC CAA GGA GAA AAA CCG ACT GCG 3', and Hes5/R, 5' CGC GGC GAA GGC TTT GCT GTG TTT CAG 3';
- *Id3*, Id3/F1, 5' CGG TCC GCA TCT CCC GAT CCA GAC A 3', and Id3/R1, 5' CGG GCG CCA GCA CCT GCG TTC 3';
- *Msx1*, Msx1/F1, 5' GAC TCC TCA AGC TGC CAG AAG ATG CTC 3', and Msx1/R, 5' GTC CTG GGC TTG CGG TTG GTC TTG TG 3';
- Ncor1, Ncor1/F, 5' CCA GCA CCT CAG TGG TGA CGA GCA 3', and Ncor1/R 5' GCC TTT CAG TTC CTA AAT AGC TTT GCC C 3';
- *Pax6*, Pax6/ForM, 5' CCA AGG GCG GTG AGC AGA TGT GTG AGA TCT TCT ATT CTA G 3', and Pax6/RevM, 5' CCC GTT GAC AAA GAC ACC ACC AAG CTG ATT CAC TC 3';
- *Sip1*, mZeb2/F2, 5' CGA GAG GCA TAT GGT GAC GCA CAA G 3', and mZeb2/R1, 5' CAC TGT GAA TTC TCA GGT GTT CTT TCA GGT 3';
- *Sox2*, Sox2/FEXT, 5' CGG CAC GGC CAT TAA CGG CAC ACT G 3', and Sox2/REXT, 5' GAG CAT TAT CAG ATT TTT CCT ACT CTC CTC TTT TTG 3';

Human oligos:

- *GAPDH,* hGAPDH/Fw, 5’ CAT CAC CAT CTT CCA GGA GCG AGA TCC 3’, and hGAPDH/ Rv, 5’ CAA ATG AGC CCC AGC CTT CTC CAT GG 3’;
- *EGFR,* hEGFR/Fw, 5’ GAG ACC CCC AGC GCT ACC TTG TCA TTC A 3’, and hEGFR/Rv, 5’ CCA CCA CGT CGT CCA TGT CTT CTT CAT CCA 3’;
- *PDGF,* hPDGF/Fw, 5’ CCT GCC CAT TCG GAG GAA GAG AAG CA 3’, and hPDGF/Rv, 5’ GGT GCA GCG TTT CAC CTC CAC GCA CG 3’;
- *PDGFR,* hPDGFR/Fw, 5’ ACA CTT GCT ATT ACA ACC ACA CTC AGA CAG AAG 3’, and hPDGFR/Rv, 5’ TCC TCC ACG ATG ACT AAA TAA TCC GTC ATT CCT A 3’;
- *PTEN,* hPTEN/Fw, 5’ GTT TGT GGT CTG CCA GCT AAA GGT GAA GAT A 3’, and hPTEN/ Rv, 5’ CAC AGG TAA CGG CTG AGG GAA CTC AAA G 3’;
- *NF1,* hNF1/Fw, 5’ AGG ACC TGA AGG TAT TCC ACA ATG CTC TCA A 3’, and hNF1/Rv, 5’ CTG AAG TTA CTT GGA CAG CAG TAG AAC CAA C 3’;
- *MYC,* hMYC/Fw, 5’ CCC TGG TGC TCC ATG AGG AGA CAC 3’, and hMYC/Rv, 5’ AGG AGC CTG CCT CTT TTC CAC AGA AAC A 3’;
- *MYCN,* hMYCN/Fw, 5’ GAG AGG ACA CCC TGA GCG ATT CAG ATG 3’, and hMYCN/ Rv, 5’ TGG TGA ATG TGG TGA CAG CCT TGG TGT TG 3’;
- *RB1,* hRB1/Fw, 5’ GAG GGA ACA TCT ATA TTT CAC CCC TGA AGA GTC 3’, and hRB1/Rv, 5’ CAG AAG TCC CGA ATG ATT CAC CAA TTG ATA CTA AGA 3’;
- *CDKN2a/b,* hCDKN2a/b/Fw, 5’ CTC CAC GGC GCG GAG CCC AAC T 3’, and hCDKN2a/b/ Rv, 5’ GCA GCA CCA CCA GCG TGT CCA GGA A 3’;
- *CDK4,* hCDK4/Fw, 5’ GCA TCC CAA TGT TGT CCG GCT GAT GGA 3’, and hCDK4/Rv, 5’ GGT CTA CAT GCT CAA ACA CCA GGG TTA CC 3’;
- *CDK6,* hCDK6/Fw, 5’ GCA CCC CAA CGT GGT CAG GTT GTT TGA TG 3’, and hCDK6/Rv, 5’ GGT CAA GTC TTG ATC GAC ATG TTC AAA CAC TAA A 3’;
- *CCND2,* hCCND2/Fw, 5’ CCT GCA GCA GTA CCG TCA GGA CCA A 3’, and hCCND2/Rv, 5’ TCA CAG GTC GAT ATC CCG CAC GTC TGT A 3’;
- *SOX2,* hSOX2/Fw, 5’ CGG CAC GGC CAT TAA CGG CAC ACT G 3’, and hSOX2/Rv, 5’ GTT TTC TCC ATG CTG TTT CTT ACT CTC CTC TTT TG 3’;
- *TRP53,* hTRP53/Fw, 5’ CCT CCT CAG CAT CTT ATC CGA GTG GAA G 3’, and hTRP53/Rv, 5’ CAT AGG GCAC CAC CAC ACT ATG TCG AAA AG 3’;
- *MDM2,* hMDM2/Fw, 5’ GTA TAA GTG TCT TTT TGT GCA CCA ACA G 3’, and hMDM2/Rv, 5’ TGT ACC TAC TGA TGG TGC TGT AAC CAC C 3’;

- *GLI1,* hGLI1/Fw, 5' GGA GGA AAG CAG ACT GAC TGT GCC AGA 3', and hGLI1/Rv, 5' CAG ACC AGT GCC AGC AAT GCA AGG TCC 3';
- *HES1,* hHES1/Fw, 5' CCA AAG ACA GCA TCT GAG CAC AGA AAG TCA TC 3', and hHES1/ Rv, 5' GCG AGC TAT CTT TCT TCA GAG CAT CCA AAA TC 3';
- *VEGF,* hVEGF/Fw, 5' GAA GAT GTA CTC GAT CTC ATC AGG GTA C 3', and hVEGF/Rv, 5' CAG AAG GAG GAG GGC AGA ATC ATC AC 3'.

3.14 Western blots

Western analysis was performed according to standard methods. Total cell lysates in CHAPS buffer were quantified by BCA protein assay kit (ThermoFisher #10678484) and denatured at 95°C for 5 min, prior to loading. Thirty micrograms of proteins were loaded per each lane and run on a 12% acrylamide – 0.1% SDS gel. Full details about antibodies employed are reported in Supplementary Materials and Methods. Different antigens and bACT were sequentially revealed by an ECL kit (GE Healthcare, Milan - Italy, #GERPN2109). Images were acquired by an Alliance LD2–77.WL apparatus (Uvitec, Cambridge) and analyzed by Adobe Photoshop CS2 software™ and Microsoft Excel 11 software™.

The following primary antibodies were used: anti- Emx2, mouse monoclonal, M06-4F7 antibody (Abnova #H00002018-M06), at 1:300; anti-p(Thr202/Tyr204)Erk1/2, rabbit monoclonal (Cell Signaling Technology, Leiden - The Netherlands, #4370), at 1:2000; anti-p(Ser463/465)Smad1/5/8, rabbit polyclonal (Merck-Millipore, Vimodrone - Italy, #ab3848), at 1:500; anti-p(Tyr705)Stat3, rabbit monoclonal (Cell Signaling Technology #9145), at 1:1000; anti-p(Ser727) Stat3, rabbit polyclonal (Santa Cruz, Dallas - TX, sc- 8001-R), at 1:800. A secondary HRP-conjugated anti-rabbit antibody (ThermoFisher #32260) was used at 1:2000. bACT was straightly detected by a peroxydase C-conjugated mouse monoclonal antibody (Sigma #A3854), used at 1:10,000.

3.15 Statistical analysis of results

Where it not otherwise stated, each experiment was performed at least in biological triplicate. For each experimental condition, 2,000-3,000 cells (from 20 photographic fields)were scored, by an operator (the candidate) blind of sample identity. Frequencies of immunoreactive cells were averaged and s.e.m.'s were

calculated. Results were normalized against controls. Their statistical significance was evaluated by the t-test (one-tail; unpaired).

As for the RT-PCR results, upon normalization of each gene of interest with a housekeeping gene, a t-test (one-tail; unpaired) was performed in order to acknowledge statistical significance.

4. RESULTS

4.1 *Foxg1* regulation of astrogenesis

4.1.1 *Foxg1* inhibits astrogenesis both in vivo and in vitro

Previous investigations in our lab gave evidence for both an enlargement of the NSCs compartment and reduction of astroglial output following *Foxg1* overexpression in NSCs. These studies also reported a defective progression of NSCs to early glia committed progenitors. However, these phenomena were only documented in vitro, as well as in a temporal frame *delayed* as compared to the physiological astrogliogenic schedule (Brancaccio et al., 2010). On the basis of this research study, we hypothesized that *Foxg1* might also control the developmental commitment of neural stem cells towards glial fates, so constrainin the astrogenic volume within the developing cerebral cortex.

To test this hypothesis, we decided to assess if *Foxg1* overexpression impacts the *in vivo* astroglial output of genetically manipulated NSCs, transplanted into wild type recipient brains, according to a developmentally plausible schedule. For this purpose, we engineered dissociated E12.5 cortico-cerebral precursors for conditional, TetON-driven *Foxg1* overexpression, under the control of a synthetic, Nestin gene-derivative promoter, selectively firing in NSCs. We acutely activated the transgene via doxycyclin administration and we maintained cells in pro-proliferative medium for seven days. Then, we transplanted cells into the parietal cortico-cerebral parenchyma of P0 isochronic mouse pups. Specifically, we injected a 1:1 mix of cells, made alternatively gain-of-function for *Foxg1* or a control, and labelled with EGFP and mCherry, respectively. Four days later, we sacrificed the pups and scored their brains for the astroglial outputs of the two different, transplanted precursor types (*Fig. R.1 A-A'*). Remarkably, each pool of *Foxg1*-GOF cells could be referred to the pool of control cells in the same brain. We found that, compared to controls, s100β+ derivatives of *Foxg1*-GOF precursors were reduced by 19.25 ± 6.94% ($p < 9.60 \times 10^{-6}$, n=8,8, *paired t-test*) (*Fig. R.1 C*). Brancaccio et al. showed that *Foxg1* also promotes NSCs self-renewal (Brancaccio et al., 2010). We reasoned that this might lead us to

underestimate the real impact of Foxg1 overexpression on the astrogenic power of NSCs *in vivo*. To compensate for such an effect, we evaluated the frequency of Nestin$^+$ NSCs within each precursor pool, just before transplantation (*at day 0*), and normalized the pool's astroglial output against such frequency. As expected, we found that *Foxg1* overexpression induced a 2.5-folds increase of Nestin$^+$ cell frequency (+149.76 ±6.34, p< 4.37x10^-12*,* n=3,3) in respect to the controls (*Fig. R.1 B*). This means that the same manipulation elicited a decrease of the *NSCs-normalized* s100β+ astrocytic output by 67.67%.

Then, to rule out a possible a dominant negative effect on our result, we performed a specular loss-of-function assay, with neural precursors alternatively engineered cells by an α*Foxg1-shRNA*-expressing-LV or a control (*Fig. R.1 D-D'*). To increase the sensitivity of the assay, we anticipated precursors' transplantation by 3 days, so interrogating cells which display huigher levels of *Foxg1*-mRNA (our unpublished observations). Specifically, we engineered E12.5 corticocerebral precursors, we maintained them in culture for only 4 days and we co-transplanted a 1:1 mix of them into heterochronic P0 pups. Then, we assessed the final glial output at P4. The s100β+ cells frequency did not change upon *Foxg1* manipulation (n=4,4) (*Fig. R.1 F*). However, on the day of transplantation, the frequency of Nestin+ precursors was decreased by 32.14±3.26% in α*Foxg1-shRNA* samples compared to controls (*Fig. R.1 E*). This means that Foxg1 downregulation upregulated the *NSCs-normalized* astrogenic output by 39.75 %. All together these last data confirm that, when overexpressed in NSCs, *Foxg1* exerts a genuine anti-astrogenic effect..

Interestingly, such *Foxg1* antiastrogenic activity was robustly confirmed when consequences of *Foxg1* mis-expression were re-evaluated in vitro, within the same temporal framework. That is very important, as it suggests that molecular mechanisms leading to this phenotype may be largely dissected in this simplified in vitro set-up.

In a first assay, we acutely engineered dissociated E12.5 cortico-cerebral precursors for conditional *Foxg1* overexpression, as described above for transplantation assays. We maintained cells in a pro-proliferative medium supplemented with doxycyclin for seven days. Next, we transferred cells to a poli-L-lysin-coated coverslips and kept them under pro-differentiative medium, supplemented with doxycyclin, for four additional days. Finally, we performed

cultures immunolabeling. We found a pronounced loss of S100β$^+$ astrocytes (-63.89±9.14%, p<0.003, n=4,4) (*Fig. R.2 C*), as well as a consistent reduction of Gfap$^+$ cells (-37.32±20.10%, p<0.002, n=3,3,) (*Fig. R.2 D*) upon *Foxg1* overactivation. In a second assay, astroglial cultures prepared from *Foxg1*$^{+/-}$ mice-derived cortico-cerebral precursors displayed no significant difference in the s100β$^+$ cell frequency compared to the wild type controls (*Fig. R.2 G*).

Finally, we also evaluated the frequencies of presumptive NSCs in *Foxg1*-mutant cultures and normalized the number of their S100β$^+$ and Gfap$^+$ in vitro progenies against such frequencies. At DIV4, NSCs, expressing Sox2 but not an mCherry reporter under the control of the Tubulin-α1 promoter (selectively firing in the whole neuronogenic lineage), were augmented by 89.64±10.67% (p<0.0001, n=4,4) in *Foxg1*-GOF cultures and decreased by 26.95% in *Foxg1*-LOF cultures(*Fig. R.2 B-F*). This implicates that the NSCs-normalized astrocytic output varied by -80.96% (S100β$^+$ cells) and 52.41% (Gfap$^+$ cells) in *Foxg1*-GOF cultures, as well as by + 32.93% (S100β$^+$ cells) in *Foxg1*-LOF cultures.

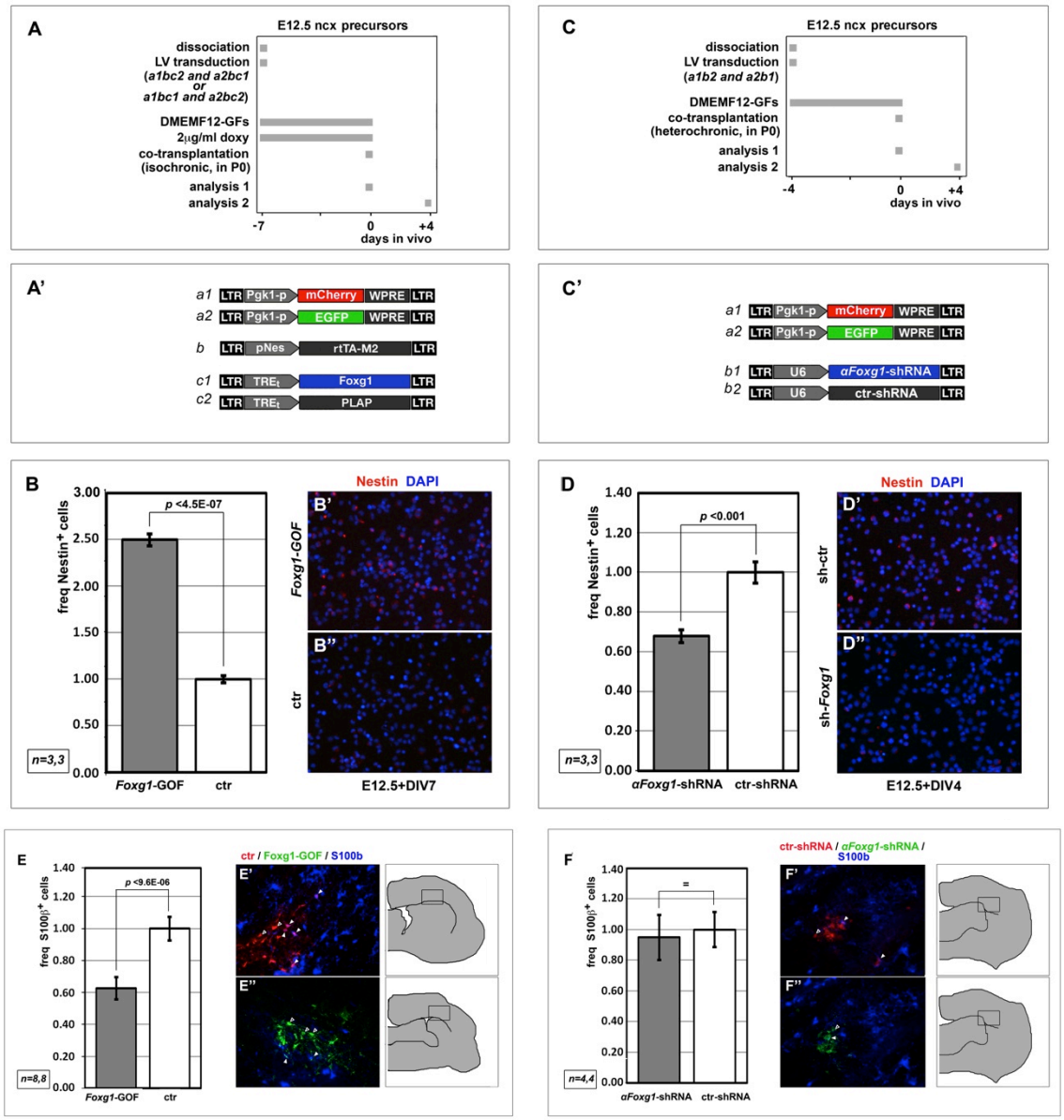

Figure R.1 Reduced astrocytogenesis upon *Foxg1* manipulation, *in vivo*. Experimental strategy and lentiviral vectors employed for its implementation are shown in (**A,A',C,C'). (B)** Frequencies of Nestin⁺ derivatives of neocortical (ncx) precursors, acutely infected with LV:*pNes/hsp68-rtTA2S-M2* and, alternatively, LV:*TREt-IRES2-PLAP* (NC) and LV:*TREt-Foxg1-IRES2* (*Foxg1*-GOF). Cells kept for 7 days under pro-proliferative medium and acutely attached on poli-L-lysin-coated coverslips; doxycyclin administered at DIV-7–0. Data normalized against sample (ctr); absolute frequency of Nestin+ cells in (ctr), 10.38±0.39%. Scale bar=s.e.m. **(B'-B'')** Examples of Nestin⁺ cells referred to in (B). **(D)** Frequencies of Nestin⁺ derivatives of cortical precursors, acutely infected with *LV:U6-ctr-shRNA* (ctr-shRNA) and, alternatively, *LV:U6-αFoxg1-shRNA* (*αFoxg1*-shRNA). Cells kept for 4 days under pro-proliferative medium and acutely attached on poli-L-lysin-coated coverslips; doxycyclin administered at DIV-4–0. Data normalized against sample (ctr); absolute frequency of Nestin+ cells in (ctr), 22.45±1.21%. Scale bar=s.e.m. **(D'-D'')** Examples of Nestin⁺ cells referred to in (D). **(E)** Frequencies of S100β⁺ astrocytes, evaluated within the parietal cortex of P4 pups among derivatives of cells engineered as in (A,A'), further labeled with either *LV:Pgk1-EGFP* (for ctr) or *LV:Pgk1-mCherry* (for *Foxg1*-GOF) and co-transplanted as a 1:1 mix into the cortical parietal parenchyma of isochronic P0 pups. Data normalized against sample (ctr); absolute frequencies of S100β⁺ (ctr), 30.38±2.24 cells. Scale bar=s.e.m. **(E'-E'')**

Examples of S100β+ cells referred to in (E). **(F)** Frequencies of S100β+ astrocytes, evaluated within the parietal cortex of P4 pups among derivatives of cells engineered as in (C,C'), further labeled with either *LV:Pgk1-EGFP* (ctr) or *LV:Pgk1-mCherry* (*αFoxg1*-shRNA) and co-transplanted in 1:1 mix into the cortical parietal parenchyma of heterochronic P0 pups. Data normalized against sample (ctr-shRNA); absolute frequencies of S100β+ (ctr-shRNA), 25.04±2.85 cells. Scale bar=s.e.m. **(F'-F'')** Examples of S100β+ cells referred to in (F). *n* is the number of biological replicates; *p*-value calculated by t-test (one-tail, unpaired) for (B)and (D), paired for (E) and (F)).

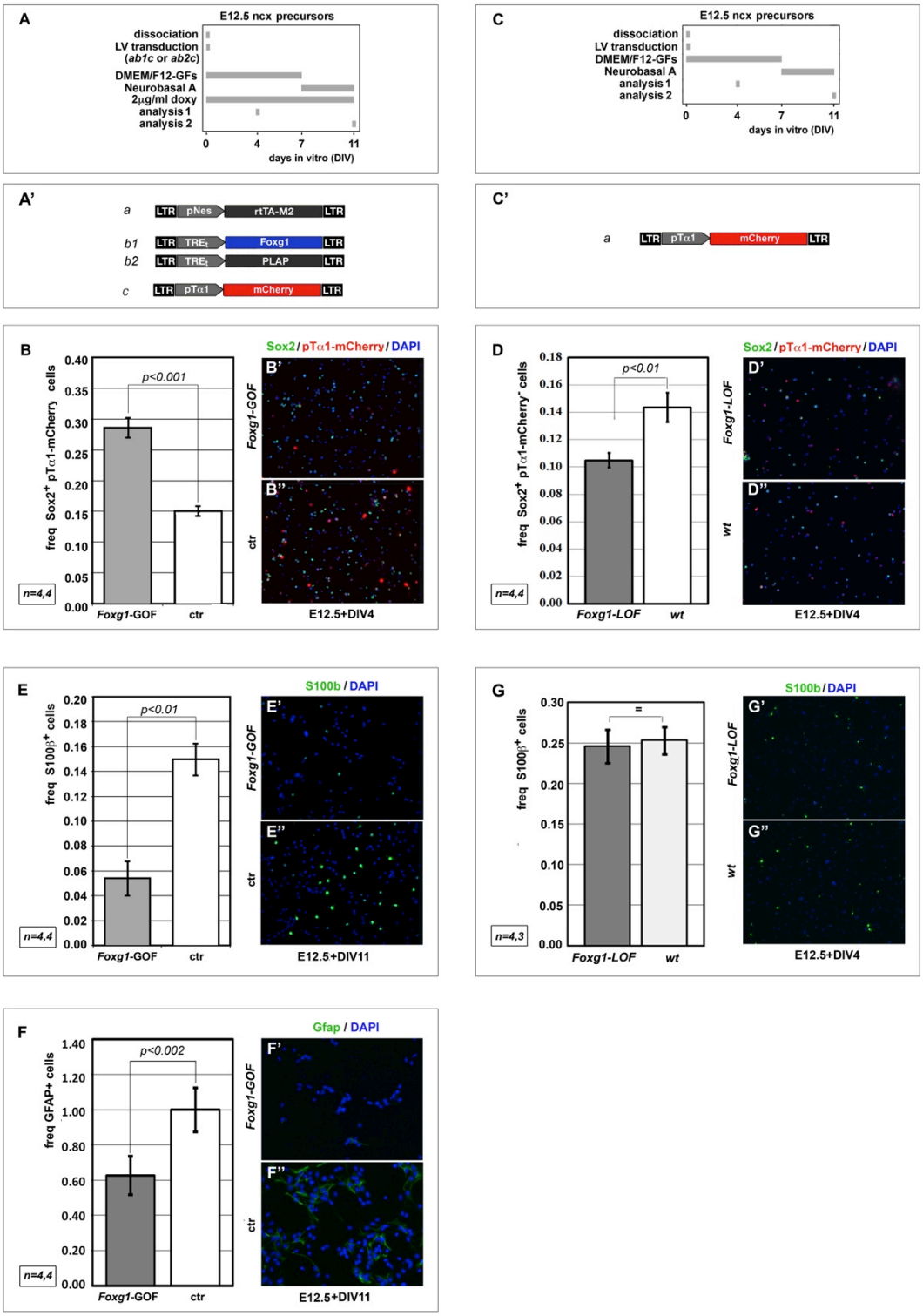

Figure R.2. Reduced astrocytogenesis upon *Foxg1* manipulation, *in vitro*. Experimental strategy and lentiviral vectors employed for its implementation are shown in **(A,A',C,C')**. **(B)** Frequencies of Sox2+-mCherry- derivatives of neocortical (ncx) precursors, acutely infected with LV:*pNes/hsp68-rtTA2S-M2*, LV:*ptα1-mCherry*, and, alternatively, LV:*TREt-IRES2-PLAP* (ctr) or LV:*TREt-Foxg1-IRES2* (*Foxg1*-GOF). Cells kept for 4 days under pro-proliferative medium and acutely attached on poly-L-lysin-coated coverslips at DIV4; doxycycline administered at DIV0-4. Cells immunoprofiled at DIV 4 (*analysis 1*, referred to in (A)). Data normalized against sample (ctr); absolute frequency of Sox2+-mCherry- cells in (ctr),

15.05±0.79%. Scale bar=s.e.m. **(B',B'')** Examples of Sox2^{+}-mCherry^{-} cells referred to in (B). **(D)** Frequencies of Sox2^{+}-mCherry^{-} cells derived from cortical precursors alternatively dissected from wild type (wt) and *Foxg1*$^{+/-}$ littermate mice (*Foxg1*-LOF), and acutely infected with *LV:ptα1-mCherry*. Cells kept for 7 days under pro-proliferative medium and 4 more days under pro-differentiative medium. Cells immunoprofiled at DIV 4 (*analysis 1*, as showed in (C)). Data normalized against sample (wt); absolute frequency of Sox2^{+}-mCherry^{-} cells in (ctr), 14.36±0.10%. Scale bar=s.e.m. **(D',D'')** Examples of Sox2^{+}-mCherry^{-} cells referred to in (D). **(E,F)** Frequencies of S100β^{+}(E) and Gfap^{+}(F) derivatives of cortical precursors, acutely infected with LV:*pNes/hsp68-rtTA2S-M2,* and, alternatively, LV:*TREt-IRES2-PLAP* (ctr) or LV:*TREt-Foxg1-IRES2* (*Foxg1*-GOF). Cells kept for 7 days under pro-proliferative medium and 4 more days under pro-differentiative medium; doxycycline administered at DIV0-11. Cells immunoprofiled at DIV 11 (*analysis 2*, as showed in (A)). Data normalized against sample (ctr); absolute frequency of S100β^{+} and Gfap^{+} cells in (ctr), 14.95±1.27 and 21.67±1.03%, respectively. Scale bar=s.e.m. (**E',E'',F',F'')** Examples of S100β^{+} and Gfap^{+} cells referred to in (E), (F), respectively. **(G)** Frequencies of S100β^{+} cells derived from cortical precursors alternatively dissected from wild type (wt) and *Foxg1*$^{+/-}$ littermate mice (*Foxg1*-LOF). Cells kept for 7 days under pro-proliferative medium and 4 more days under pro-differentiative medium. Cells immunoprofiled at DIV 11 (*analysis 2*, referred to in (C)). Data normalized against sample (wt); absolute frequency of S100β^{+} cells in (wt), 25.36±1.70%. Scale bar=s.e.m. (**G'-G'')** Examples of S100β^{+} cells referred to in (G). *n* is the number of biological replicates; *p*-value calculated by t-test (one-tail, unpaired).

4.1.2 Preliminary dissection of molecular mechanisms underlying *Foxg1* regulation of astrogenesis

As far as we know, the key molecular pathways modulating astroglial differentiation play a prominent role in transcriptional control of glial genes. Therefore, we considered the possibility to use trascriptional regulation of glial genes as a starting model to dissect molecular mechanisms mediating *Foxg1* anti-astrogenic activity. For this purpose, we wondered if, apart from down-regulating the frequency of astroglial cells, *Foxg1* is able to dampen *Gfap*-mRNA levels. We engineered E14.5 cortico-cerebral precursors for TetON-controlled *Foxg1* overexpression, driven by the constitutive *Pgk1* promoter. We plated cells on poli-ornithin/fibronectin treated coverslips, under NeurobasalA medium supplemented with B27, 200µM L-glutammine, Pen/Strept and doxyciclin. At DIV3 we administered a 24 hours-long pulse of 50ng/ml BMP4 and 30ng/ml LIF. Finally, at DIV4 we harvested cells for RNA extraction (*Fig. R.3 A-B)* and evaluated *Gfap*-mRNA levels by qRT-PCR. We found that *Gfap*-mRNA was decreased by 49.92±13% upon *Foxg1* overactivation (p<0.021, n=6,6) (*Fig. R.3 C*). Remarkably, when *Gfap*-mRNA levels were further normalized against the frequency of Nestin⁺ cells (evaluated in *Foxg1*-GOF cultures at the time of RNA extraction), this decrease was even more pronounced (-64.78%). This suggests that, in addition to its general negative impact on astrogenesis progression, *Foxg1* may specifically down-regulate *Gfap* transcription.

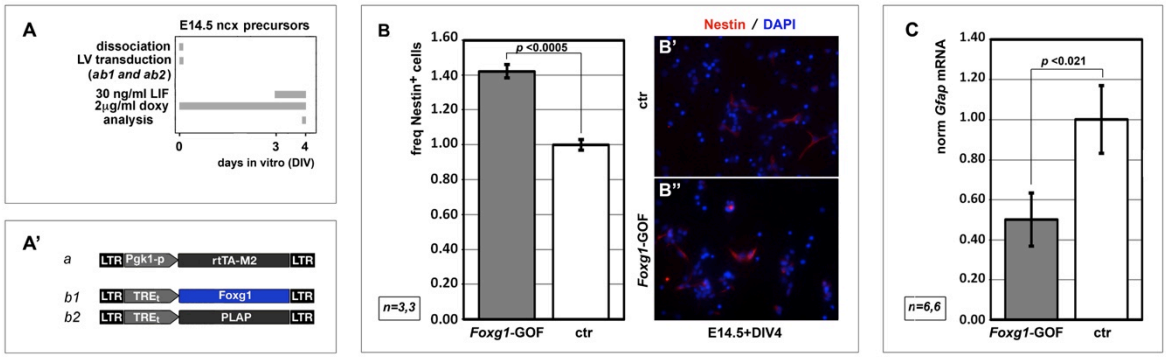

Figure R.3. *Foxg1* represses *Gfap* transcription. Experimental strategy and lentiviral vectors employed for its implementation are shown in **(A,A'). (B)** Frequencies of Nestin⁺ derivatives of neocortical (ncx) precursors, acutely infected with LV:*pPgk1-rtTA2S-M2* and, alternatively, LV:*TREt-IRES2* (ctr) or LV:*TREt-Foxg1-IRES2* (*Foxg1*-GOF). Cells acutely attached on poly-ornithin/fibronectin-coated coverslips, kept for 4 days under NeurobasalA medium supplemented with B27, 200µM L-glutammine, Pen/Strept; doxycyclin administered

at DIV0–4. Cells immunoprofiled at DIV4. Data normalized against sample (ctr); absolute frequency of Nestin$^+$ cells in (ctr), 8.63±0.27%. Scale bar=s.e.m. **(B'-B'')** Examples of Nestin$^+$ cells referred to in (B). **(C)** *Gfap*-mRNA levels in derivatives of precursors acutely infected with LV:*pPgk1-rtTA2S-M2* and, alternatively, LV:*TREt-IRES2* (ctr) or LV:*TREt-Foxg1-IRES2* (*Foxg1*-GOF). Cells acutely attached on poly-ornithin/fibronectin-coated coverslips, kept for 4 days under NeurobasalA medium supplemented with B27, 200μM L-glutammine, Pen/Strept, GFs; doxycyclin administered at DIV0–4. Data double-normalized, against endogenous *Gapdh*-mRNA and (ctr) values. *n* is the number of biological replicates; *p*-value calculated by t-test (one-tail, unpaired).

To clarify mechanisms dampening *Gfap*-mRNA levels in *Foxg1*-GOF precursors, we decided to profile these precursors for: (1) functional levels of pathways modulating glial genes transcription, and (2) the epigenetic state of *Gfap* chromatinWe started from the first part, while the second one will be the focus of a dedicated follow up study. Here we provide partial results about the issue (1). This functional dissection will be completed in a dedicated follow up study.

We preliminarily evaluated the global availability of key effectors modulating Gfap transcription in *Foxg1*-GOF cultures. For this purpose, we overactivated *Foxg1* in E12.5 cortico-cerebral precursors and we kept them in pro-proliferative conditions for seven days. Then, we harvested cells for protein extraction and Western Blot analysis (*Fig. R.4 A,D)*. We found that neither p(Tyr^{705})Stat3 nor p(Ser$^{463/465}$)Smad1,5,8 levels were changed upon *Foxg1* manipulation (*Fig. R.4 B-C*). Interestingly, immunofluorescence profiling of the whole cell population revealed that nuclear ErbB4-ICD levels levels were augmented by 12.13±2.79% (*Fig. R.4 H,I)*. Conversely, nuclear NCoR immunolabeling displayed no significant difference (*Fig. R.4 K,L*).

Next, we restricted our analysis to the Nestin^{+} NSC compartment, where the histo-genetic choice subject of our interest is taken. We limited *Foxg1* overexpression to this compartment and immunoprofiled nuclei of its cells for the four effectors mentioned above. As for the evaluation of pStat3 and pSmad1,5,8, we immunolabelled cells after a 1hour pulse of 30ng/ml Lif and 50mg/ml Bmp4, respectively. Intriguingly, we found a significant decrease of both pStat3 and pSmad1,5,8, by 58.28±1.99% (p< 2.54x10^-10, n=300,310) and 52.91±2.34% (p< 5.78x10^-23, n=270,220), respectively, upon *Foxg1* overexpression (*Fig R.5 B,C* and *Fig. R.5 E,F*). The average ErbB4-ICD signal did not vary (*Fig R.5 H,I*). Surprisingly, NCoR, which had been found unmodified in the whole cell population, was significantly, albeit moderately upregulated (+14.18±2.83%, p< 0.0002, n=212,281) ((*Fig R.5 K,L*). In synthesis, as many as three modifications potentially accounting for *Foxg1* anti-astrogenic activity were found: a decrease of pStat3 and pSmad1,5,8, namely an index of diminished Jak/Stat and Bmp pro-astrogenic signaling, respectively, and an increase of NCoR, possibly associated to augmented ErbB4 anti-gliogenic signalling.

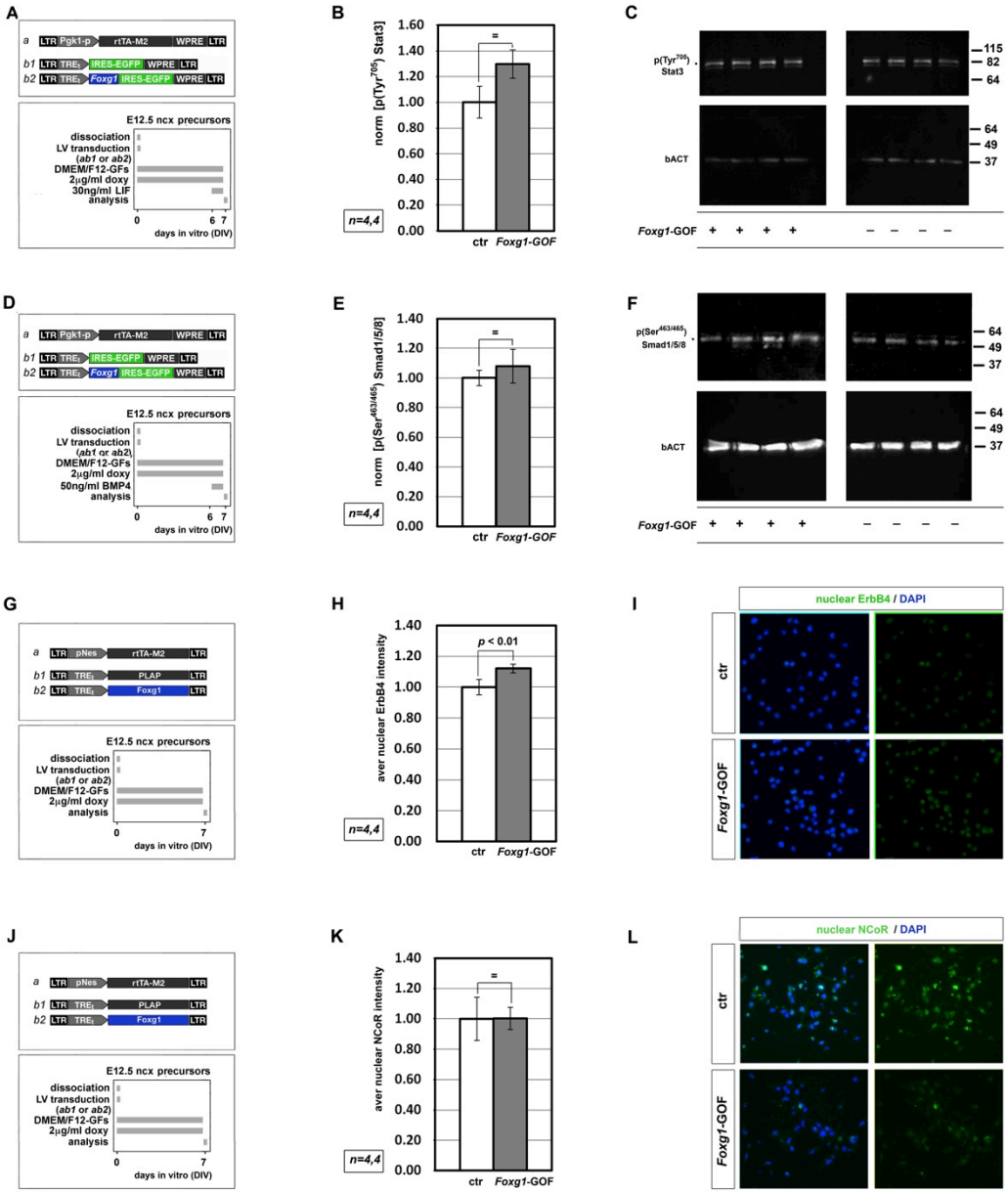

Figure R.4. Immunoprofiling of *Foxg1* gain-of-function cortico-cerebral cultures for key intracellular signalling transducers, within the whole population. Experimental strategies and lentiviral vectors employed for their implementation are shown in (**A,D,G,J).** Western blot **e**valuation of **(A-C)** p(Tyr^{705})Stat3 and **(D-F)** p(Ser^{463}/Ser^{465})Smad1/5/8 protein levels in derivatives of neocortical (ncx) precursors, acutely infected with LV:*pPgk1-rtTA2S-M2* and, alternatively, LV:*TREt-IRES2-EGFP* (ctr) or LV:*TREt-Foxg1-IRES2-EGFP* (*Foxg1*-GOF). Cells kept for 7 days under pro-proliferative medium; doxycyclin administered at DIV0–7. Lif (A-C) and Bmp4 (D-F) added to the medium 24 hours prior to analysis. Cells immunoprofiled at DIV7. Data normalized against sample (ctr). Evaluation of **(G-H)** p(Tyr^{1284})ErbB4-ICD and **(J-K)** NCoR protein levels within the nucleus of derivatives of cortical precursors, acutely infected with LV:*pNes/hsp68-rtTA2S-M2,* and, alternatively, LV:*TREt-IRES2-PLAP* (ctr) or LV:*TREt-Foxg1-IRES2* (*Foxg1*-GOF). Cells kept for 7 days under pro-proliferative medium and attached on poly-L-lysin-coated coverslips at DIV7; doxycyclin administered at DIV0–7. Cells immunoprofiled at DIV7. Data normalized against sample (ctr). *n* is the number of biological replicates; *p*-value calculated by t-test (one-tail, unpaired). **(I,L)** Examples of ErbB4-ICD$^+$ and NCoR$^+$ cells referred to in (H) and (K), respectively. In all figures, values normalized against controls.

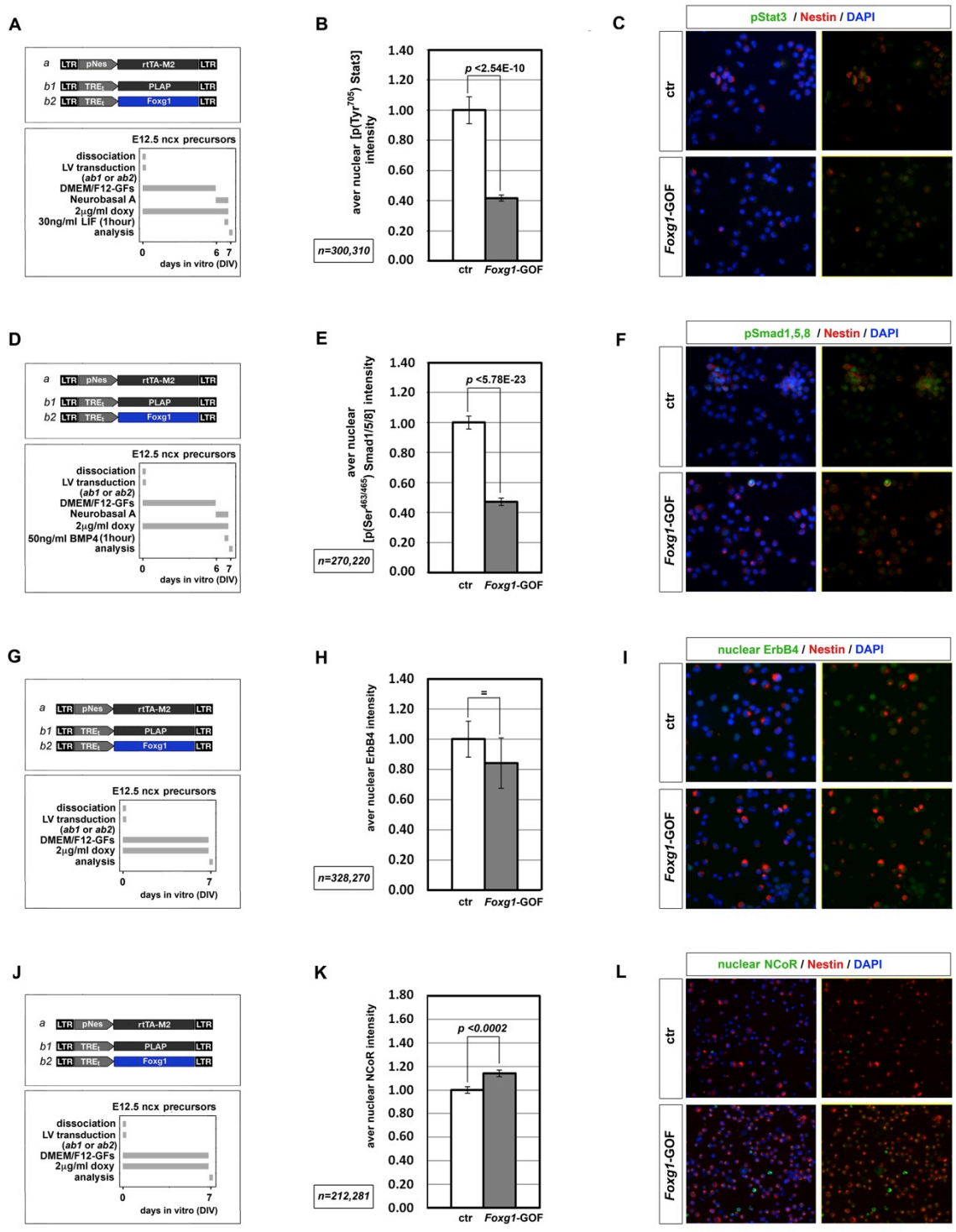

Figure R.5. Immunoprofiling of *Foxg1* gain-of-function cortico-cerebral cultures for key intracellular signalling transducers, within the neural stem cell population. Experimental strategies and lentiviral vectors employed for thei implementation are shown in **(A,D,G,J).** Evaluation of **(B)** p(Tyr^{705})Stat3, **(E)** p(Ser^{463}/Ser^{465})Smad1/5/8, **(H)** p(Tyr^{1284})ErbB4-ICD and **(K)** NCoR protein levels within the nucleus of Nestin+ derivatives of neocortical (ncx) precursors, acutely infected with LV:*pNes/hsp68-rtTA2S-M2,* and, alternatively, LV:*TREt-IRES2-PLAP* (ctr) or LV:*TREt-Foxg1-IRES2* (*Foxg1*-GOF). Cells kept for 7 days under pro-proliferative medium and attached on poly-L-lysin-coated coverslips at DIV6, under Neurobasal A medium, supplemented with B27, 200µM L-glutammine, Pen/Strept, GFs; doxycyclin administered at DIV0–7; Lif (A-C) and Bmp4 (D-F) added to the

medium 1 hour prior to the analysis. Cells immunoprofiled at DIV7. Data normalized against sample (ctr). *n* is the number of biological replicates; *p*-value calculated by t-test (one-tail, unpaired). **(C)**, **(F)**, **(I)** and **(L)** Examples of p(Tyr^{705})Stat3^{+}/Nestin^{+}, p(Ser^{463}/Ser^{465})Smad1/5/8^{+}/Nestin^{+}, p(Tyr^{1284})ErbB4-ICD^{+}/Nestin^{+} and NCoR^{+}/Nestin^{+} cells referred to in (B), (E), (H) and (K), respectively.

To assess functional relevance of the moderate NCoR upregulation observed, we tried to rescue the S100β^{+} output of *Foxg1*-GOF cultures, by knocking down *Tab2*, whose protein product is essential to anti-astrogenic NCoR activity upon ErbB4 stimulation. We engineered E12.5 precursors for conditional *Foxg1* overexpression, in the presence of a short hairpin against Tab2 (αTab2-shRNA) or a control. We kept cells in pro-proliferative conditions for seven days, and then transferred them to poly-L-lisine coverslips under pro-differentiative Neurobasal A medium for four days. Finally, we immunolabeled cells for S100β marker (*Fig. R.6 A*). Remarkably, αTab2-shRNA rescued the astroglial output of *Foxg1*-GOF samples, while not increasing S100β^{+} cell frequency in controls (*Fig. R.6 B,C*). This suggests that the ErbB4/Tab2/NCoR pathway is a likely key mediator of *Foxg1* antiastrogenic activity.

However, to complete the reconstruction of the antigliogenic cascades ruled by *Foxg1*, further in depth analysis of transactive pathways and epigenetic state of chromatin they converge on will be required.

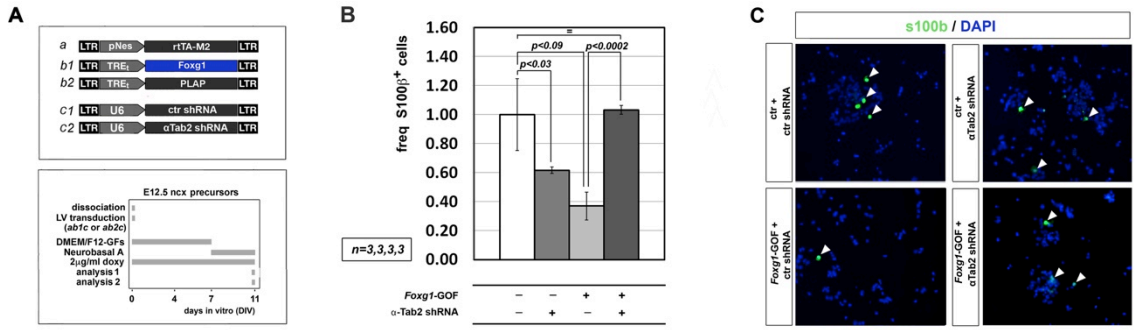

Figure R.6 Tab2 mediate antiastrogenic properties of *Foxg1* in derivatives of E12.5 cortico-cerebral precursors. Experimental strategy and lentiviral vectors employed for its implementation are shown in (**A). (B)** Frequencies of S100β^{+} derivatives of neocortical (ncx) precursors, acutely infected with LV:*pNes/hsp68-rtTA2S-M2,* and, alternatively, LV:*TREt-IRES2-PLAP* (ctr) or LV:*TREt-Foxg1-IRES2* (*Foxg1*-GOF) and also LV:*U6p-ctr-shRNA* or LV:*U6p-αTab2-shRNA*. Cells kept for 7 days under pro-proliferative medium and 4 more days under pro-differentiative medium; doxycycline administered at DIV0-11. Cells immunoprofiled at DIV 11. Data normalized against *PLAP^{+}/ctr-shRNA^{+}* control sample (ctr) absolute frequency of

S100β+ in (ctr), 21.36±5.27%. Scale bar=s.e.m. *n* is the number of biological replicates; *p*-value calculated by t-test (one-tail, unpaired). **(C)** Examples of S100β+ cells referred to in (B).

4.2 *Emx2* regulation of astrogenesis

4.2.1 *Emx2* overexpression reduces astrogenesis

We previously reported that prolonged *Emx2* overexpression in early pallial NSCs results in a substantial decrease of their ultimate glial output. We suspected that this could be due to a precocious shrinkage of the proliferating astrogenic pool (Brancaccio et al., 2010). These observations were made in vitro. To verify if this also happens in vivo, we injected a plasmid driving *Emx2* overexpression into the lateral ventricular cavity of P0 brains and electroporated it into periventricular precursors of the posterior parietal wall. Four days later, we sacrificed pups and inspected heavily electroporated regions of their neocortices for distribution of astroglial cells. As expected, we found that $S100\beta^+$ astrocytes and $S100\beta^+Ki67^+$ astroglial proliferating progenitors laying above a periventricular border of defined length were down regulated by 27.87±6.90% ($p<0.049$, $n=5,5$) and 47.85±5.97% ($p<0.006$, $n=5,5$), respectively, compared to controls (*Fig. R.7 A,B,E*). To rule out that this result was due to a dominant negative effect, astrogenesis was also scored in the posterior cortex of E17.5 *Emx2*$^{-/+}$ embryos. Here, frequencies of $S100\beta^+$ astrocytes and $S100\beta^+Ki67^+$ astroglial proliferating progenitors were upregulated by 33.24±11.03% ($p<0.040$, $n=5.5$) and 129.61±6.74% ($p<0.063$, $n=3.3$), respectively (*Fig. R.7 C,D,F*), suggesting that dampening of astrogenesis is a genuine function exerted by Emx2 in vivo.

Then, in order to set up an in vitro model suitable to dissect molecular mechanisms underlying *Emx2* antiastrogenic activity, we engineered dissociated E12.5 cortico-cerebral precursors for conditional Emx2 overexpression. We activated the transgene at in vitro equivalent of perinatal age and finally evaluated the astroglial output. Immunoprofiling of engineered cultures at DIV21 revealed that, similarly to in vivo, $S100\beta^+$ cells were reduced by 31.88±7.10% ($p<0.007$, n=3,3), compared to controls (*Fig. R8 A*). Interestingly, the decrease of these cells was preceded by a shrinkage of the astrogenic proliferating pool, -66.78±10.31% at DIV13 compared to controls ($p<0.003$, $n=3,3$) (*Fig. R8 B,C*). Consistently, BrdU uptake within the astrogenic lineage was also diminished (*Suppl. Fig. S.3*). Noticeably, in both controls and *Emx2*-GOF cultures, almost 9/10 of $S100\beta^+$ cells (87.14±2.69% and

89.72±0.83%, respectively, with $p<0.205$ and $n=3,3$) were also immunoreactive for the established Aldolase C (AldoC) pan-astrocytic marker (*Suppl. Fig. S.1 A,B*).

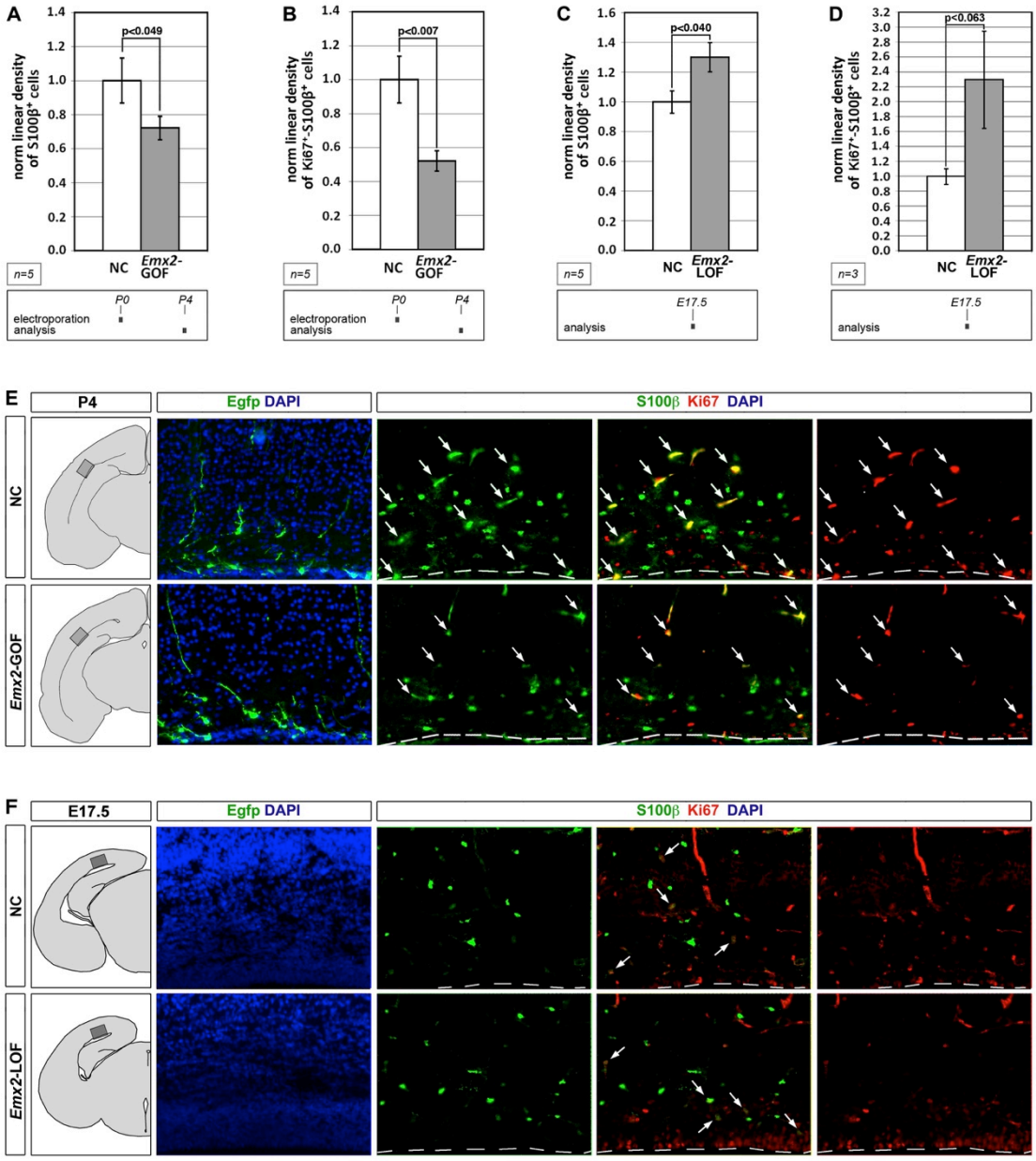

Figure R.7. Reduced astrocytogenesis upon *Emx2* manipulation, in vivo. (A, B) Linear densities of S100β+ astrocytes and S100β+Ki67+ astroglial proliferating progenitors in the posterior parietal cortex of P4 pups electroporated at P0 with a pCMVIRES2-*EGFP* control (NC) and, alternatively, a constitutive pCMV-*Emx2*-IRES2-EGFP expressor plasmid (*Emx2*-GOF). Data normalized against sample (NC); absolute frequencies of S100β+ and S100β+Ki67+ cells in (NC), 40.9±5.4 cells/100 mm and 11.7±1.6 cells/100 mm, respectively. Scale bar=s.e.m. **(C, D)** Linear densities of S100β+ astrocytes and S100β+Ki67+ astroglial proliferating progenitors in the posterior parietal cortex of E17.5 embryos heterozygous for an *Emx2* null allele and their littermate wild type controls. Data normalized against sample (NC); absolute frequencies of S100β+ and S100β+Ki67+ cells in (NC), 9.6±0.8 cells/100 mm

and 1.7±0.2 cells/100 mm, respectively. Scale bar=s.e.m. **(E)** Examples of S100β$^+$Ki67$^+$ cells (arrows) referred to in (B), located in highly electroporated regions highlighted with anti-EGFP immunofluorescence on adjacent sections. **(F)** Examples of S100β$^+$Ki67$^+$ cells (arrows) referred to in (D).

Moreover, only <1/10 of them (8.43±1.80% and 6.38±0.79%, respectively, with p<0.178 and n=3,3) also expressed the oligodendrocytic marker CNPase (Supp. Info. Fig. S1C,D). That confirms that these S100β$^+$ cells were to large extent astrocytes. Finally, to get further insights into *Emx2* mechanisms of action, we run a gain-of-function test similar to the one described in *Fig. R.8*, however mixing lentivirus-engineered precursors with an excess of naive, wild type precursors (in a 1:9 ratio), just before transgene activation. Remarkably, even in this case, the fraction of engineered cells expressing S100b was reduced upon *Emx2* overactivation, by 36.75±1.39% (p<0.002 and n=3,3) (*Suppl. Fig. S.2*). This means that the Emx2 impact on astrogenesis relies to large extent on cell autonomous mechanisms.

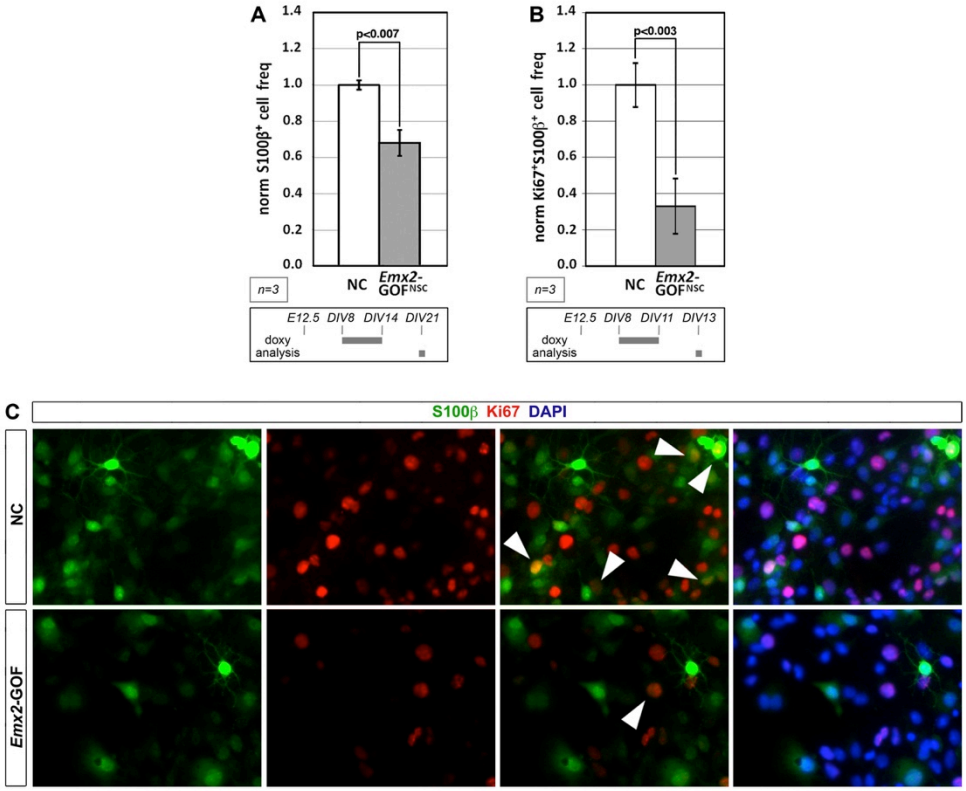

Figure R.8. Reduced astrocytogenesis upon *Emx2* overexpression, in vitro. (A) Frequencies of S100β⁺ derivatives of cortical precursors, acutely infected with LV:*pNes/hsp68-rtTA2S-M2* and, alternatively, LV:*TREt-IRES2-EGFP* (NC) and LV:*TREt-Emx2-IRES2-EGFP* (*Emx2*-GOF). Cells kept for 2 weeks under anti-differentiative medium and 1 more week under pro-differentiative medium; doxycyclin administered at DIV8–14. Data normalized against sample (NC); absolute frequency of S100β+ cells in (NC), 17.52±0.54%. Scale bar=s.e.m. **(B)** Frequencies of S100β⁺Ki67⁺ derivatives of cortical precursors, acutely infected as in (A). Cells kept for 11 days under antidifferentiative medium and 2 more days under GF-supplemented pro-differentiative medium; doxycyclin administered at DIV8–11. Data normalized against sample (NC); absolute frequency of NC S100β⁺Ki67⁺ cells, 10.48±0.72%. Scale bar=s.e.m. **(C)** Examples of S100β⁺Ki67⁺ cells (arrowheads) referred to in (B).

4.2.2 Molecular mechanisms mediating antiastrogenic properties of *Emx2*

To get hints on molecular mechanisms mediating such astrogenesis reduction, we monitored a few established genes promoting the expansion of the astrogenic proliferating pool: EgfR ((Mayer et al., 2009; Viti et al., 2003)), Fgf9 (Lum et al., 2009) and Sip1 (Seuntjens et al., 2009). Interestingly, Emx2 downregulated *EgfR* and *Fgf9* by 31.10±6.74% (p<0.008, n=3) and 49.24±8.23% (p<0.025; n=3), respectively, while not affecting *Sip1* (*Fig. R.9 A*). Consistently, *EgfR*-mRNA and *Fgf9*-mRNA were upregulated in isochronic *Emx2*$^{+/-}$ cultures, by circa 74.60±31.21% (p<0.07, n=3) and 29.78±1.18% (p<0.069, n=2), respectively (*Fig. R.9 B*).

Intriguingly, FACS profiling of NSC-restricted-Emx2-GOF cultures revealed no significant change in frequencies of EgfR^{+} NSCs. Conversely, it showed a delayed and pronounced reduction of EgfR levels within the astrogenic compartment (*Fig. R.9 C,D*), pointing to an indirect regulation of EgfR by Emx2.

To assay functional relevance of EgfR and Fgf9 down regulation to *Emx2* depression of astrogenesis, we delivered a lentivector driving constitutive EgfR expression to Emx2-GOF cultures at DIV8 and, alternatively, we supplemented these cultures with exogenous Fgf9. Both treatments rescued the normal astroglial output. When they were administered to Emx2-wt cultures, this parameter was not affected (*Fig. R.9 E,F*). Remarkably, both EgfR and Fgf9 also rescued the shrinkage of the astrogenic proliferating pool induced by *Emx2* (*Fig. R.9 G,H*). Finally, the amplitude of astrogenesis reduction elicited by either *Emx2* overexpression in NSCs or Egf removal from the culturing medium at astrocytogenesis peak time were comparable (*Suppl. Fig. S.4*). Altogether, these data strongly support the hypothesis that both EgfR and Fgf9 downregulation mediate the *Emx2* impact on astrogenesis.

Regarding molecular mechanisms underlying *Emx2* activity, poor sensitivity of EgfR and Fgf9 levels to exogenous Fgf9 addition and EgfR overexpression, respectively (*Suppl. Fig. S.5*), suggested that *Emx2* regulation of astrogenesis may proceed along two different pathways.

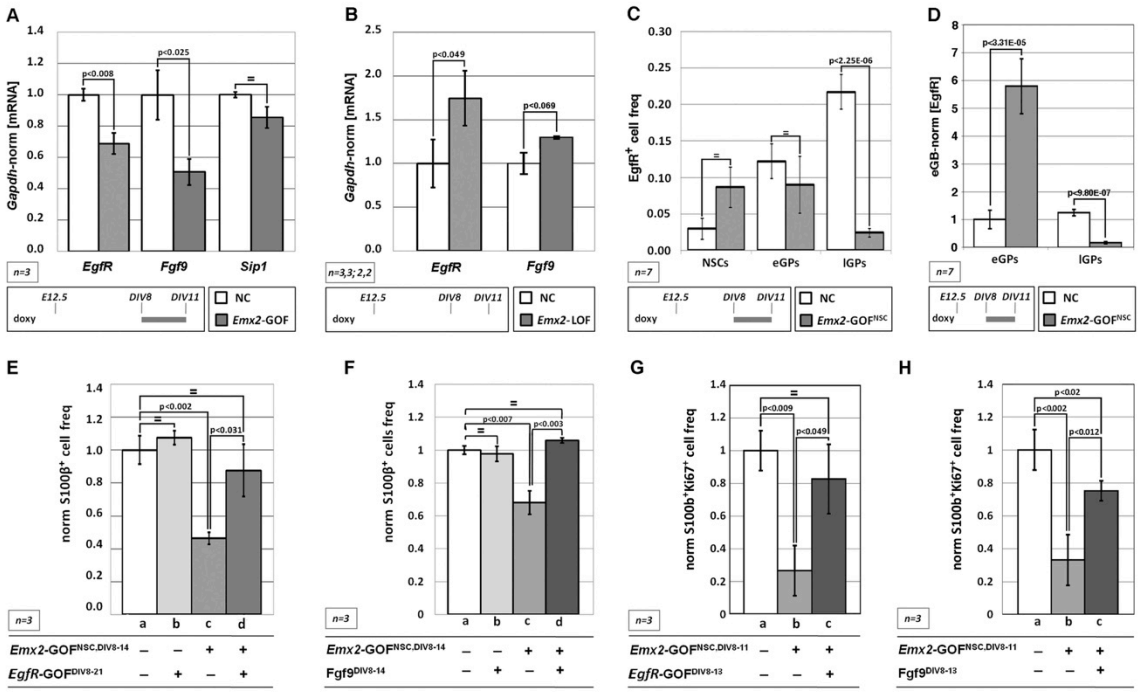

Figure R.9. *EgfR* and *Fgf9* mediate antiastrogenic properties of *Emx2* in derivatives of E12.5 cortico-cerebral precursors. **(A)** *EgfR*-, *Fgf9*-, and *Sip1*-mRNA levels in derivatives of precursors acutely infected with LV:*pPgk1-rtTA2S-M2* and, alternatively, LV:*TREt-IRES2-EGFP*(NC) or LV:*TREt-Emx2-IRES2-EGFP* (*Emx2*-GOF). Cells kept for 11 days under anti-differentiative medium; doxycyclin administered at DIV8–11. Data double-normalized, against endogenous Gapdh-mRNA and (NC) values. **(B)** EgfR- and Fgf9-mRNA levels in derivatives of wild type (NC) and $Emx2^{+/-}$ (*Emx2*-LOF) precursors. Culture conditions and data normalization as in (A). **(C)** Frequencies of EgfR expressing elements in derivatives of precursors acutely infected with LV:*pNes/hsp68-rtTA2S-M2*, LV:*pTa1-mCherry* and, alternatively, LV:*TREt-IRES2-EGFP* (NC) or LV:*TREt-Emx2-IRES2-EGFP* (*Emx2*-GOF^{NSC}). Culture conditions as in (A), standard Egf replaced by Alexa 555-tagged Egf at DIV9–11. FACS-profiling after terminal anti-A2B5-APC labeling. Frequencies of EgfR-expressing cells evaluated within the neural stem cells (NSCs), early glial progenitors (eGPs), and late glial progenitors (lGPs) compartments. **(D)** EgfR cytofluorescence levels in $EgfR^+$ glial progenitors, normalized against eGPs. In (C, D), different precursor types recognized according to the following profiles: NCS=*pNes*-$EGFP^+$/antiA2B5-APC^-/pTa1-$mCherry^-$; eGPs=*pNes*-$EGFP^+$/antiA2B5-APC^+/pTa1-$mCherry^-$; lGPs=*pNes*-$EGFP^-$/antiA2B5-APC^+/pTa1-$mCherry^-$). **(E)** Frequencies of S100β+ derivatives of cortical precursors, acutely infected with LV:*pNes/hsp68-rtTA2S-M2* (a-d), LV:*TREt-IRES2-EGFP* (a, b) and LV:*TREt-Emx2-IRES2-EGFP* (c, d), and subsequently (DIV8) superinfected with LV:*TREt-luc* (a, c) and LV:*pPgk1-EgfR* (b, d). Cells kept for 2 weeks under anti-differentiaive medium and 1 more week under pro-differentiative medium; doxycyclin administered at DIV8–14. Data normalized against sample (a); absolute frequency of $S100\beta^+$ cells in (a), 19.95±1.72%. p(Emx2/EgfR interaction, 2-ways ANOVA)< 0.10. **(F)** Frequencies of $S100\beta^+$ derivatives of cortical precursors, acutely infected with LV:*pNes/hsp68-rtTA2S-M2* (a-d), LV:*TREt-IRES2-EGFP* (a, b) and LV:*TREt-Emx2-IRES2-EGFP* (c, d), and subsequently (DIV8) exposed to Fgf9 (b, d). Cells kept for 2 weeks under anti-differentiative medium and 1 more week under pro-differentiative medium; doxycyclin administered at DIV8–14. Data normalized against sample (a); absolute frequency of $S100\beta^+$ cells in (a), 17.07±0.45%. p(Emx2/Fgf9 interaction, 2-ways ANOVA)<0.002. **(G)** Frequencies of $S100\beta^+Ki67^+$ derivatives of cortical precursors, acutely infected as in (E) and superinfected at DIV8 with LV:*pPgk1-EgfR* (c) and LV:*TREt-EGFP* (a, b). Cells kept for 11 days under anti-differentiative medium, supplemented with doxycyclin at DIV8–11, and 2 more

days under GF-supplemented pro-differentiative medium. Data normalized against sample (NC); absolute frequency of (NC) $S100\beta^+Ki67^+$ cells, 9.81±0.54%. Scale bar=s.e.m. **(H)** Frequencies of $S100\beta^+Ki67^+$ derivatives of cortical precursors, acutely infected as in (F) and supplemented with Fgf9 at DIV8 (c). Cells kept for 11 days under anti-differentiative medium, supplemented with doxycyclin at DIV8–11, and 2 more days under GF-supplemented pro-differentiative medium. Data normalized against sample (NC); absolute frequency of (NC) $S100\beta^+Ki67^+$ cells, 10.32±0.61%. Scale bar=s.e.m.

As for *Emx2*-dependent EgfR regulation, we speculated that a key role might be played by Bmp signaling. In fact, *Emx2* promotes this signaling, by downregulating its established inhibitors Noggin and Fgf8 ((Bilican et al., 2008; Fukuchi-Shimogori and Grove, 2003; Shimogori et al., 2004)), while Bmps, in turn, inhibit EgfR expression (Lillien and Raphael, 2000). We confirmed the *Emx2* capability to enhance Bmp signaling in our system, by assessing the up regulation of two well-known endogenous reporters of Bmp signaling, *Id3* and *Msx1* (Hollnagel et al., 1999) (*Fig. R.10 A*).

Then, as expected, we found that Bmp inhibition by LDN193189 restored EgfR expression levels in an *Emx2*- GOF environment, while not affecting them in controls (*Fig. R.10 D*).

Concerning Fgf9, its expression might rely on Sox2, which is specifically promoted by signals triggering astrocytic proliferation (Bani-Yaghoub et al., 2006). Emx2 might down regulate Fgf9 by inhibiting the Sox2 activation elicited by Brn2 (Mariani et al., 2012), which is expressed in a variety of neural cells including the astrogenic lineage (Abe et al., 2012). We found that Emx2 overexpression almost silenced Sox2 in cortico-cerebral precursors at astrogenesis peak time (*Fig. R.10 B,C*). Furthermore, Sox2 overexpression rescued Fgf9 levels in an Emx2-GOF environment (*Fig. R.10 E*). This confirms that Sox2 is implicated as a key mediator of Emx2-dependent Fgf9 regulation. As expected, we also found that Brn2 overexpression rescued Fgf9 levels in an *Emx2*-GOF environment, while not affecting them in controls (*Suppl. Fig. S.6*).

Finally, we wondered if Bmp signaling and Sox2 are also implicated in the regulation of Fgf9 and EgfR, respectively.

Interestingly, we observed that both Bmp inhibition by LDN193189 and Sox2 overexpression were able to rescue the inhibition of these two genes elicited by *Emx2* (*Fig. R.10 F,G*). Intriguingly, however, Bmp inhibition in the absence of *Emx2*

overexpression did not affect *Fgf9* (*Fig. R.10 F, compare a and b*). On the other side, while *Emx2* downregulated *Fgf9* in control conditions (*Fig. R.10 F, compare a and c*), it increased *Fgf9*- mRNA levels by >2.25-folds upon Bmp signaling inhibition (*Fig. R.10 F, compare b and d*). This suggests that Bmp signaling might inhibit *Fgf9* expression by antagonizing a hypothetical, *Emx2*-dependent stimulatory pathway (*Fig. R.10 H, question mark*).

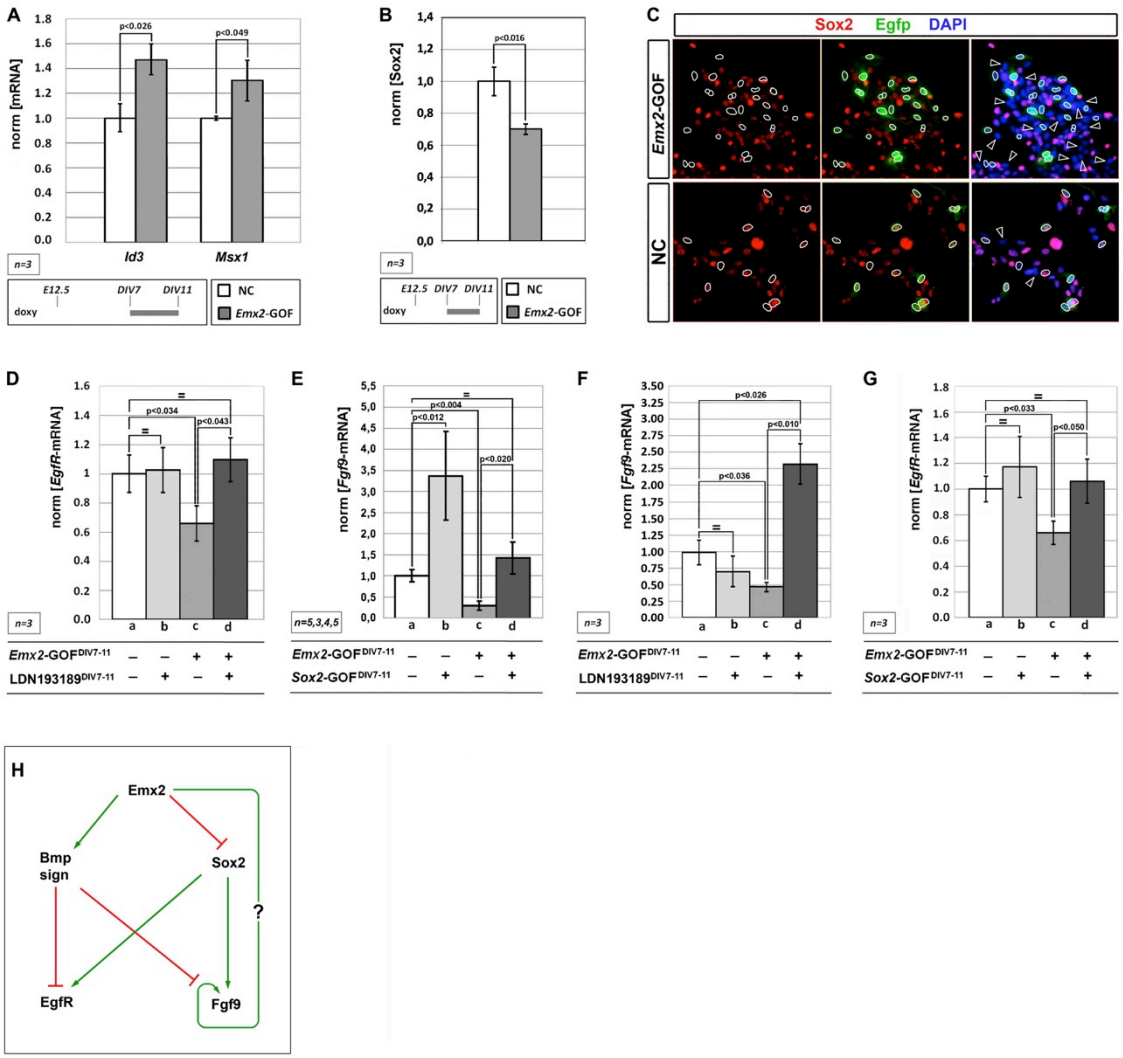

Figure R.10. Emx2 represses EgfR and Fgf9 by enhancing Bmp signaling and inhibiting Sox2. (A) Upregulation of the Bmp targets Id3 and Msx1 in preparations of E12.5 cortico-cerebral precursors, acutely infected with LV:*pPgk1p-rtTA2S-M2* (*Emx2*-GOF, NC), LV:*TREt-IRES2-EGFP* (NC) and LV:*TREt-Emx2-IRES2-EGFP* (*Emx2*-GOF), grown in anti-differentiative medium and subsequently (DIV8) exposed to doxycyclin. Data double-normalized against Gapdh and NC. **(B)** Sox2 levels in cultures of cortico-cerebral precursors prepared as in (A), evaluated by immunofluorescence. Data normalized against NC. **(C)** Distribution of Sox2 immunoreactivity and EGFP fluorescence in cells referred to in (B). Circles delineate heavily

infected cells displaying residual EGFP fluorescence despite of PFA fixation, while arrows point to Sox2-negative cells. **(D)** EgfR-mRNA levels in preparations of E12.5 cortico-cerebral precursors, acutely infected with LV:*Pgk1prtTA2 S-M2* (a-d), LV:*TREt-IRES2-EGFP* (a, b) and LV:*TREt-Emx2-IRES2-EGFP* (c, d), grown in anti-differentiative medium and subsequently (DIV8) exposed to doxycyclin (a-d) and the Bmp-inhibitor LDN193189 (b, d). p(Emx2/LDN193189 interaction, 2-ways ANOVA)< 0.01. **(E)** Fgf9-mRNA levels in preparations of E12.5 cortico-cerebral precursors, acutely infected with LV:*Pgk1p-rtTA2S-M2* (a-d), LV:*TREt-IRES2-EGFP* (a, b), LV:*TREt-Emx2-IRES2-EGFP* (c, d) and LV:*TREt-Sox2* (b, d), grown in anti-differentiative medium and subsequently (DIV8) exposed to doxycyclin (a–d). p(Emx2/Sox2 interaction, 2-ways ANOVA) < 0.04. **(F, G)** Fgf9- and EgfR-mRNA levels in reparations of cortico-cerebral precursors described in (D) and (E), respectively. p(*Emx2*/LDN193189 interaction, 2-ways ANOVA) < 0.001 and p(*Emx2*/Sox2 interaction, 2-ways ANOVA)< 0.5. In (D–G), data double-normalized against Gapdh and samples (a). **(H)** Synopsis of epistatic relationships among Emx2 and mediators of its antiastrogenic activity, inferred from data reported in (A–G). The question mark highlights a hypothetical regulatory branch possibly accounting for data in (Fbd). In (A, B, D–G), Scale bar= s.e.m.

4.2.3 Relevance of *Emx2* dynamics to perinatal burst of astrogenesis

Since neuronogenesis peak time, cortico-cerebral precursors can sense exogenous gliogenic signals and relay them to the nucleus, where chromatin of glial genes is already prone to transcription (Barnabé-Heider et al., 2005; Hatada et al., 2008). Nevertheless, astrogenesis mounts only 4–5 days later,after neuronogenesis completion. Late-embryonic arousal of astrogenic cytokines has been shown to be a main determinant of this schedule (Barnabé-Heider et al., 2005). We hypothesized that high Emx2 levels displayed by multipotent precursors within the neuronogenic time window (Gulisano et al., 1996) could contribute to such schedule, by shrinking the embryonic astrogenic pool and limiting its eventual output.

To test this prediction, first, we compared *Emx2* expression levels in embryonic and perinatal neural precursors. As expected, we found that *Emx2*-mRNA, normalized against three genes mainly active within multipotent precursors of the apical domain, Sox2, Pax6, and Hes5 (http://developingmouse. brain-map.org), progressively decreased from E14.5 to E18.5, concomitantly with the arousal of astrogenesis (*Fig. R.11 A–C*). Then, to corroborate this result, we scored expression levels of the Emx2 protein, using two antibodies. First, we evaluated Sox2-normalized Emx2 immunofluorescence levels in acutely dissociated, single Sox2+ precursors, by means of a mouse monoclonal antibody. Interestingly, such levels resulted almost halved in precursors originating from P0 neocortices compared to their E12.5 counterparts (*Fig. R.11 D,E*). Moreover, we immunoprofiled coronal sections from

E12.5 and E18.5 brains with a rabbit polyclonal antibody. Here, we observed that Emx2 immunoreactivity was extremely high in the E12.5 pallium, while being barely detectable in periventricular layers of the E18.5 neocortex (*Fig. R.11 F*).

Finally, to assess the effects elicited by short term Emx2 overexpression in embryonic NSCs, we challenged embryonic precursors by a Lif-supplemented, pro-differentiative medium.

Wild type precursors kept under Lif for 4 days generated $GFAP^+$ and $S100\beta^+$ cells at frequencies far above untreated controls (not shown). Remarkably, Emx2 overexpression reduced these frequencies by 76.22±4.07% ($p<0.0004$, $n=3$) and 40.16±9.17% ($p<0.02$, $n=3$), respectively (*Fig. R.11 G,H*). Consistently, neural cultures heterozygous for an *Emx2*-null mutation, kept under Lif for 2 days, gave rise to an almost double $S100\beta^+$ cell output compared to controls (191.85±22.81%, with $p<0.015$, $n=3$, see *Fig. R.11 I*). All this confirmed our predictions.

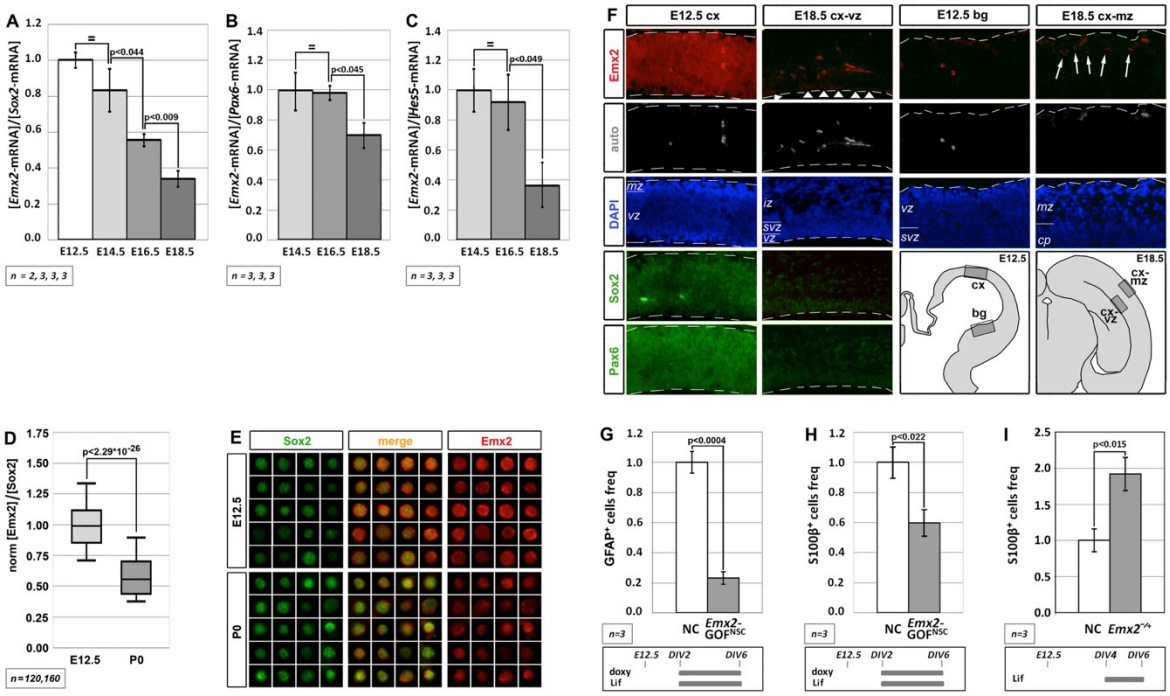

Figure R.11. High Emx2 expression in embryonic cortical NSCs dampens astrogenesis. **(A–C)** Time course profile of *Emx2*-mRNA in the embryonic neocortex. qRT-PCR results normalized against two genes highly expressed in apical multipotent precursors, *Sox2* and *Pax6*, and the NSC marker *Hes5*, and further normalized against E12.5 (A) and E14.5 (B, C) data. (**D**) Distribution of Sox2-normalized Emx2 immunofluorescence levels in acutely dissociated, single Sox2$^+$ precursors originating from E12.5 and P0 neocortices. For each box-plot, bars represent 1st decile, 1st quartile, median, 3rd quartile and 9th decile, respectively. (**E**) Example of Sox2$^+$ cells referred to in (D). (**F**) Distribution of Emx2 immunoreactivity in frontal sections of E12.5 and E18.5 telencephala. Emx2 immunoreactivity (1st row) is compared to endogenous autofluorescence (2nd row) and DAPI staining (3rd row) from the same E12.5 and E18.5 sections, as well as with Sox2 (4th row) and Pax6 (5th row) immunoreactivities from adjacent sections. Emx2 immunoreactivity is very strong in the ventricular zone of E12.5 cortex (1st row, 1st column). It is absent in the same layer of E12.5 basal ganglia (1st row, 3rd column), shown here as an internal, tissuematched, negative control. Arrowheads point to E18.5 periventricular cells weakly immunoreactive for Emx2 (1st row, 2nd column). Arrows indicate Emx2$^+$ Cajal-Retzius cells within the marginal zone, shown here as an internal positive control (1st row, 4th column). Abbreviations: cx, cortex; bg, basal ganglia; vz, ventricular zone; svz, subventricular zone; iz, intermediate zone; cp, cortical plate; mz, marginal zone. (**G, H**) Frequencies of GFAP$^+$ and S100β$^+$ elements originating from E12.5 cortico-cerebral precursors, acutely infected with LV:*pNes/hsp68-rtTA2^S-M2* and, alternatively, LV:*TREt-IRES2-EGFP* (NC) or LV:*TREt-Emx2-IRES2-EGFP (Emx2-GOF^{NSC}*). Cells kept under anti-differentiative medium at DIV1-2 and under Neurobasal A/B27/glutamax at DIV3–6; Lif and doxycyclin administered at DIV3–6. Data normalized against NC samples; absolute frequencies of GFAP$^+$ and S100β$^+$ cells in (NCs), 36.55±62.62% and 46.32±64.86%, respectively. Scale bar = s.e.m. (**I**) Frequencies of S100β$^+$ elements originating from E12.5 cortico-cerebral precursors, wild type and heterozygous for an *Emx2*-null mutation. Cells kept under anti-differentiative medium at DIV1-3 and under Neurobasal A/B27/glutamax at DIV4–6; Lif administered at DIV4–6. Data normalized against (NC) samples; absolute frequencies of S100β$^+$ cells in (NCs), 17.29 ± 62.74%. Scale bar=s.e.m.

4.3 *Emx2* overexpression in glioblastoma multiforme: a therapeutical application

4.3.1 *Emx2* overexpression kills glioblastoma cells *in vitro*

To assess if *Emx2* can antagonize glioblastoma multiforme, we overexpressed its coding sequence in 2 GBM lines (U87MG and T98G) as well as in GBM cell cultures originating from 5 different patients (GbmA, GbmB, GbmC, GbmD and GbmE), via lentiviral vectors and TetON technology. As controls, we employed the corresponding GBM cultures, infected by *Egfp*- or *Emx2*-encoding lentiviruses and kept in the presence or absence of doxycycline, respectively (*Fig. R.12 A,B and Suppl.Fig. S7*). In all cases, the activation of the *Emx2* transgene arrested the expansion of the culture and led to its collapse, usually within 7-8 days, never beyond the 22nd day (*Fig. R.12 C-I*). As we detected in *Emx2*-gain of function (-GOF) GbmA, GbmB and GbmC samples (*Fig. R.12 L-O*), this possibly reflected a decrease of the proliferating fraction (up to -34.5±5.3%, $p<0.01$, in GbmB) (*Fig. R.12 L,M*) and an increase of the apoptotic fraction (up to 539.7±90.5%, $p<0.001$, in GbmB) (*Fig. R.12 N-O*). Intriguingly, G1-to-S phase progression was not affected (*Suppl. Fig. S.8*).

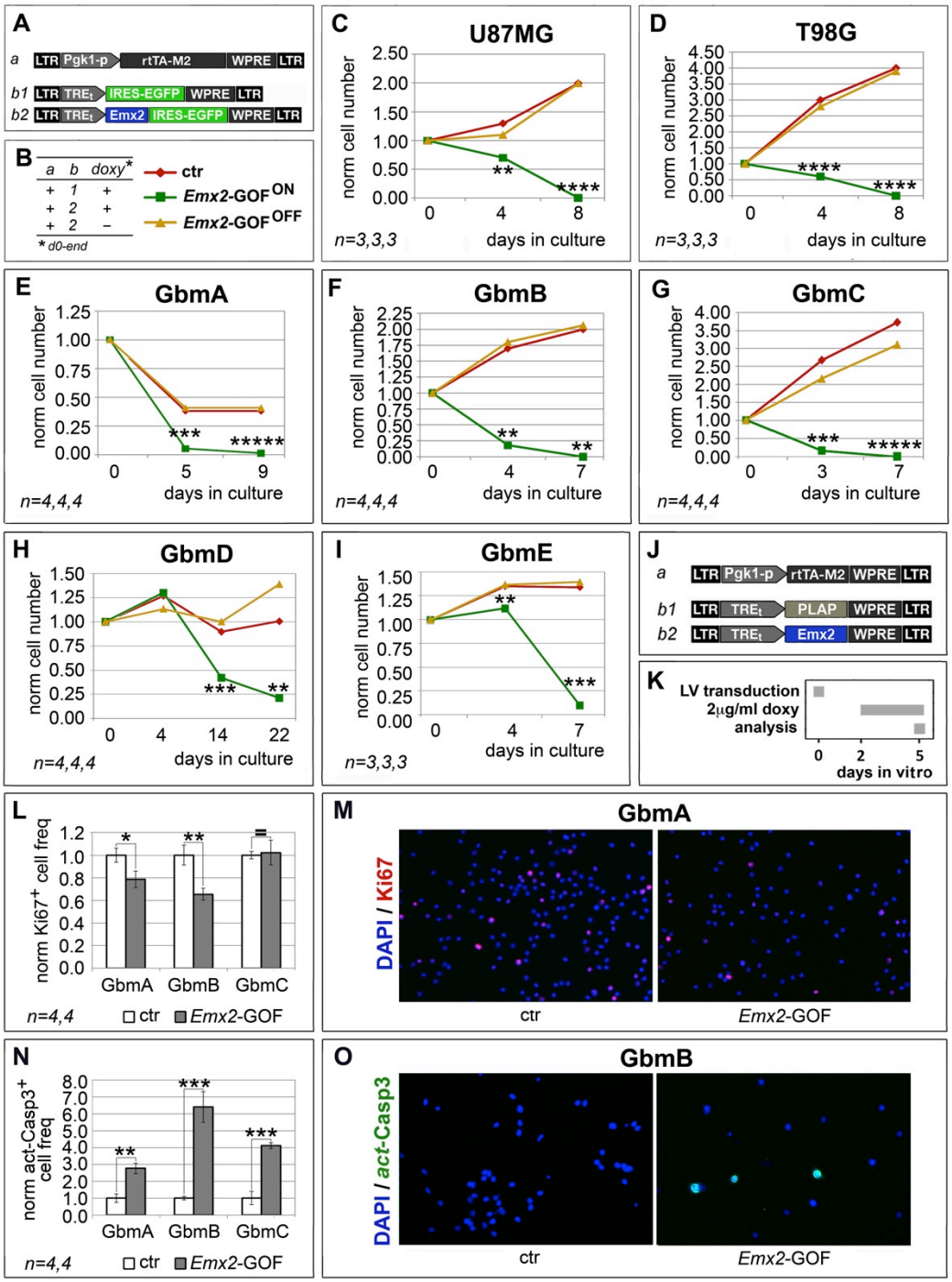

Figure R.12. Population dynamics of *Emx2* gain-of-function GBM cultures. *In vitro* kinetic progression of U87MG, T98G, GbmA, GbmB, GbmC, GbmD and GbmE GBM lines **C-I.**, engineered by lentiviral vectors and TetON technology as in **A, B.**, and kept as adherent **C, D.** or floating cultures **E-I.**, under Fgf2 and Egf. Ki67+ proliferating **L, M.** and activated-Casp3+ apoptotic **N, O.** fractions of GbmA, GbmB and GbmC glioblastoma cells, engineered by control (**J.**, a-b1) and *Emx2*-GOF (J, a-b2) lentiviral sets, and kept as floating cultures according to the timetable in **K.** Cell numbers were normalized against *t*=0 values (C-I), or control values **L, N.** [As for (L, N), absolute average control cell frequencies were: 0.207, 0.155 and 0.131 (Ki67+, in GbmA, GbmB and GbmC cultures, respectively); 0.001, 0.012 and 0.012 (actCasp3+, in GbmA, GbmB and GbmC cultures, respectively)]. *n* is the number of biological replicates. *p*-value was calculated by t-test (one-tail, unpaired): **p<0.05*, ***p<0.01*, ****p<0.001*, *****p<0.0001*, ******p<0.00001*.

Table R.1. Biased mRNA profiling of *Emx2* gain-of-function GBM cultures.

t	Gbm A 3d	Gbm B 3d	Gbm C 3d	Gbm D 3d	U87-MG 4d	gene function
EGFR	0.25 ±0.06 *n=4,4; p<0.03*	0.78 ±0.03 *n=4,4; p<0.05*	0.61 ±0.04 *n=4,4; p<0.001*	0.37 ±0.13 *n=4,4; p<0.02*	0.48 ±0.02 *n=4,4; p<0.0005*	RTK signaling
PDGF	0.40 ±0.004 *n=4,4; p<0.03*	ns	ns	**1.74 ±0.12** *n=4,4; p<0.002*	ns	
PDGFRA	ns	0.75 ±0.11 *n=4,4; p<0.05*	0.80 ±0.07 *n=4,4; p<0.04*	0.55 ±0.01 *n=4,4; p<0.0001*	0.16 ±0.10 *n=4,4; p<0.0001*	
PTEN	ns	1.54 ±0.23 *n=4,4; p<0.05*	ns	**0.30 ±0.03** *n=4,4; p<0.01*	ns	
NF1	ns	ns	ns	**0.26 ±0.01** *n=3,3; p<0.009*	ns	
MYC	ns	ns	ns	0.83 ±0.04 *n=4,4; p<0.04*	ns	cell cycle control
MYCN	0.55 ±0.03 *n=3,3; p<0.02*	ns	ns	0.40 ±0.06 *n=4,4; p<0.01*	ns	
RB1	ns	**0.45 ±0.16** *n=4,4; p<0.02*	ns	**0.46 ±0.04** *n=4,4; p<0.004*	ns	
CDKN2A	ns	2.68 ±0.37 *n=4,4; p<0.01*	ns	**0.22 ±0.01** *n=4,4; p<0.02*	ns	
CDKN2B	ns	2.68 ±0.37 *n=4,4; p<0.01*	ns	**0.22 ±0.01** *n=4,4; p<0.02*	ns	
CDK4	0.48 ±0.07 *n=3,3; p<0.005*	ns	ns	0.81 ±0.06 *n=4,3; p<0.02*	0.72 ±0.08 *n=4,4; p<0.02*	
CDK6	0.30 ±0.02 *n=3,3; p<0.01*	ns	ns	0.36 ±0.004 *n=4,3; p<0.002*	ns	
CCND2	0.16 ±0.06 *n=3,3; p<0.04*	ns	ns	**1.17 ±0.03** *n=4,4; p<0.005*	ns	
SOX2	0.30 ±0.04 *n=4,4; p<0.02*	0.60 ±0.06 *n=4,4; p<0.03*	0.70 ±0.11 *n=4,4; p<0.04*	0.19 ±0.01 *n=4,4; p<0.00001*	ns	other malignancy-related
HES1	2.56 ±0.37 *n=3,3; p<0.008*	8.02 ±0.27 *n=4,4; p<0.0001*	1.38 ±0.05 *n=4,4; p<0.001*	1.28 ±0.02 *n=4,4; p<0.02*	4.34 ±0.80 *n=4,4; p<0.004*	
GLI1	ns	**2.60 ±0.65** *n=4,4; p<0.05*	ns	**2.90 ±0.25** *n=4,4; p<0.001*	ns	
TRP53	ns	2.87 ±0.57 *n=4,4; p<0.008*	4.58 ±0.87 *n=3,3; p<0.01*	**0.67 ±0.05** *n=4,4; p<0.001*	**0.66 ±0.08** *n=4,4; p<0.04*	
MDM2	ns	ns	ns	0.46 ±0.06 *n=4,3; p<0.03*	ns	
VEGF	ns	ns	ns	ns	ns	

Table R.1. mRNA levels of presumptive mediators of *Emx2* anti-oncogenic activity in GBM cells engineered as in Figure 1A. Seven days after lentiviral transduction, doxycyclin was added at 2 µg/ml. RNA samples were collected at time "*t*" after doxycyclin addition. qRT-PCR results, normalized against *GAPDH* and further normalized against their own negative controls, are shown as average ± s.e.m. Values possibly accounting for *Emx2* anti-oncogenic activity are highlighted in blue. ns, not significant. *n* is the number of biological replicates. *p*-value was calculated by t-test (one-tail, unpaired).

4.3.2 *Emx2* antagonizes glioblastoma by a pleiotropic impact on malignancy-related processes

To cast light on molecular mechanisms underlying *Emx2* impact on GBM kinetics, we overexpressed its coding sequence in 5 GBM samples and scored mRNA levels of selected genes involved in their malignancy. These genes include: (a) a group implicated in relaying mitogenic signals along RTK cascades (*EGFR, PDGF, PDGFRA, PTEN, NF1*), (b) a group involved in the control of early G1/late G1 checkpoint (*MYC, MYCN, RB1, CDKN2A, CDKN2B, CDK4, CDK6, CCND2*), and (c) a more heterogeneous group dealing with a variety of malignancy-related processes, such as stemness, apoptosis, neovasculogenesis (*SOX2, HES1, GLI1, TRP53, MDM2, VEGF*). In all samples analyzed, *Emx2* significantly altered the expression of group (a) genes, consistently with its antioncogenic activity. It downregulated *EGFR* in all cases. In addition, it decreased *PDGF* and *PDGFRA* in 1 and 4 cases, respectively, and increased *PTEN*, in 1 case (*Table R.1*). In a large subset of samples, *Emx2* also modulated mRNA levels of group (b) genes, again in agreement with its antioncogenic activity (*Table R.1*). These genes include - in particular - *CDK4* and *CDK6*, mastering the early G1 checkpoint (decreased in 3 and 2 cases, respectively). Finally, *Emx2* downregulated *SOX2* in 4 samples and increased *TRP53* and *HES1* expression, in 2 and 5 samples, respectively (*Table R.1*).

To complement mRNA profiling, we also monitored *Emx2* overexpressing GBM cells for key phospho-proteins involved in malignancy-related, intracellular signal transduction *(Fig. R.13* and *Suppl. Fig. S.9*). We found a significant decrease of p(Thr202/Tyr204)Erk1/2 (-40.3±6.3%, $p<0.005$, see Figure 2C, 2D). This may stem from depressed EGF and PDGF signalling. It may be a key determinant of the kinetic behaviour of *Emx2*- GOF GBM cells (Veliz et al., 2015). Furthermore, we detected a robust increase of p(Ser463/465)Smad1,5,8 (+100%, $p<0.003$, see *Fig. R.13 E,F*). This is an index of enhanced Bmp signalling, which was shown to be instrumental to *Emx2*- dependent inhibition of astroblast proliferation (Falcone et al., 2015). Finally, we found that Stat3 phosphorylation levels in Tyr705 and Ser727, crucial to self-renewing abilities of GBM cells (Park et al., 2013), were unchanged (*Fig. R.13 G-J*).

Next, we tested the functional relevance of selected mRNA/protein changes described above to the *Emx2* antioncogenic activity. For this purpose, we chose a few

"X" agents neutralizing such changes and evaluated their capability to rescue the original GBM kinetic profiles (*Fig. R.14 A-C*).

First, we tried to restore the basic expansion rate of GbmA and GbmC cultures, previously made gain-of-function for *Emx2*, by transducing them with an *EGFR*-expressing transgene (*Fig. R.14 A, rescue X1*). This manipulation slowed down the decline of these cultures, however only in a partial and temporary fashion (*Fig. R.14 D,G*). A similar effect was elicited by overexpression of the stemness-factor *SOX2* (*Fig. R.14 A, rescue X2*) in *Emx2*- GOF GbmA and GbmC (*Fig. R.14 E,H*). Noticeably, neither *EGFR* nor *SOX2* overexpression perturbed GBM kinetics in control conditions (*Fig. R.14 D,E,G,H*).

Moreover, we tried to counteract *HES1*, one of the main *Emx2*-responders, whose overexpression was previously linked to proliferation arrest in a variety of contexts [19–21]. To this aim, we delivered its established functional antagonist *HES6* (Gratton et al., 2003) to GBM cells (*Fig. R.14 A, rescue X3*). This manipulation slowed down the collapse of GbmA and GbmC cultures overexpressing *Emx2*, while not fully preventing it (*Fig. R.14 F,I*). Conversely, *HES6* overexpression did not promote GBM expansion in control conditions (*Fig. R.14 F,I*).

Next, we tried to restore RTK signalling defects evoked by *Emx2* (*Fig. R.13 C,D*), providing GBM cultures with an excess of Fgf9 (*Fig. R.14 A, rescue X4*). This is a key ligand down-regulated by *Emx2* (Falcone et al., 2015) and proven to promote proliferation within the astrocytic lineage (Seuntjens et al., 2009). Also, we silenced BMP signalling (*Fig. R.14 A, rescue X5*), already proposed as a key therapeutic tool against GBM (Li et al., 2014; Piccirillo et al., 2006). Both manipulations slowed down the decline of *Emx2*-GOF GbmA cultures, however only to a partial extent (*Fig. R.14 J,K*). Neither Fgf9 nor BMP-inhibitor delivery promoted an expansion of control GbmA cells (*Fig. R.14 J,K*).

Finally, in addition to *Emx2* impact on transcription, we considered the possibility that the anti-oncogenic activity of this protein could be strenghtened by its capability to chelate the translational factor Eif4e (Nédélec et al., 2004). In agreement with this prediction, *Eif4e* overexpression in *Emx2*-GOF U87MG cultures (*Fig. R.14 A, rescue X6*) delayed their decline, while not affecting U87MG controls (*Fig. R.14 L*).

All that suggests that *Emx2* may act by perturbing a number of genes and metabolic nodes crucial to GBM aggressiveness. It points at *Emx2* as a promising

therapeutic tool to simultaneously attack a variety of key effectors of GBM malignancy.

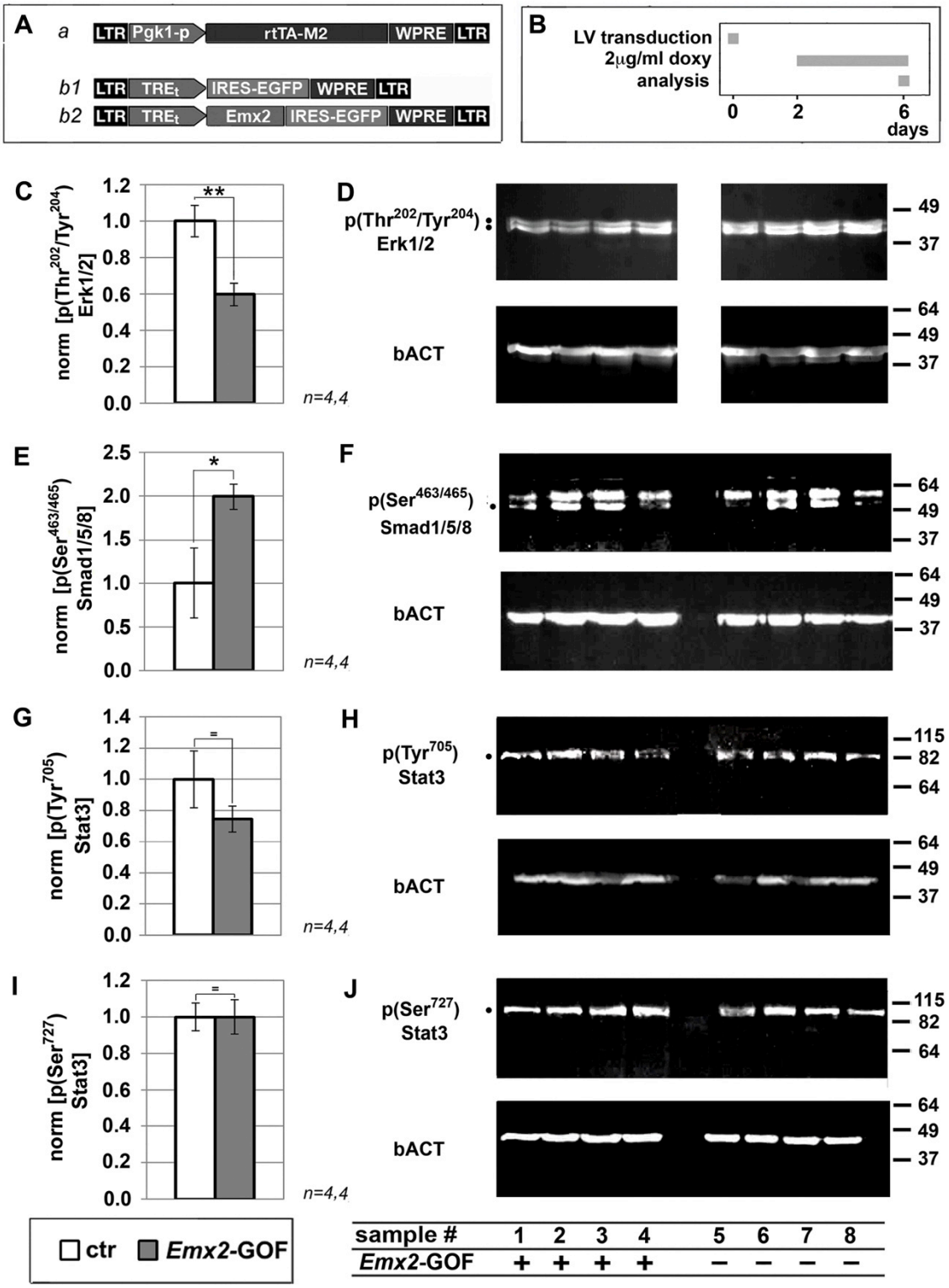

Figure R.13. Immunoprofiling of *Emx2* gain-of-function GBM cultures for key intracellular signaling transducers. Western blot evaluation of p(Thr^{202}/Tyr^{204})Erk1/2 **(C, D)** p(Ser^{463}/Ser^{465})Smad1/5/8 **(E,F)** p(Tyr^{705})Stat3 **(G,H)** and p(Ser^{727})Stat3 **(I,J)** levels in U87 cell samples, engineered as in **A, B.** Values were normalied against controls. *n* is the number of biological replicates. *p*-value was calculated by t-test (one-tail, unpaired): **p<0.05*, ***p<0.01*.

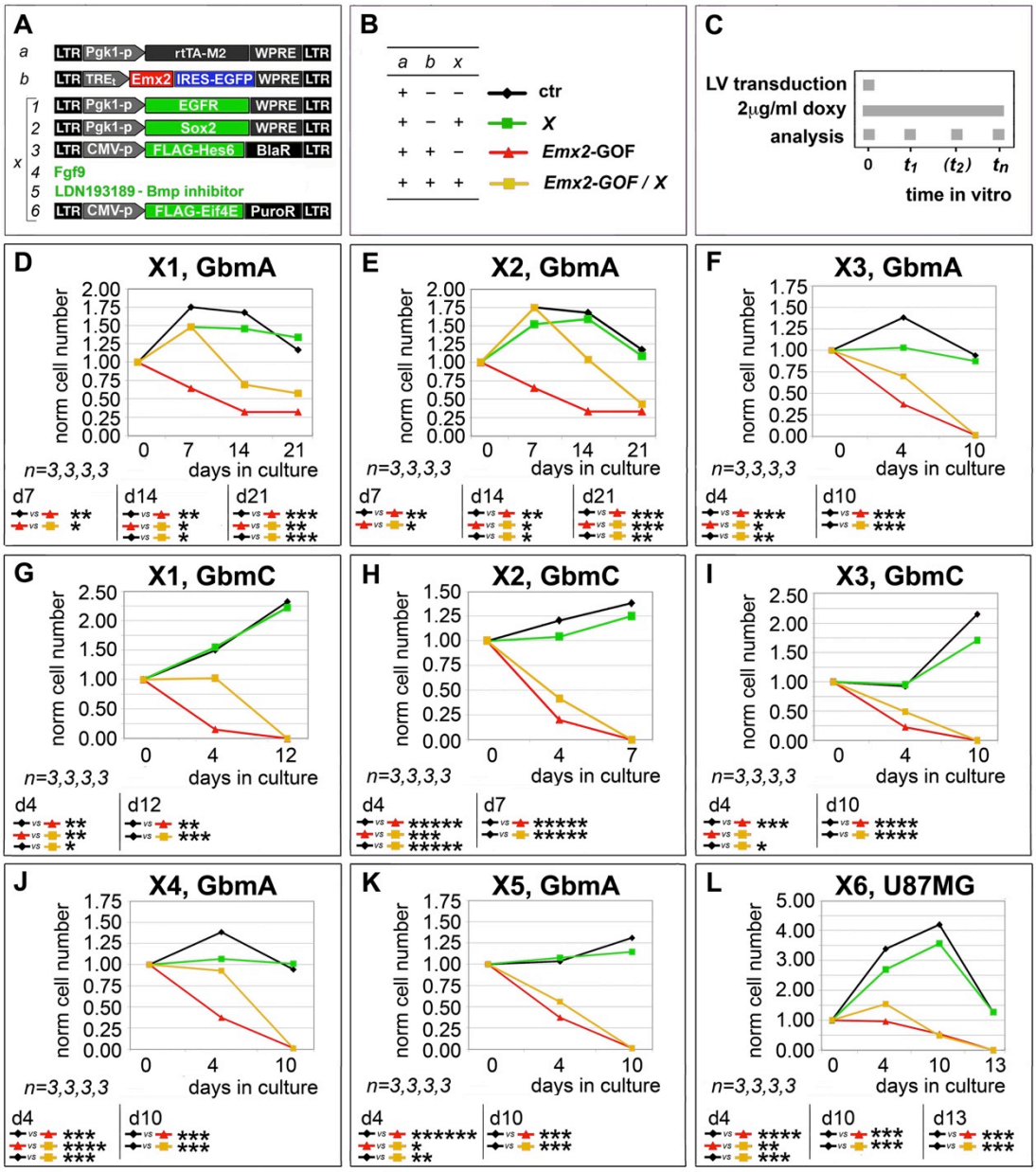

Figure R.14. Rescue of *Emx2* antioncogenic activity via modulation of its presumptive mediators. GBM cells were engineered and cultured as in (**A-C)** In particular, lentiviruses harboring an *IRES-EGFP* or a *PLAP* module under the control of a *TREt* promoter were used as controls for "b" and "X1, X2, X3, X6", respectively. Cells were scored for the capability of selected "X" agents (restoring presumptive mediators of *Emx2* anti-oncogenic activity) to rescue their control kinetic profiles (**D-L)** *n* is the number of biological replicates. *p*-value was calculated by t-test (one-tail, unpaired).

4.3.3 *Emx2* overexpression is suitable to antagonize GBM *in vivo*

To assess the portability of *Emx2* antioncogenic activity *in vivo*, we transplanted engineered GBM cells (U87MG, GbmA, GbmC and GbmD) into the neocortical parenchyma of P4 wild-type mouse pups. Specifically, we injected a 1:1 mix of cells, made alternatively gain-of-function for *Emx2* or a control, and labelled with Egfp and mCherry, respectively. One week later, we sacrificed the animals and scored each brain for the ratio between the number of *Emx2*-GOF cells (Egfp+) and the number of control cells (mCherry^{+}). This ratio was equal to 0.40±0.05 (p<0.099, n=3), 0.44±0.13 (p<0.049, n=4), 0.34±0.12 (p<0.025, n=4) and 0.29±0.04 (p<0.006, n=4), for U87MG, GbmA, GbmC and GbmD, respectively (*Fig. R.15*). (In a previous pilot test run with Egfp+ and mCherry+ GBM cells not harboring additional transgenes, this ratio was close to 1) (*Suppl. Fig. S.10*).

To complement this analysis, we investigated if Emx2 overexpression may increase the survival time of GBM-transplanted mice in a classical long-term assay. To this aim, we transplanted engineered, EGFP-labeled GBM cells (U87MG) into the striatum of 5 weeks old nude mice. In particular, we injected 300,000 *Emx2*-GOF cells to a former group and 300,000 control cells to the other group. Remarkably, we found that mice transplanted with *Emx2*-GOF GBM cells displayed a median survival of 55 days against the 35 days of the control group (p<0.001, n=14,14) (*Fig. R.16*). Together with the previous set of in vivo experiments, these results indicate that *Emx2* exerts a robust antioncogenic activity even *in vivo.*

Disappontingly, *Emx2* overexpression in pyramidal neurons is highly toxic (our unpublished data). Therefore, generalized *Emx2* delivery to the diseased brain of GBM patients would not be a suitable approach. To circumvent this issue, we thought to restrict therapeutic *Emx2* overexpression to tumor precursor cells, by putting it under the control of a cis-active element selectively firing in neural stem cells *(Fig. R.17 A, "Nes-p"; Suppl. Fig. S.11*). Remarkably, this design turned out to be feasible, as it successfully replicated the kinetic outcome elicited upon generalized *Emx2* overexpression (compare *Fig. R.17 C,D and Fig. R.12 E,F*).

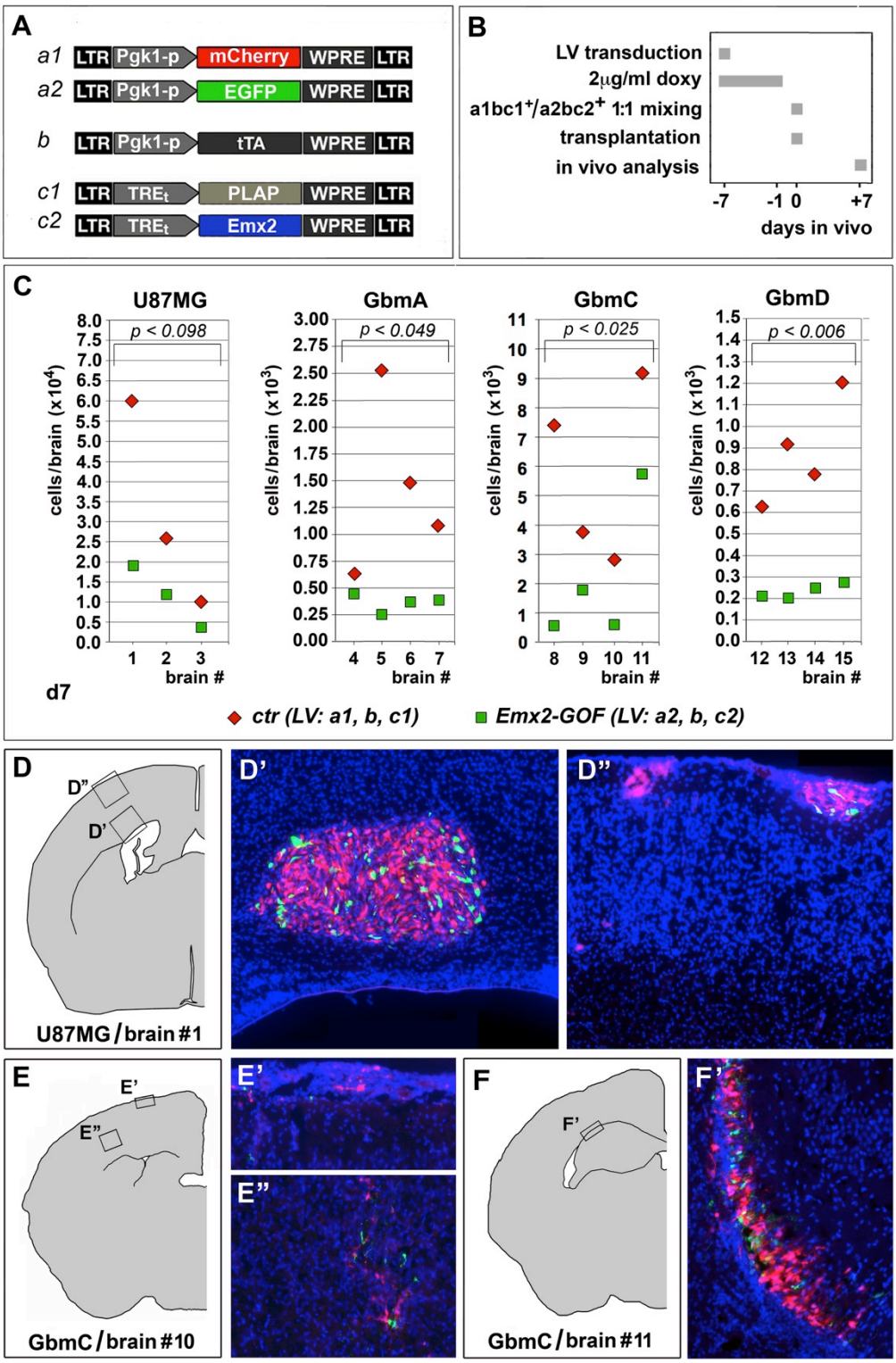

Figure R.15. *Emx2* antioncogenic activity *in vivo,* short-term experiments. Experimental strategy and lentiviral vectors employed for its implementation are shown in **(A,B).** A 1:1 mix of differently fluoro-labelled, *Emx2*-GOF and control engineered GBM cells was transplanted into the cortical parenchyma of P4 wild type mouse pups. One week later, engrafted cells of different genotypes were scored in every single brain (**C-F').** 3-4 different brains were analyzed for every GBM line tested. *p*-value was calculated by t-test (one-tail, paired).

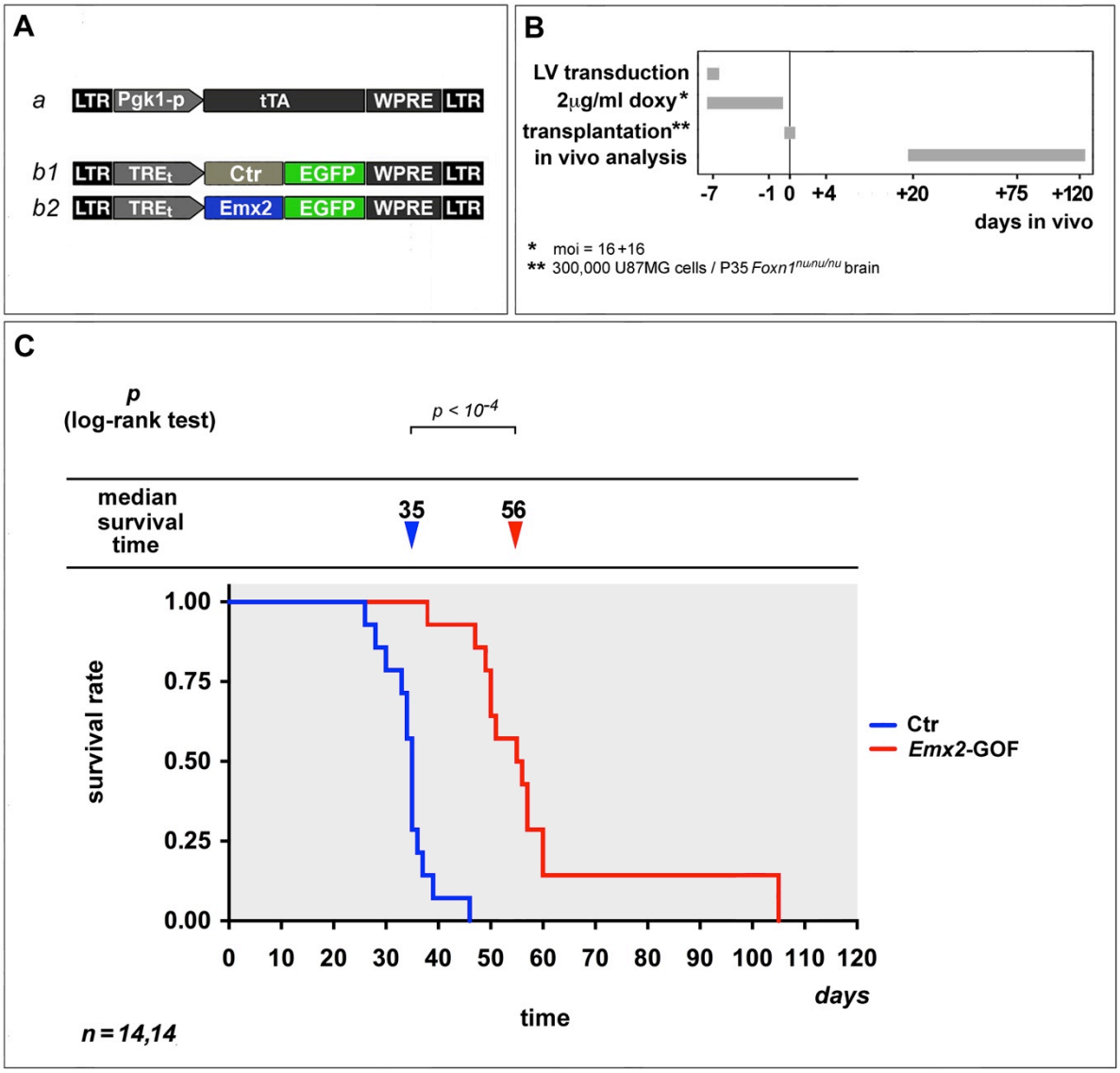

Figure R.16 *Emx2* antioncogenic activity *in vivo,* long-term survival tests. Experimental strategy and lentiviral vectors employed for its implementation are shown in **(A,B).** EGFP-labelled, *Emx2*-GOF or control engineered GBM cells were transplanted into the cortical parenchyma of juvenile immunosuppressed (Foxn1$^{nu/nu}$) mice. Animal survival was scored. *n* is the number of mice for each group. *p*-value was calculated by long-rank test.

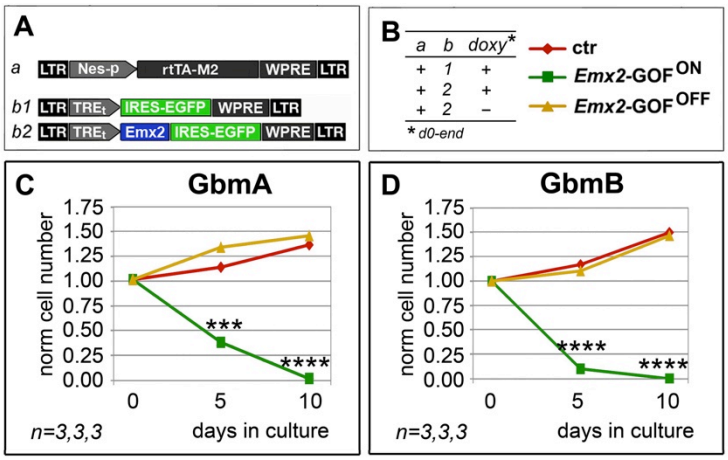

Figure R.17. Persisting antioncogenic efficacy of *Emx2* upon neural nestin enhancer-restricted overexpression. *In vitro* kinetic progression of GbmA and GbmB lines **(C,D)**, engineered by lentiviral vectors and TetON technology as in **(A,B)**, and kept as floating cultures, under Fgf2 and Egf. Cell numbers were normalized against *t*=0 values. *n* is the number of biological replicates. *p*-value was calculated by t-test (one-tail, unpaired): ****p<0.001*, *****p<0.0001*.

Figures from *R.7* to *R.11* were adapted from (Falcone et al., 2015) and *Figures* from *R.12* to *R.17* were adapted from (Falcone et al., 2016).

5. DISCUSSION

In this study, I investigated the neurodevelopmental role of two transcription factors involved in the inhibition of astrogenesis and the exploitability of one of them for gene therapy of glioblastoma multiforme tumor.

Astrocytes generation within the developing cerebral cortex is a finely regulated process. Astrogenesis begins in the middle of the neuronogenic temporal window, it spreads as soon as neurogenesis reaches its end and it peaks up after neuronogenesis completion. The astrocytic output mainly depends on two factors: commitment of multipotent precursors toward astroglial fates and kinetic-differentiative progression of the astrogenic proliferating pool. The proper sizing of the astrocytic compartment is crucial for the adult brain functions. A deficit of this compartment may alter excitability and information processing abilities of neural tissues. An uncontrolled proliferation of astroglial cells in the adult may give rise to severe pathologies, among which GBM, representing one of the most aggressive malignant brain tumors in humans.

Our research study gave robust evidence for *Foxg1* and *Emx2* limiting mouse cortico-cerebral astrogenesis. This antiastrogenic activity is upheld by the outcomes of a variety of experimental manipulations we performed, in vivo and in vitro. Specifically, we found that *Foxg1* inhibits the commitment of early neural precursors to astroglial fates, while *Emx2* antagonizes astroblast proliferation. Moreover, we proved that *Emx2* may be employed as a therapeutical tool to counteract GBM.

******

In the first part of this work, we showed that *Foxg1* overexpression in early neural stem cells inhibits cortico-cerebral astrogenesis, both in vitro and in vivo (*Fig.R. 1* and *Fig. R.2*). Therefore, we investigated the molecular mechanisms leading to such outcome, referring to the regulation of the well-known *Gfap* glial gene as a model. We found that *Foxg1* inhibits *Gfap* transcription. We reasoned that this may be due to a mis-regulation of the transactive pathways impinging on *Gfap* promoter

and/or an altered accessibility of its chromatin. We focused our attention on the first issue. To have an overall comprehension of the underlying molecular dynamics, we straightly monitored the ultimate, nuclear transactive effectors which regulate glial genes transcription. We detected a decrease of both pStat3 and pSmad1,5,8 as well as a concomitant increase of NCoR levels in neural stem cells overexpressing *Foxg1* (*Fig. R.5*). Moreover, we found that suppression of Tab2, a NCoR cofactor crucial to *Gfap* transrepression, restored wild type astrogenic rates in *Foxg1*-GOF cultures (*Fig. R.6*). All together, these results strongly suggest that *Foxg1* antagonizes NSC-to-astrocyte progenitor progression, due to its pleiotropic impact on transactive pathways modulating such progression.

Cortico-cerebral astrogenesis is sharply regulated thanks to the integration of signals provided by several regulatory pathways and the controlled accessibility of glial chromatin. The regulation of glial genes transcription (mostly *Gfap* and *s100β*) is a milestone for the study of pro- and anti-gliogenic programs. Therefore, we started to investigate *Foxg1* activity by measuring its impact on *Gfap* transcription. Once demonstrated that *Foxg1* down-regulates *Gfap* mRNA levels, we wanted to understand if this effect is due to its impact on the transducing pathways, to a direct induction of chromatin closure, or both. We started from the first issue. In preliminary tests, we quantified the final molecular effectors of the most important pathways involved in astrogenesis regulation, within the whole *Foxg1*-GOF neural cell population. Results of these tests led us to the provisional conclusion that ErbB4-intracellular domain (ErbB4-ICD) could be the key mediator of *Foxg1* antiastrogenic activity. Strikingly, when the analysis was restricted to the stem cell compartment (upon Foxg1 overexpression in such compartment), the scenario turned out to be radically different. We found more concurrent mechanisms, different from ErbB4 misregulation, through which *Foxg1* could lead to the inhibition of glial commitment.

Firstly, pStat3 levels reduction suggested an impact of *Foxg1* on the main pro-astrogenic cascade, the Jak/Stat pathway. Secondly, the decrease of pSmad1,5,8 provided evidence of a dampened Bmp signaling. (Actually, relevance of both changes to impaired astrogenic progression still waits for functional validation). Noticeably, these results were obtained in the presence of saturating levels of Lif and Bmp4, respectively. This suggests a defective sensibility of the corresponding sensing/transducing pathway to relay information from cell plasmamembrane to

nucleus, rather than a decreased ligand availability. Interestingly, Foxg1 has been previously demonstrated to chelate and inhibit the pSmad1 BMP4-signalling effector (Rodriguez et al., 2001; Seoane et al., 2004; Vezzali et al., 2016). Next, pSmad1 normally binds to pStat1,3 and enhances its transactivating power (Fukuda et al., 2007; Onishi et al., 2014). Moreover, pStat1,3 transactivates genes encoding for key components of its own pathway (Ichiba et al., 1998). Therefore, the pStat3 decrease triggered by *Foxg1* overexpression might simply reflect the depression of the Bmp axis. Alternatively, reduced NSC sensitivity to Lif-family ligands might be induced by *other Foxg1*-dependent mechanisms, distinct from Bmp pathway depression. This issue has to be experimentally investigated.

Finally, the well-known NCoR transcriptional corepressor may also be crucial to *Gfap* transcription inhibition. In the context of ErbB4 pathway, ErbB4-ICD is complexed with NCoR thanks to a Tab2 cofactor bridge. The resulting ternary complex translocates into the nucleus where it represses glial genes transcription. We measured both ErbB4 and NCoR nuclear immunofluorescence levels in neural stem cells in culture. We found an increase of NCoR, while not observing significant changes in ErbB4-ICD. Therefore, we speculated that NCoR could be the actual limiting factor, dictating the inhibitory tone exerted by the NCoR:Tab2:ErbB4-ICD complex on the Gfap promoter upon *Foxg1* manipulation. To confirm that such pathway is instrumental to *Foxg1* antiastrogenic action, we suppressed *Tab2* expression, thanks to the RNAi technique. In the presence of a short hairpin against *Tab2*, we observed a rescue of the astroglial output delivered by *Foxg1*-GOF samples, suggesting that our inference was correct. Intriguingly, an excess of NCoR:Tab2:ErbB4-IC complex could further divert RbpJk from interacting with Notch intracellular domain (NICD), so further dampening the Notch pro-glial pathway. This aspect needs to be investigated.

Foxg1 regulation of astrogenesis adds to numerous other functions exerted by this gene in the developing cerebral cortex (Hanashima et al., 2004; Fasano et al., 2009; Danesin et al., 2009; Hanashima et al., 2007; Kumamoto et al., 2013; Martynoga et al., 2005; Pancrazi et al., 2015) and echoes the impact that its *Drosophila m.* homolog *Slp* exerts on fruitfly gliogenesis (Mondal et al., 2007). Actually, at the moment we have strong evidences of Foxg1 ability to antagonize astrogenesis, as well

some interesting hints about the underying molecular mechanisms. However, three fundamental issues still remain to be cleared.

First, we need to secure *Foxg1* physiological relevance to proper temporal articulation of astrogenesis. For this purpose, we have to rigorously evaluate the Foxg1 protein and mRNA content of cerebral stem cells, at different developmental stages. We expect to detect higher Foxg1 levels around neuronogenesis' midpoint, and progressively decreasing levels when astrogenesis is about to reach its peak level. Moreover, we have to perform in utero electroporation of *Foxg1*-GOF and *Foxg1*-LOF plasmids into mid-neuronogenic, periventricular neural stem cells and subsequently analyze their ultimate astrogenic output.

Second, we need to go deeper into the dissection of the effects that *Foxg1* exerts on different pro- and anti-gliogenic pathways. This can result in a complex picture envisioning more than only one single mediator.

Third, we have to shed light on a possible *Foxg1* involvement in the epigenetic regulation of astroglial genes. This transcription factor might recruit additional epigenetic effectors on gial genes chromatinenes, keeping it not suitable to get transcribed. We will investigate all these themes in a dedicated follow-up study, so to broaden our knowledge as regards this multifaceted transcription factor that is essential during development.

******

As for the second part of this work, we showed that *Emx2* overexpression in corticocerebral stem cells inhibits astrogenesis, largely in a cell autonomous way. This was due to decreased proliferation of astrocyte-committed progenitors, resulting in a severe reduction of their ultimate astroglial output (*Figs. R.7 and R.8*, and *Suppl. Figs. S1, S2,* and *S3*). We found that *Emx2* inhibits astrogenesis by downregulating EgfR and Fgf9 (*Fig. R.9* and *Suppl. Fig. S.4*) via Bmp signaling promotion and Sox2 suppression (*Fig. R.10* and *Suppl. Fig. S.6*). Finally, we provided evidence that in vivo temporal progression of *Emx2* expression levels in neural stem cells contributes to restrain astrocyte generation during the neuronogenic phase (*Fig. R.11*).

As reported above, a key determinant of cortico-cerebral astrogenic rates is the accurate sizing of the proliferating astrogenic pool. In this context, a special role is played by the Egf signaling axis and Fgf9, as key promoters of astrogenesis. Despite of saturating levels of Tgfa/Egf ligands throughout the embryonic life (Assimacopoulos et al., 2003; Burrows et al., 1997), EgfR expression, very low in the early pallium, progressively increases as neuronogenesis proceeds (Burrows et al., 1997; Viti et al., 2003) and our data not shown). This limits the pallial competence to activate the Egf signaling axis, at least up to birth (Burrows et al., 1997). Similarly, Fgf9 expression, prominent after birth, is very poor during prenatal life, when it results limiting for glioblasts proliferation (Seuntjens et al., 2009). Here we demonstrated that Emx2 acts as a master gene coordinating proper temporal progression of both EgfR and Fgf9.

Emx2-dependent repression of EgfR was previously documented within the developing urogenital apparatus (Kusaka et al., 2010). Here we found that it also occurs within the astrogenic lineage. Conversely, Emx2-dependent repression of Fgf9 is a fully novel finding. Here we provided evidence that both EgfR and Fgf9 regulation rely on Emx2-dependent increase of Bmp signaling and dampening of Sox2. Finally, we showed that time course progression of Emx2 levels in cortico-cerebral NSCs contributes to postpone the bulk of astrogenesis to postnatal ages.

Emx2 regulation of astrogenesis adds to a number of earlier developmental processes mastered by this gene, including pancortical specification, neuronogenesis, arealization and lamination (Mallamaci et al., 2000a, 2000b, Muzio et al., 2002, 2005). It points to Emx2 as a potential therapeutic tool for the control of reactive astrogliosis (Sofroniew, 2009) and competitive diversion of neural precursors to neuronogenesis, for purposes of brain repair (Burns et al., 2009). Moreover, these findings inspired us to exploit *Emx2* as a possible tool for the treatment of glioblastoma multiforme tumor, which constitutes the third part of this work.

******

As for the last part of this work, we showed that *Emx2* overexpression in a number of GBM cultures forced them to collapse, by promoting cell death and inhibiting cell proliferation. *Emx2* impact on GBM metabolism was complex and a number of genes and pathways sensitive to its overexpression were co-involved in its

antitumoral activity. Remarkably, such activity was confirmed *in vivo*, upon transplantation of conditionally engineered tumor cells into the neocortical parenchyma of mouse neonates and juvenile immunotolerant mice. Last but not least, restricting *Emx2* overexpression to presumptive tumor stem cells replicated the outcome of generalized gene overexpression.

Multiple bodies of correlative data suggest that *EMX2* downregulation could contribute to the genesis of GBMs. The COSMIC database (http://cancer.sanger .ac.uk/cosmic) reports two distinct homozygous *EMX2* deletions occurring in 2 out of 801 gliomas (data not shown). Analysis of Allen Brain - Ivy Glioblastoma Atlas data showed us that *EMX2*-mRNA levels are specifically reduced by ≥2-folds in GBM tumors with respect to surrounding tissue (*Suppl. Fig. S.12*). Next, in the majority of glioblastoma cultures analyzed in the present study, endogenous *EMX2*-mRNA was undetectable. When it was present, its level was lower than in astrogenic, fetal cortico-cerebral NSCs (*Suppl. Fig. S.13*). Finally, a consistent scenario was found in acutely immunopanned GBM astrocytes, compared to astrocytes purified from the surrounding healthy tissue (Zhang et al., 2016). Albeit intriguing, all these correlative data are obviously not sufficient to draw firm conclusions about *EMX2* role in GBM etiopathogenesis, which was out of the aims of the present study. Nevertheless, our data suggest that, regardless of its role in the oncogenic process, *Emx2* may be a powerful tool for counteracting GBM tumors.

Subject of this study were two established GBM cell lines (U87MG and T98G) and five tumor cultures derived from operated GBM patients. Promisingly, all of them robustly responded to *Emx2* and rapidly collapsed, because of defective proliferation and exaggerated cell death (*Fig. R.12* and *Suppl.. Fig. S.8*).

Noticeably, their molecular responses were complex and not stereotyped (*Table R.1*), possibly reflecting GBM etiopathogenetic heterogeneity (Brennan et al., 2013; Sturm et al., 2014; Verhaak et al., 2010)). The vast majority of molecular changes evoked by *Emx2* were consistent with its antitumor activity (*Table R.1* and *Fig. R.13*), a selection of them was proven to be instrumental to it (*Fig. R.14*). However, in no case, counteracting each of these changes could fully restore original kinetic properties of the cultures (*Fig. R.14*). All this means that *Emx2* antioncogenic efficacy may emerge as a consequence of its ability to attack a *variety* of metabolic nodes crucial to malignancy. In addition to a robust inhibition of GBM expansion, this

ability might help preventing selection of drug-resistant clones and recurrencies. Intriguingly, a number of *Emx2*-repressed and -stimulated genes reported above are the very same affected by duplications and deletions in late stage glioma cancers, respectively (Brennan et al., 2013). This further suggests that our manipulation could be therapeutically effective on a variety of high grade gliomas, regardless of their primary molecular origin.

Remarkably, *Emx2* overexpression elicited a pronounced anti-GBM activity even *in vivo* (*Fig. R.15* and *Fig. R.16*). This was found by cotransplanting conditionally engineered tumor cells, alternatively expressing *Emx2* or a control transgene, into the cortical parenchyma of wild type mouse pups and scoring the outcome one week later. This is a novel experimental setup, allowing to preliminarly assess antioncogenic power *in vivo*, quickly, in an immunocompetent environment, and in the presence of strong progliogenic cues. Consistently, juvenile immunotolerant mice, transplanted by engineered human U87MG cells according to the classical orthotopic approach (Higgins et al., 2013), underwent a pronounced increase of their average survival time upon *Emx2* overexpression. Finally, of particular therapeutic interest is the fact that a collapse of engineered GBM cultures also occurred when *Emx2* overexpression was restricted to Nes-p+ precursor cells (*Fig. R.17*). These cells, in fact, are likely to include tumor initiating cells (TICs), from which tumor recurrencies are supposed to originate. Such cells may escape even the attack by the most advanced oncolytic vectors developed against GBM.

All these results point to *Emx2* as a novel, promising tool for GBM therapy. However, for this purpose, the study of interaction of *Emx2* overexpression with the standard therapy for GBM, as well as the selection of a more appropriate, not-genotoxic vectors for gene delivery, are mandatory. Moreover, an in depth exploration of mechanisms mediating *Emx2* activity, by unbiased GBM transcriptome profiling, is also due. These issues are the subject of a dedicated follow-up study, currently running in our lab.

6. SUPPLEMENTARY MATERIAL

6.1 SUPPLEMENTARY RESULTS AND DISCUSSION

Evaluating the *Emx2* expression gain elicited in cortico-cerebral multipotent neural precursors at astrogenesis peak times.

To compare the outcome of our artificial manipulation of *Emx2* levels with the physiological dynamics of this gene in ageing neural precursors, we coinfected E12.5 cortico-cerebral precursors with constitutively active LV:*pPgk1p-rtTA2^{S}-M2* and LV:*TREt-Emx2-IRES2-EGFP*. We kept them in culture for 7 days under GFs plus additional 4 days under GFs and doxycyclin, and finally compared them with controls by qRTPCR. *Emx2*-mRNA, normalized against *Gapdh*, resulted to be upregulated by 33.4±7.5 folds ($p<0.007$; n=3).

Remarkably, *Emx2* products are mainly confined to multipotent precursors and their immediate derivatives within the apical proliferative compartment (Mallamaci et al., 1998, and http://developingmouse.brain-map.org). Moreover, such cells amount to about 7% of primary cerebral cultures set up with a protocol similar to the present one (see (Brancaccio et al., 2010), *Fig. R.8*). All this suggests that, in control conditions, multipotent precursors within our neural cultures should express *Emx2* at levels about 100/7 higher than the average level estimated for the whole cell population.

Consequently, the gain of *Emx2* expression we elicited within these precursors could be approximately calculated by dividing the *Emx2* expression gain as evaluated over the whole population, 33.4±7.5, by the ratio between the baseline *Emx2* level in multipotent precursors and the average baseline level in the whole population, 100/7. Therefore it should be close to 33.4/(100/7), i.e. 2.3. Interestingly, the reciprocal of this value is similar to the variation of *Hes5*-normalized *Emx2*-mRNA levels we detected in the cortex between E16.5 and E18.5 (*Fig. R.10 A-C*). This suggests that our lentiviral/TetON transgene could largely compensate for the drop of *Emx2* expression which occurs in multipotent precursors at the time of the neuronogenic-to-astrogenic transition.

6.2 SUPPLEMENTARY FIGURES

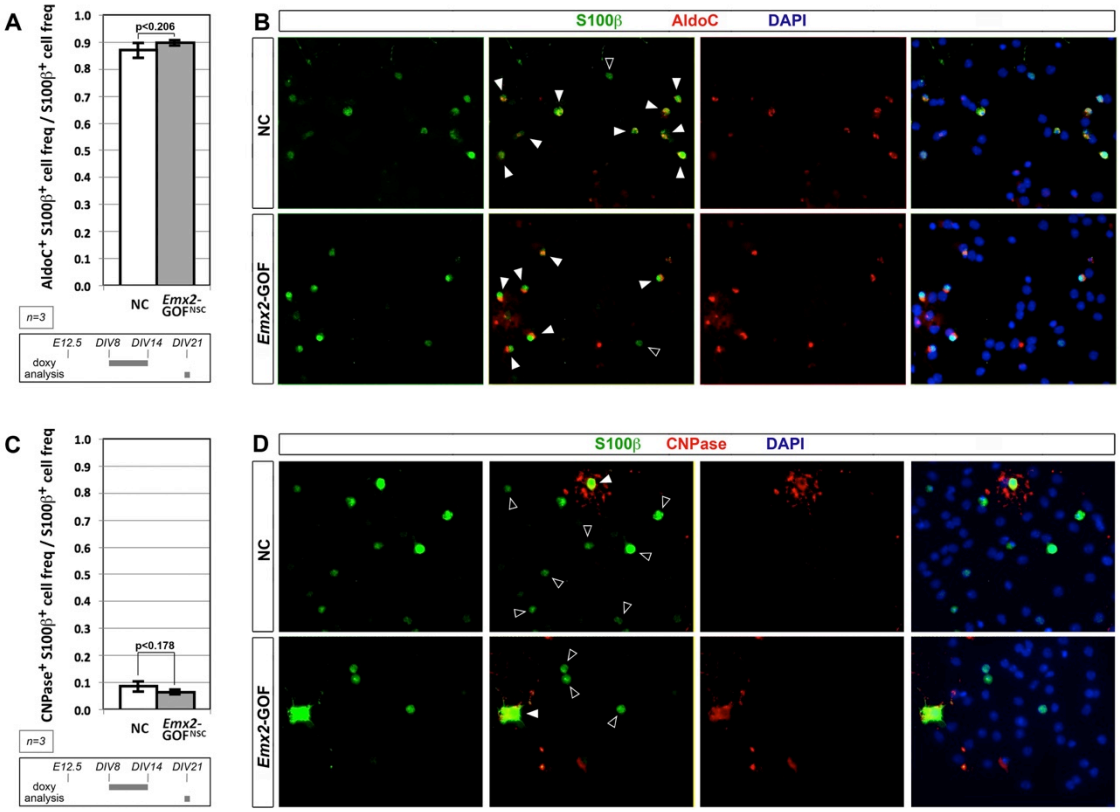

Supplementary Figure S.1. Aldolase C and CNPase expression within the S100b⁺ compartment upon *Emx2* overexpression in vitro. Fractions of S100b⁺ cells also expressing the pan-astrocytic marker Aldolase C (AldoC) **(A)** or the oligodendrocyte lineage marker CNPase **(C)**, evaluated in engineered neural cultures set up as described for Fig. 2A. Evaluation of the AldoC⁺ and CNPase⁺ frequencies restricted to the S100b⁺ population, data normalized against sample (NC). **(B)** and **(D)** shown are examples of engineered cultures referred to in (A) and (C), respectively. Here, solid and empty arrowheads point to S100b⁺ cells expressing or not-expressing the other marker, respectively.

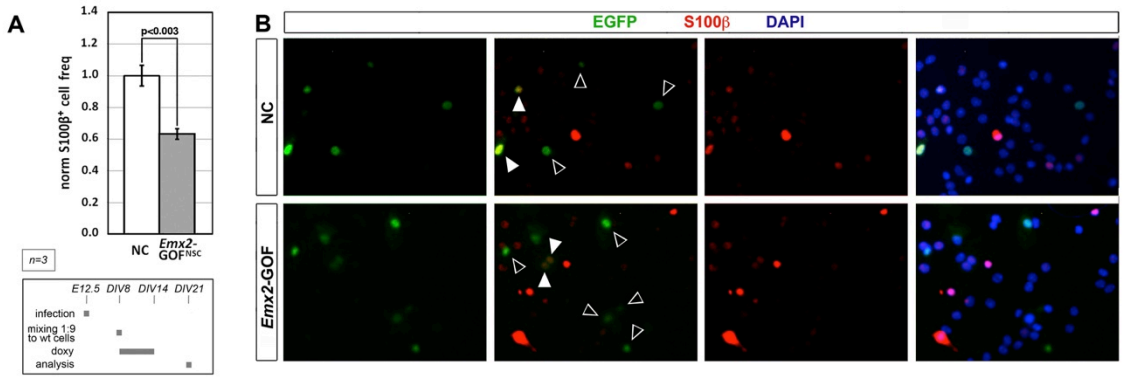

Supplementary Figure S.2. Reduced astrocytogenesis upon *Emx2* overexpression, in vitro, evaluation of cell-autonomous effects. (A) Frequencies of S100b+ derivatives of cortical precursors, acutely labeled with the constitutive EGFP-expressor LV:*pPgk1-EGFP*, as well as infected with the NSC-restricted rtTA2S-M2-expressor LV:*pNes/hsp68-rtTA2S-M2* and, alternatively, LV:*TREt-IRES2-EGFP* (NC) or LV:*TREt-Emx2-IRES2-EGFP* (*Emx2*-GOF). Cells kept for 1 week under anti-differentiative medium, mixed at DIV8 with an excess of wild-type, age-matched cells from the same original pool (1:9), kept another week under anti-differentiative medium and one more week under pro-differentiative medium; doxycyclin administered at DIV8-14. Evaluation of the S100b+ fraction restricted to engineered, EGFP+ cells, data normalized against sample (NC). Absolute frequency of S100b+ cells within the (NC) EGFP+ population, 19.63 ± 0.73%. Scalebar = s.e.m. In **(B)**, shown are examples of engineered cultures referred to in (A). Here, solid and empty arrowheads point to EGFP+ cells expressing or not-expressing S100b+, respectively.

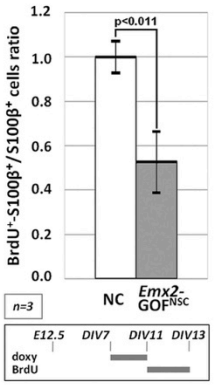

Supplementary Figure S.3. Proliferation rates within the astrogenic lineage upon *Emx2* overexpression in vitro. Percentages of S100b+ cells also expressing the intermitotic marker Ki67, evaluated in engineered neural cultures set up as described for Fig. 2B and pulsed by BrdU at DIV12-13.

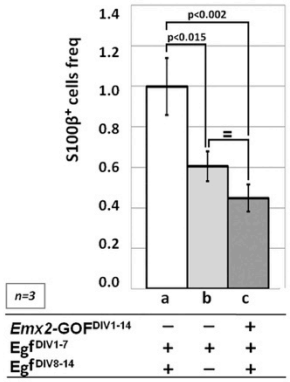

Supplementary Figure S.4. Sensitivity of astrogenesis to Egf removal. Frequencies of S100b$^+$ derivatives of cortical precursors, acutely infected with LV:*pNes/hsp68-rtTA2^S-M2* and, alternatively, LV:*TREt-IRES2-EGFP* (a,b) and LV:*TREt-Emx2-IRES2-EGFP* (c). Cells kept for 2 weeks under anti-differentiative medium and one more week under pro-differentiative medium; doxycyclin and Egf temporally restricted according to the table. Data normalized against sample (a); absolute frequency of S100b$^+$ cells in (a), 17.70±2.49%.

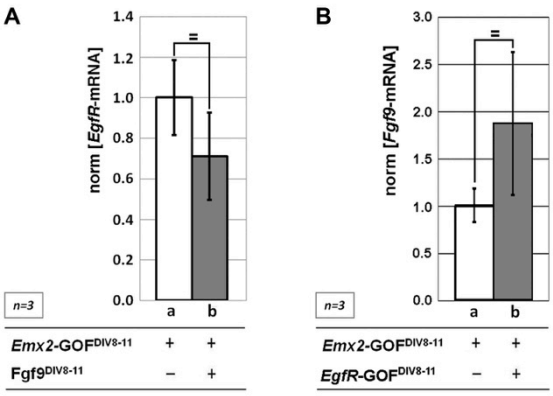

Supplementary Figure S.5. Absence of *EgfR*/*Fgf9* cross-talk in *Emx2*-GOF neural cultures. (A,B) *EgfR*- and *Fgf9*-mRNA levels in preparations of E12.5 cortico-cerebral precursors, acutely infected with LV:*pPgk1p-rtTA2^S-M2* and LV:*TREt-Emx2-IRES2-EGFP* (a,b), grown in anti-differentiative medium and subsequently (DIV8) exposed to doxycyclin. In (A), the (b) sample was also exposed to Fgf9, since day 8. In (B), sample (a) and (b) were further superinfected at day 8, with LV:*TREt-IRES2-EGFP* and LV:*pCCLsin.PPT.hPGK.EGFR.pre*, respectively. In both (A) and (B), data double-normalized, against *Gapdh* and samples (a). Scalebar = s.e.m.

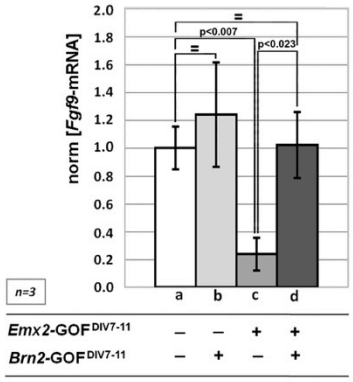

Supplementary Figure S.6. *Brn2* rescues *Emx2*-dependent *Fgf9* downregulation. *Fgf9*-mRNA levels in preparations of E12.5 cortico-cerebral precursors, acutely infected with LV:*Pgk1p-rtTA2^{S}-M2* (a-d), LV:*TREt-IRES2-EGFP* (a,b), LV:*TREt-Emx2-IRES2-EGFP* (c,d) and LV_*TREt-Brn2* (b,d), grown in anti-differentiative medium and subsequently (DIV8) exposed to doxycyclin (a-d). *p*(*Emx2*/*Brn2* interaction, 2-ways ANOVA)<0.12. Data double-normalized against *Gapdh* and sample (a). Scalebar = s.e.m.

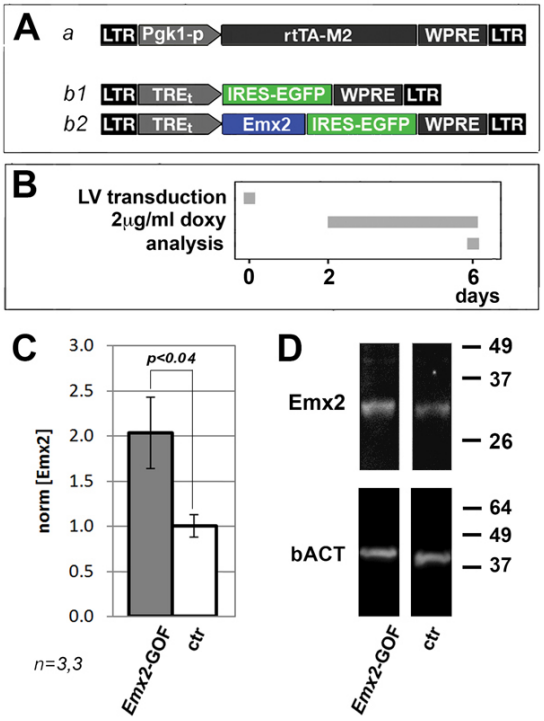

Supplementary Figure S.7. Comparison of Emx2/EMX2 protein levels in U87MG cells in baseline conditions and upon *Emx2* overexpression. Evaluation of Emx2/EMX2 levels in U87MG cell samples, engineered as in (A,B). Values were normalized against controls. n is the number of biological replicates. p-value was calculated by t-test (one-tail, unpaired): *p<0.05.

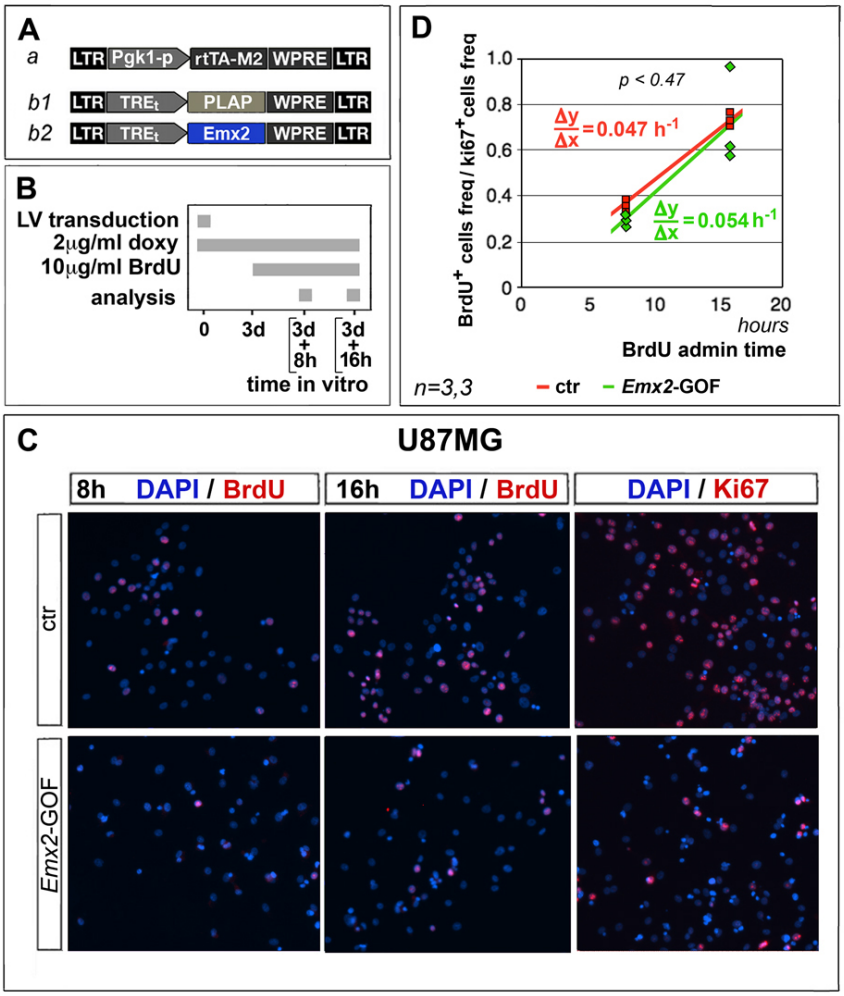

Supplementary Figure S.8. Evaluation of G1-to-S phase progression of U87MG GBM cells upon *Emx2* overexpression. U87MG cells were engineered by lentiviral vectors and TetON technology as in (**A**), kept as adherent cultures and provided with doxycyclin and BrdU as in (**B**). 8 or 16 hours after BrdU administration, cells were immunoprofiled for BrdU and further scored for Ki67 immunoreactivity (**C**). Ki67$^+$ cell frequency-normalized BrdU$^+$ cell frequencies (y) were plotted against BrdU administration times (x). Slopes, Dy/Dx, representing the progression rate of G1 cells into S-phase, were calculated. Finally, statistical significance of their difference was evaluated by ANCOVA (one-way, unpaired) (**D**). *n* is the number of biological BrdU replicates. Absolute frequencies of Ki67$^+$ cells were 0.538±0.026 and 0.197±0.003,in control and *Emx2*-GOF cultures, respectively (n=3,3; p<0.0001, by ANOVA, one-way, unpaired).

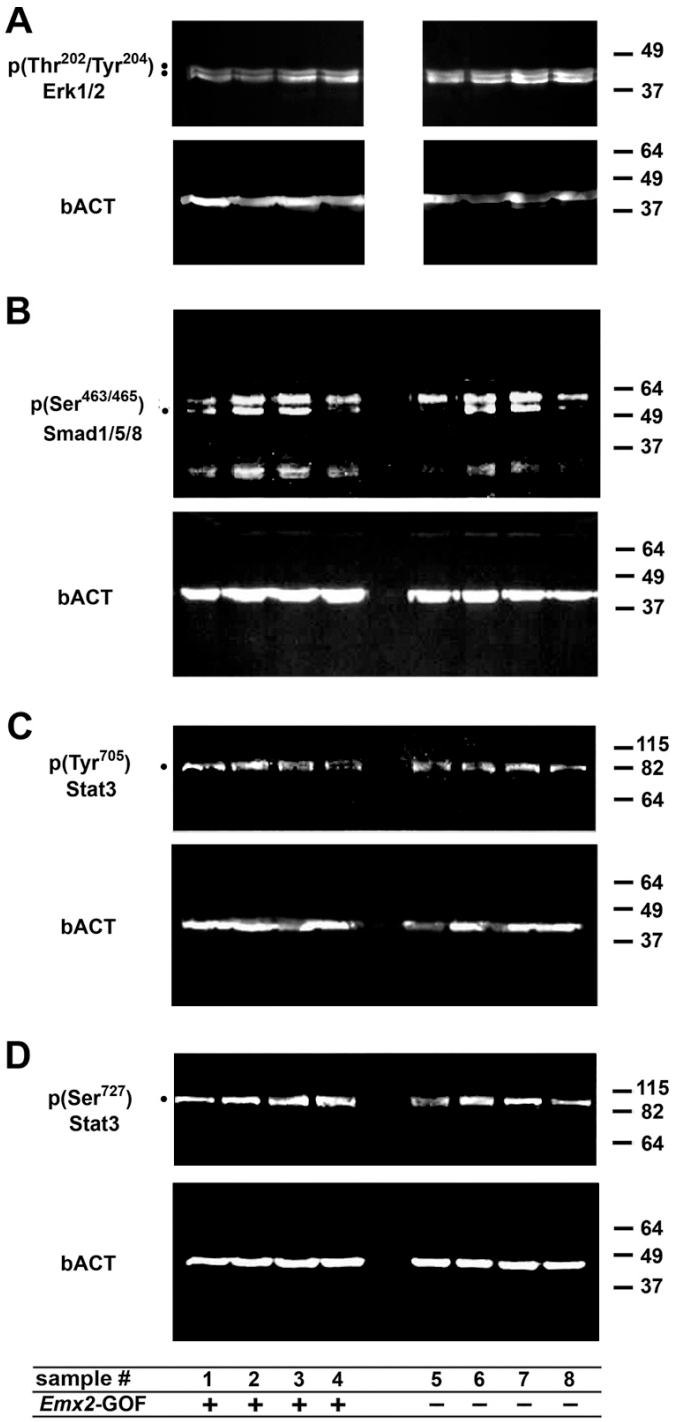

Supplementary Figure S.9. Wider representation of western blots shown in Fig. 2. This representation includes at least 6 bandwidths above and below the diagnostic band. In (**C**) and (**D**) the top edge of the upper photograph corresponds to the slot line.

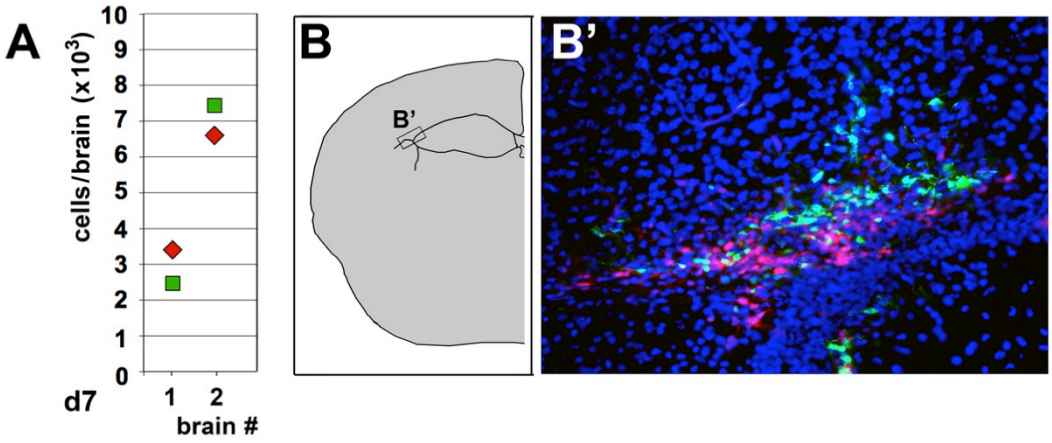

Supplementary Figure S.10. Balanced survival of Egfp- and mCherry-labelled GBM cells upon co-transplantation into the neonatal cortical parenchyma. (**A-B'**) The assay was run similar to Fig. 4. Here cells, originating from GbmA line, were only transduced with constitutevely expressed fluoroprotein genes, mixed 1:1 and co-transplanted into 2 brains. *p*-value was calculated by t-test (one-tail, paired).

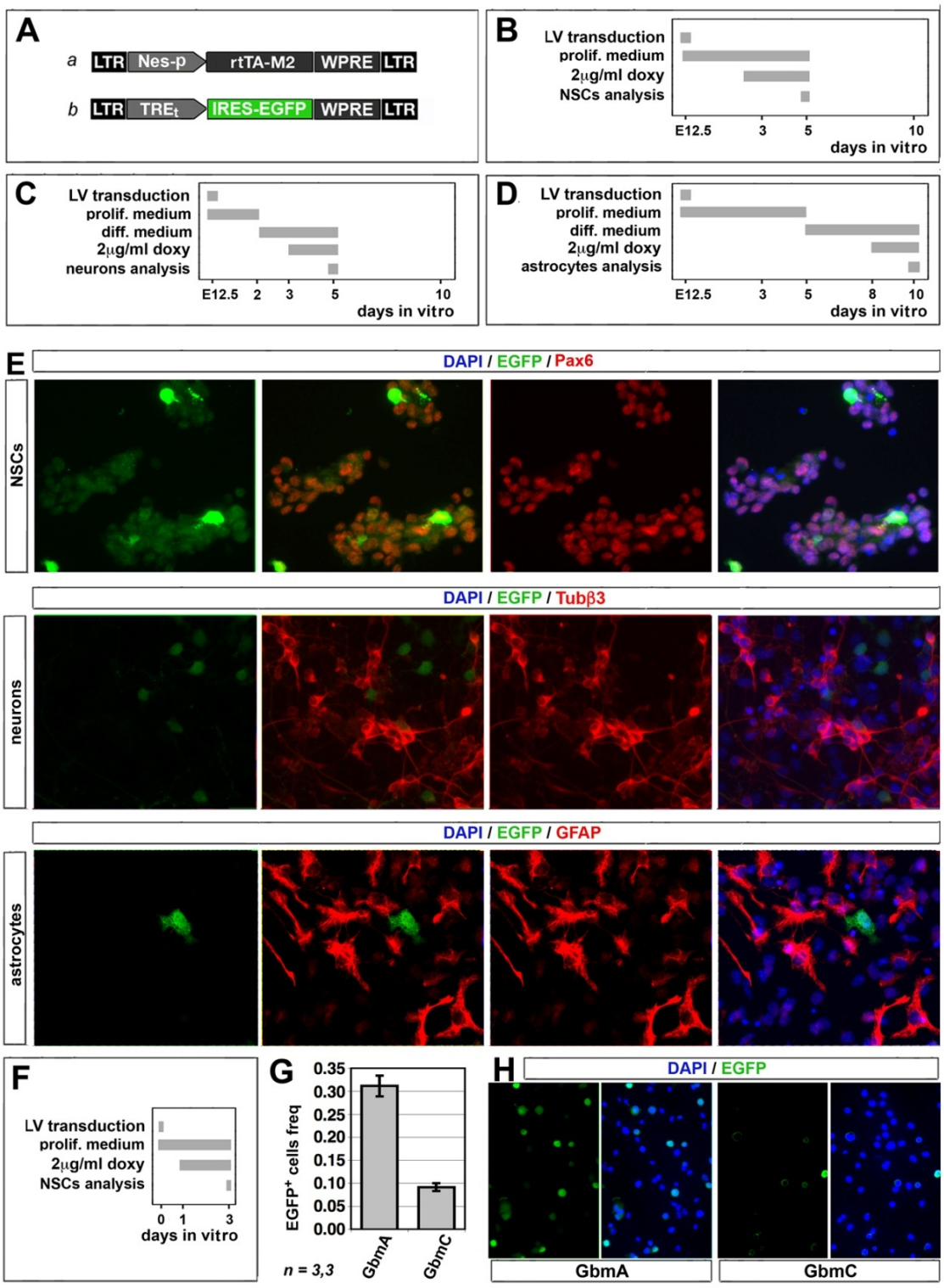

Figure S.11. Restriction of Nes-p promoter activity to embryonic neural stem cells and a subset of glioblastoma cells. E12.5 murine neural stem cells (NSCs) were engineered and cultured as shown in (**A-D**). Cells were immunoprofiled at different days in vitro as shown in (**B-D**), for EGFP, driven by Nes-p promoter, and, alternatively, Pax6, Tubb+ and GFAP (**E**). GbmA and GbmC glioblastoma cells were engineered and cultured as shown in (**A,F**) and eventually immunoprofiled for EGFP (**G,H**).*n* = number of biological replicates. bars = s.e.m.'s.

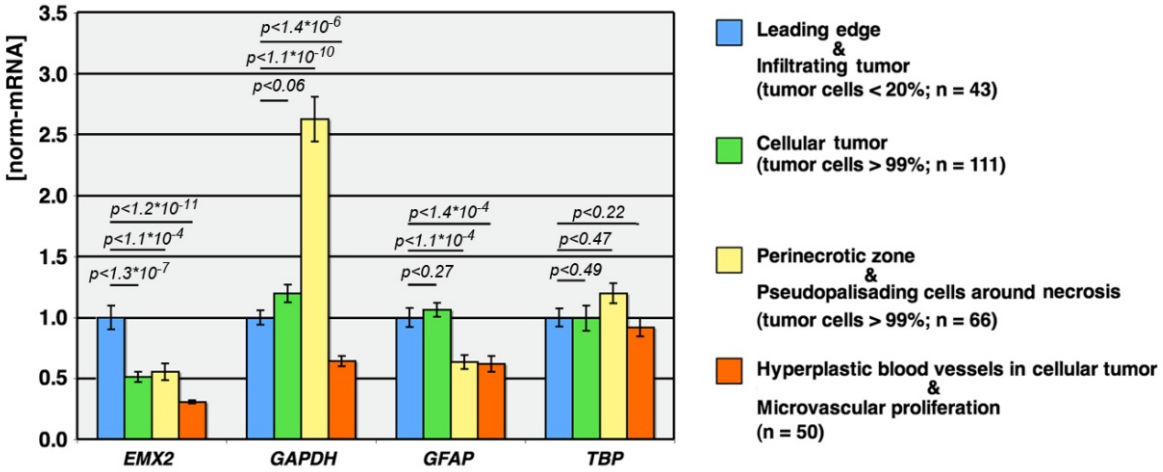

Supplementary Figure S.12. Expression levels of *EMX2* and *GAPDH*, *GFAP* and *TBP* control genes in a set of human glioblastoma lesions. z-score-normalized RNASeq data,referring to (a) leading edge and infiltrating tumor, (b) cellular tumor, (c) perinecrotic zone and pseudopalisading cells around necrosis, and (d) hyperplastic blood vessels in cellular tumor and microvascular proliferation, were downloaded from the "Allen Brain Atlas - Ivy Glioblastoma Atlas Project" on 04.14.2016. They were averaged and statistically evaluated by t-test (one-way, unpaired). n = number of biological replicates. bars = s.e.m.'s.

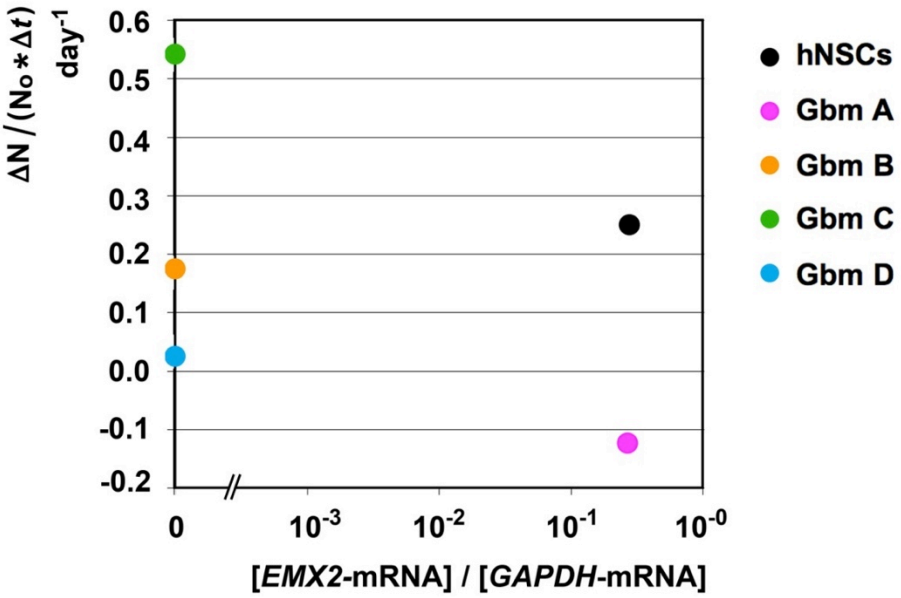

Supplementary Figure S.13. Relationship between endogenous *EMX2*-mRNA levels and normalized expansion rate of distinct GBM cells. Here GBM culture growth was evaluated over the full times shown in Fig. 1 and the $\Delta N/\ \Delta t$ expansion rates were normalized against the N_0 initial number of cultured cells.

A

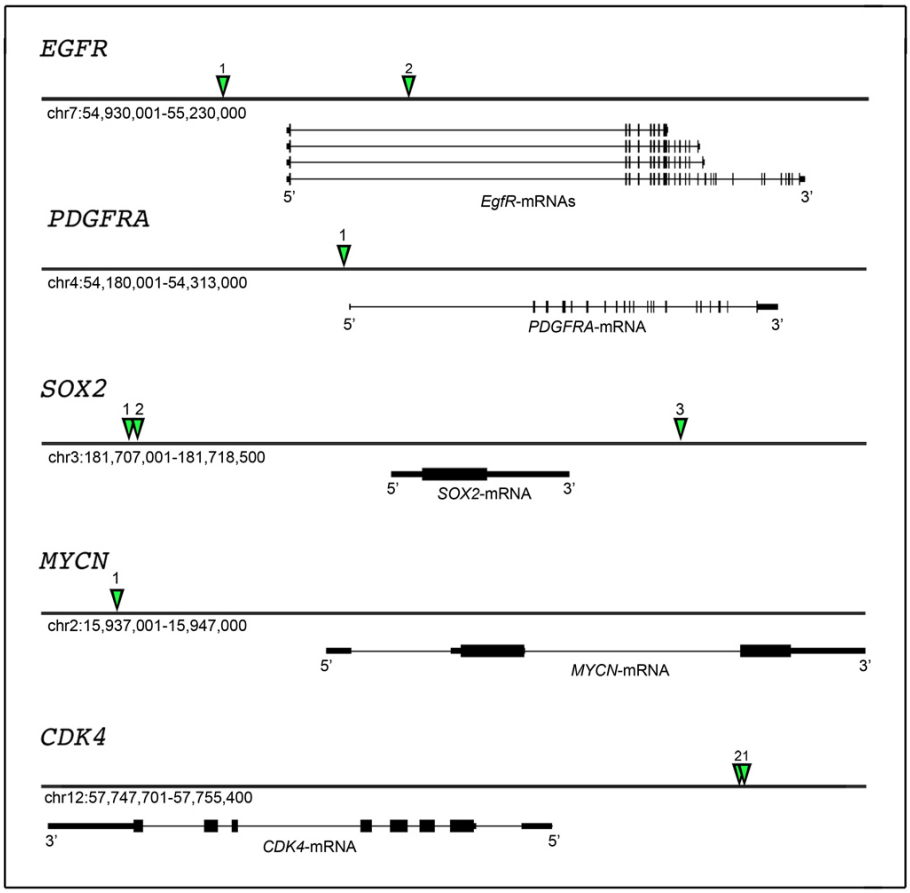

B

gene	EMX2-BS	
		human NNNNNNNN EMX2-BS-sequence NNNNNNNNN mouse NNNNNNNN EMX2-BS-sequence NNNNNNNNN
EGFR	1	hsa TTGGGTTCCAAAGGG AATAATTAAG ATTGGAGCAAAACCT mmu TTGAAATCTAAAGGG GCTAATTAAG ATAGGAGAAACGTCT
	2	hsa AGAAATAGCTTGCAA AATAATTAAC TACTGATCATTTATA mmu TGGAACACTTTGAAG AATAATTAAC TGCTGCTCATTCAAT
PDGFRA	1	hsa CATTCAAATTAGGCA GGTAATTACT ACCAGAAGGACAACT mmu CATTTAAATTAGGCA GGTAATTACT ACCAGAAGAGCAACT
SOX2	1	hsa TGGTCGTCAAACTCT GCTAATTAGC AATGCTGAGAAATTC mmu TGGTCGTCAAACTCT GCTAATTAGC AATGCTGAGAAATTC
	2	hsa CTTGGCTAGTTCTCA CCTAATTACT GCAAGTTAAACCTCT mmu CTTGGCTAGTTCTC- GCTAATTACT GCAACTTAAACCTCT
	3	hsa CAAGGCATTTTCCCC CCTAATTAAT GCAGAGACTCTAAAA mmu CTAGGCAGGTTCCCC TCTAATTAAT GCAGAGACTCTAAAA
MYCN	1	hsa AGATTCAGACTTG---------TCAGTAATTACTGGCTTGCATTAAAAG mmu AGATTCAGACTTGCTGGTAATTTCAGTAATTGCTGGTTTGCATTAAGAG
CDK4	1,2	hsa CATACTGGGAAAAAA TTTAATTAGT GAAAG AGTAATTAAC AGAAGAAGGGAGGGG mmu GACACTGAGAAAAAA ATTAATTAGC AAAAG AGTAATTAAC AGAA-AAGGGAGGGA

Supplementary Figure S.14. In silico prediction of EMX2-binding sites in genes down-regulated by EMX2. (A) Target genes and their surroundings were scanned by Jaspar software (http://jaspar.genereg.net/cgi-bin/jaspar_db.pl) for putative EMX2-binding sites, with relative profile score >0.95. Primary hits were further filtered for human/mouse conservation (by Blastn, according to the "Somewhat similar sequences" protocol) and mapped, as green arrowheads, to the corresponding human loci (as in the UCSC draft hg38). (**B**) Sequences of putative human EMX2-binding sites and their murine counterparts referred to in (A).

7. BIBLIOGRAPHY

Abe, Y., Ikeshima-Kataoka, H., Goda, W., Niikura, T., and Yasui, M. (2012). An astrocyte-specific enhancer of the aquaporin-4 gene functions through a consensus sequence of POU transcription factors in concert with multiple upstream elements. J. Neurochem. *120*, 899–912.

Adachi, T., Takanaga, H., Kunimoto, M., and Asou, H. (2005). Influence of LIF and BMP-2 on differentiation and development of glial cells in primary cultures of embryonic rat cerebral hemisphere. J. Neurosci. Res. *79*, 608–615.

Altmann, C.R., and Brivanlou, A.H. (2001). Neural patterning in the vertebrate embryo. Int. Rev. Cytol. *203*, 447–482.

Asano, H., Aonuma, M., Sanosaka, T., Kohyama, J., Namihira, M., and Nakashima, K. (2009). Astrocyte Differentiation of Neural Precursor Cells is Enhanced by Retinoic Acid Through a Change in Epigenetic Modification. STEM CELLS *27*, 2744–2752.

Assimacopoulos, S., Grove, E.A., and Ragsdale, C.W. (2003). Identification of a Pax6-Dependent Epidermal Growth Factor Family Signaling Source at the Lateral Edge of the Embryonic Cerebral Cortex. J. Neurosci. *23*, 6399–6403.

Bani-Yaghoub, M., Tremblay, R.G., Lei, J.X., Zhang, D., Zurakowski, B., Sandhu, J.K., Smith, B., Ribecco-Lutkiewicz, M., Kennedy, J., Walker, P.R., et al. (2006). Role of Sox2 in the development of the mouse neocortex. Dev. Biol. *295*, 52–66.

Barnabé-Heider, F., and Miller, F.D. (2003). Endogenously produced neurotrophins regulate survival and differentiation of cortical progenitors via distinct signaling pathways. J. Neurosci. Off. J. Soc. Neurosci. *23*, 5149–5160.

Barnabé-Heider, F., Wasylnka, J.A., Fernandes, K.J.L., Porsche, C., Sendtner, M., Kaplan, D.R., and Miller, F.D. (2005). Evidence that Embryonic Neurons Regulate the Onset of Cortical Gliogenesis via Cardiotrophin-1. Neuron *48*, 253–265.

Barnes, A.P., Lilley, B.N., Pan, Y.A., Plummer, L.J., Powell, A.W., Raines, A.N., Sanes, J.R., and Polleux, F. (2007). LKB1 and SAD kinases define a pathway required for the polarization of cortical neurons. Cell *129*, 549–563.

Bhat, K.M., van Beers, E.H., and Bhat, P. (2000). Sloppy paired acts as the downstream target of wingless in the Drosophila CNS and interaction between sloppy paired and gooseberry inhibits sloppy paired during neurogenesis. Dev. Camb. Engl. *127*, 655–665.

Bilican, B., Fiore-Heriche, C., Compston, A., Allen, N.D., and Chandran, S. (2008). Induction of Olig2 precursors by FGF involves BMP signalling blockade at the Smad level. PloS One *3*, e2863.

Bishop, K.M., Goudreau, G., and O'Leary, D.D. (2000). Regulation of area identity in the mammalian neocortex by Emx2 and Pax6. Science *288*, 344–349.

Bonni, A., Sun, Y., Nadal-Vicens, M., Bhatt, A., Frank, D.A., Rozovsky, I., Stahl, N., Yancopoulos, G.D., and Greenberg, M.E. (1997). Regulation of gliogenesis in the central nervous system by the JAK-STAT signaling pathway. Science *278*, 477–483.

Brancaccio, M., Pivetta, C., Granzotto, M., Filippis, C., and Mallamaci, A. (2010). Emx2 and Foxg1 Inhibit Gliogenesis and Promote Neuronogenesis. STEM CELLS *28*, 1206–1218.

Brennan, C.W., Verhaak, R.G.W., McKenna, A., Campos, B., Noushmehr, H., Salama, S.R., Zheng, S., Chakravarty, D., Sanborn, J.Z., Berman, S.H., et al. (2013). The Somatic Genomic Landscape of Glioblastoma. Cell *155*, 462–477.

Burns, T.C., Verfaillie, C.M., and Low, W.C. (2009). Stem cells for ischemic brain injury: a critical review. J. Comp. Neurol. *515*, 125–144.

Burrows, R.C., Wancio, D., Levitt, P., and Lillien, L. (1997). Response diversity and the timing of progenitor cell maturation are regulated by developmental changes in EGFR expression in the cortex. Neuron *19*, 251–267.

Calegari, F., and Huttner, W.B. (2003). An inhibition of cyclin-dependent kinases that lengthens, but does not arrest, neuroepithelial cell cycle induces premature neurogenesis. J. Cell Sci. *116*, 4947–4955.

Cao, F., Hata, R., Zhu, P., Ma, Y.-J., Tanaka, J., Hanakawa, Y., Hashimoto, K., Niinobe, M., Yoshikawa, K., and Sakanaka, M. (2006). Overexpression of SOCS3 inhibits astrogliogenesis and promotes maintenance of neural stem cells. J. Neurochem. *98*, 459–470.

Caric, D., Raphael, H., Viti, J., Feathers, A., Wancio, D., and Lillien, L. (2001). EGFRs mediate chemotactic migration in the developing telencephalon. Dev. Camb. Engl. *128*, 4203–4216.

Cebolla, B., and Vallejo, M. (2006). Nuclear factor-I regulates glial fibrillary acidic protein gene expression in astrocytes differentiated from cortical precursor cells. J. Neurochem. *97*, 1057–1070.

Cebolla, B., Fernández-Pérez, A., Perea, G., Araque, A., and Vallejo, M. (2008). DREAM mediates cAMP-dependent, Ca2+-induced stimulation of GFAP gene expression and regulates cortical astrogliogenesis. J. Neurosci. Off. J. Soc. Neurosci. *28*, 6703–6713.

Cheng, P.-Y., Lin, Y.-P., Chen, Y.-L., Lee, Y.-C., Tai, C.-C., Wang, Y.-T., Chen, Y.-J., Kao, C.-F., and Yu, J. (2011). Interplay between SIN3A and STAT3 Mediates Chromatin Conformational Changes and GFAP Expression during Cellular Differentiation. PLOS ONE *6*, e22018.

Cohen, S.M., and Jürgens, G. (1990). Mediation of Drosophila head development by gap-like segmentation genes. Nature *346*, 482–485.

Craig, C.G., Tropepe, V., Morshead, C.M., Reynolds, B.A., Weiss, S., and van der Kooy, D. (1996). In vivo growth factor expansion of endogenous subependymal neural precursor cell populations in the adult mouse brain. J. Neurosci. Off. J. Soc. Neurosci. *16*, 2649–2658.

Dalton, D., Chadwick, R., and McGinnis, W. (1989). Expression and embryonic function of empty spiracles: a Drosophila homeo box gene with two patterning functions on the anterior-posterior axis of the embryo. Genes Dev. *3*, 1940–1956.

Danesin, C., Peres, J.N., Johansson, M., Snowden, V., Cording, A., Papalopulu, N., and Houart, C. (2009). Integration of telencephalic Wnt and hedgehog signaling center activities by Foxg1. Dev. Cell *16*, 576–587.

Dehay, C., and Kennedy, H. (2007). Cell-cycle control and cortical development. Nat. Rev. Neurosci. *8*, 438–450.

Del Bene, F. (2011). Interkinetic nuclear migration: cell cycle on the move. EMBO J. *30*, 1676–1677.

Deneen, B., Ho, R., Lukaszewicz, A., Hochstim, C.J., Gronostajski, R.M., and Anderson, D.J. (2006). The transcription factor NFIA controls the onset of gliogenesis in the developing spinal cord. Neuron *52*, 953–968.

Derouet, D., Rousseau, F., Alfonsi, F., Froger, J., Hermann, J., Barbier, F., Perret, D., Diveu, C., Guillet, C., Preisser, L., et al. (2004). Neuropoietin, a new IL-6-related cytokine signaling through the ciliary neurotrophic factor receptor. Proc. Natl. Acad. Sci. U. S. A. *101*, 4827–4832.

Dou, C.L., Li, S., and Lai, E. (1999). Dual role of brain factor-1 in regulating growth and patterning of the cerebral hemispheres. Cereb. Cortex N. Y. N 1991 *9*, 543–550.

Ernst, M., and Jenkins, B.J. (2004). Acquiring signalling specificity from the cytokine receptor gp130. Trends Genet. *20*, 23–32.

Falcone, C., Filippis, C., Granzotto, M., and Mallamaci, A. (2015). Emx2 expression levels in NSCs modulate astrogenesis rates by regulating EgfR and Fgf9. Glia *63*, 412–422.

Falcone, C., Daga, A., Leanza, G., and Mallamaci, A. (2016). Emx2 as a novel tool to suppress glioblastoma. Oncotarget *7*, 41005–41016.

Fan, G., Martinowich, K., Chin, M.H., He, F., Fouse, S.D., Hutnick, L., Hattori, D., Ge, W., Shen, Y., Wu, H., et al. (2005). DNA methylation controls the timing of astrogliogenesis through regulation of JAK-STAT signaling. Development *132*, 3345–3356.

Fasano, C.A., Phoenix, T.N., Kokovay, E., Lowry, N., Elkabetz, Y., Dimos, J.T., Lemischka, I.R., Studer, L., and Temple, S. (2009). Bmi-1 cooperates with Foxg1 to maintain neural stem cell self-renewal in the forebrain. Genes Dev. *23*, 561–574.

Fox, I.J., and Kornblum, H.I. (2005). Developmental profile of ErbB receptors in murine central nervous system: Implications for functional interactions. J. Neurosci. Res. *79*, 584–597.

Fricker-Gates, R.A., Winkler, C., Kirik, D., Rosenblad, C., Carpenter, M.K., and Björklund, A. (2000). EGF infusion stimulates the proliferation and migration of embryonic progenitor cells transplanted in the adult rat striatum. Exp. Neurol. *165*, 237–247.

Fukuchi-Shimogori, T., and Grove, E.A. (2003). Emx2 patterns the neocortex by regulating FGF positional signaling. Nat. Neurosci. *6*, 825–831.

Fukuda, S., Abematsu, M., Mori, H., Yanagisawa, M., Kagawa, T., Nakashima, K., Yoshimura, A., and Taga, T. (2007). Potentiation of Astrogliogenesis by STAT3-Mediated Activation of Bone Morphogenetic Protein-Smad Signaling in Neural Stem Cells. Mol. Cell. Biol. *27*, 4931–4937.

Galli, R., Fiocco, R., De Filippis, L., Muzio, L., Gritti, A., Mercurio, S., Broccoli, V., Pellegrini, M., Mallamaci, A., and Vescovi, A.L. (2002). Emx2 regulates the proliferation of stem cells of the adult mammalian central nervous system. Dev. Camb. Engl. *129*, 1633–1644.

Gangemi, R.M.R., Daga, A., Muzio, L., Marubbi, D., Cocozza, S., Perera, M., Verardo, S., Bordo, D., Griffero, F., Capra, M.C., et al. (2006). Effects of Emx2 inactivation on the gene expression profile of neural precursors. Eur. J. Neurosci. *23*, 325–334.

García-Marqués, J., and López-Mascaraque, L. (2013). Clonal identity determines astrocyte cortical heterogeneity. Cereb. Cortex N. Y. N 1991 *23*, 1463–1472.

Garrett, T.P.J., McKern, N.M., Lou, M., Elleman, T.C., Adams, T.E., Lovrecz, G.O., Zhu, H.-J., Walker, F., Frenkel, M.J., Hoyne, P.A., et al. (2002). Crystal structure of a truncated epidermal growth factor receptor extracellular domain bound to transforming growth factor alpha. Cell *110*, 763–773.

Ge, W.-P., Miyawaki, A., Gage, F.H., Jan, Y.N., and Jan, L.Y. (2012). Local generation of glia is a major astrocyte source in postnatal cortex. Nature *484*, 376–380.

Götz, M., and Huttner, W.B. (2005). The cell biology of neurogenesis. Nat. Rev. Mol. Cell Biol. *6*, 777–788.

Grandbarbe, L., Bouissac, J., Rand, M., Hrabé de Angelis, M., Artavanis-Tsakonas, S., and Mohier, E. (2003). Delta-Notch signaling controls the generation of neurons/glia from neural stem cells in a stepwise process. Dev. Camb. Engl. *130*, 1391–1402.

Gratton, M.-O., Torban, E., Jasmin, S.B., Theriault, F.M., German, M.S., and Stifani, S. (2003). Hes6 promotes cortical neurogenesis and inhibits Hes1 transcription repression activity by multiple mechanisms. Mol. Cell. Biol. *23*, 6922–6935.

Grove, E.A., Tole, S., Limon, J., Yip, L., and Ragsdale, C.W. (1998). The hem of the embryonic cerebral cortex is defined by the expression of multiple Wnt genes and is compromised in Gli3-deficient mice. Dev. Camb. Engl. *125*, 2315–2325.

Guha, A., Feldkamp, M.M., Lau, N., Boss, G., and Pawson, A. (1997). Proliferation of human malignant astrocytomas is dependent on Ras activation. Oncogene *15*, 2755–2765.

Gulisano, M., Broccoli, V., Pardini, C., and Boncinelli, E. (1996). Emx1 and Emx2 show different patterns of expression during proliferation and differentiation of the developing cerebral cortex in the mouse. Eur. J. Neurosci. *8*, 1037–1050.

Guruharsha, K.G., Kankel, M.W., and Artavanis-Tsakonas, S. (2012). The Notch signalling system: recent insights into the complexity of a conserved pathway. Nat. Rev. Genet. *13*, 654–666.

Gutin, G., Fernandes, M., Palazzolo, L., Paek, H., Yu, K., Ornitz, D.M., McConnell, S.K., and Hébert, J.M. (2006). FGF signalling generates ventral telencephalic cells independently of SHH. Dev. Camb. Engl. *133*, 2937–2946.

Hajós, F., Woodhams, P.L., Bascó, E., Csillag, A., and Balázs, R. (1981). Proliferation of astroglia in the embryonic mouse forebrain as revealed by simultaneous immunocytochemistry and autoradiography. Acta Morphol. Acad. Sci. Hung. *29*, 361–364.

Hamasaki, T., Leingärtner, A., Ringstedt, T., and O'Leary, D.D.M. (2004). EMX2 regulates sizes and positioning of the primary sensory and motor areas in neocortex by direct specification of cortical progenitors. Neuron *43*, 359–372.

Hanashima, C., Shen, L., Li, S.C., and Lai, E. (2002). Brain factor-1 controls the proliferation and differentiation of neocortical progenitor cells through independent mechanisms. J. Neurosci. Off. J. Soc. Neurosci. *22*, 6526–6536.

Hanashima, C., Li, S.C., Shen, L., Lai, E., and Fishell, G. (2004). Foxg1 Suppresses Early Cortical Cell Fate. Science *303*, 56–59.

Hanashima, C., Fernandes, M., Hebert, J.M., and Fishell, G. (2007). The role of Foxg1 and dorsal midline signaling in the generation of Cajal-Retzius subtypes. J. Neurosci. Off. J. Soc. Neurosci. *27*, 11103–11111.

Hatada, I., Namihira, M., Morita, S., Kimura, M., Horii, T., and Nakashima, K. (2008). Astrocyte-Specific Genes Are Generally Demethylated in Neural Precursor Cells Prior to Astrocytic Differentiation. PLOS ONE *3*, e3189.

He, F., Ge, W., Martinowich, K., Becker-Catania, S., Coskun, V., Zhu, W., Wu, H., Castro, D., Guillemot, F., Fan, G., et al. (2005). A positive autoregulatory loop of Jak-STAT signaling controls the onset of astrogliogenesis. Nat. Neurosci. *8*, 616–625.

Hébert, J.M., and McConnell, S.K. (2000). Targeting of cre to the Foxg1 (BF-1) locus mediates loxP recombination in the telencephalon and other developing head structures. Dev. Biol. *222*, 296–306.

Hegi, M.E., Sciuscio, D., Murat, A., Levivier, M., and Stupp, R. (2009). Epigenetic deregulation of DNA repair and its potential for therapy. Clin. Cancer Res. Off. J. Am. Assoc. Cancer Res. *15*, 5026–5031.

Herculano-Houzel, S. (2011). Not all brains are made the same: new views on brain scaling in evolution. Brain. Behav. Evol. *78*, 22–36.

Hermanson, M., Funa, K., Koopmann, J., Maintz, D., Waha, A., Westermark, B., Heldin, C.H., Wiestler, O.D., Louis, D.N., von Deimling, A., et al. (1996). Association of loss of heterozygosity on chromosome 17p with high platelet-derived growth factor alpha receptor expression in human malignant gliomas. Cancer Res. *56*, 164–171.

Higgins, D.M., Wang, R., Milligan, B., Schroeder, M., Carlson, B., Pokorny, J., Cheshier, S.H., Meyer, F.B., Weissman, I.L., Sarkaria, J.N., et al. (2013). Brain tumor stem cell multipotency correlates with nanog expression and extent of passaging in human glioblastoma xenografts. Oncotarget *4*, 792–801.

Hirabayashi, Y., Suzki, N., Tsuboi, M., Endo, T.A., Toyoda, T., Shinga, J., Koseki, H., Vidal, M., and Gotoh, Y. (2009). Polycomb Limits the Neurogenic Competence of Neural Precursor Cells to Promote Astrogenic Fate Transition. Neuron *63*, 600–613.

Hollnagel, A., Oehlmann, V., Heymer, J., Rüther, U., and Nordheim, A. (1999). Id genes are direct targets of bone morphogenetic protein induction in embryonic stem cells. J. Biol. Chem. *274*, 19838–19845.

Houart, C., Westerfield, M., and Wilson, S.W. (1998). A small population of anterior cells patterns the forebrain during zebrafish gastrulation. Nature *391*, 788–792.

Huang, Y., Myers, S.J., and Dingledine, R. (1999). Transcriptional repression by REST: recruitment of Sin3A and histone deacetylase to neuronal genes. Nat. Neurosci. *2*, 867–872.

Icardi, L., Mori, R., Gesellchen, V., Eyckerman, S., Cauwer, L.D., Verhelst, J., Vercauteren, K., Saelens, X., Meuleman, P., Leroux-Roels, G., et al. (2012). The Sin3a repressor complex is a master regulator of STAT transcriptional activity. Proc. Natl. Acad. Sci. *109*, 12058–12063.

Ichiba, M., Nakajima, K., Yamanaka, Y., Kiuchi, N., and Hirano, T. (1998). Autoregulation of the Stat3 Gene through Cooperation with a cAMP-responsive Element-binding Protein. J. Biol. Chem. *273*, 6132–6138.

Ichikawa, M., Shiga, T., and Hirata, Y. (1983). Spatial and temporal pattern of postnatal proliferation of glial cells in the parietal cortex of the rat. Brain Res. *285*, 181–187.

Jacinto, F.V., and Esteller, M. (2007). MGMT hypermethylation: a prognostic foe, a predictive friend. DNA Repair *6*, 1155–1160.

Jepsen, K., Solum, D., Zhou, T., McEvilly, R.J., Kim, H.-J., Glass, C.K., Hermanson, O., and Rosenfeld, M.G. (2007). SMRT-mediated repression of an H3K27 demethylase in progression from neural stem cell to neuron. Nature *450*, 415–419.

Jones, P.L., Jan Veenstra, G.C., Wade, P.A., Vermaak, D., Kass, S.U., Landsberger, N., Strouboulis, J., and Wolffe, A.P. (1998). Methylated DNA and MeCP2 recruit histone deacetylase to repress transcription. Nat. Genet. *19*, 187–191.

Kageyama, R., Ohtsuka, T., Hatakeyama, J., and Ohsawa, R. (2005). Roles of bHLH genes in neural stem cell differentiation. Exp. Cell Res. *306*, 343–348.

Kamakura, S., Oishi, K., Yoshimatsu, T., Nakafuku, M., Masuyama, N., and Gotoh, Y. (2004). Hes binding to STAT3 mediates crosstalk between Notch and JAK–STAT signalling. Nat. Cell Biol. *6*, 547–554.

Kamijo, T., Weber, J.D., Zambetti, G., Zindy, F., Roussel, M.F., and Sherr, C.J. (1998). Functional and physical interactions of the ARF tumor suppressor with p53 and Mdm2. Proc. Natl. Acad. Sci. U. S. A. *95*, 8292–8297.

Kanski, R., Strien, M.E. van, Tijn, P. van, and Hol, E.M. (2014). A star is born: new insights into the mechanism of astrogenesis. Cell. Mol. Life Sci. *71*, 433–447.

Kao, H.Y., Ordentlich, P., Koyano-Nakagawa, N., Tang, Z., Downes, M., Kintner, C.R., Evans, R.M., and Kadesch, T. (1998). A histone deacetylase corepressor complex regulates the Notch signal transduction pathway. Genes Dev. *12*, 2269–2277.

Kimura, J., Suda, Y., Kurokawa, D., Hossain, Z.M., Nakamura, M., Takahashi, M., Hara, A., and Aizawa, S. (2005). Emx2 and Pax6 function in cooperation with Otx2 and Otx1 to develop caudal forebrain primordium that includes future archipallium. J. Neurosci. Off. J. Soc. Neurosci. *25*, 5097–5108.

Kishi, Y., Fujii, Y., Hirabayashi, Y., and Gotoh, Y. (2012). HMGA regulates the global chromatin state and neurogenic potential in neocortical precursor cells. Nat. Neurosci. *15*, 1127–1133.

Knoepfler, P.S., Zhang, X., Cheng, P.F., Gafken, P.R., McMahon, S.B., and Eisenman, R.N. (2006). Myc influences global chromatin structure. EMBO J. *25*, 2723–2734.

Koblar, S.A., Turnley, A.M., Classon, B.J., Reid, K.L., Ware, C.B., Cheema, S.S., Murphy, M., and Bartlett, P.F. (1998). Neural precursor differentiation into astrocytes requires signaling through the leukemia inhibitory factor receptor. Proc. Natl. Acad. Sci. U. S. A. *95*, 3178–3181.

Kopan, R., and Ilagan, M.X.G. (2009). The Canonical Notch Signaling Pathway: Unfolding the Activation Mechanism. Cell *137*, 216–233.

Kornblum, H.I., Hussain, R., Wiesen, J., Miettinen, P., Zurcher, S.D., Chow, K., Derynck, R., and Werb, Z. (1998). Abnormal astrocyte development and neuronal death in mice lacking the epidermal growth factor receptor. J. Neurosci. Res. *53*, 697–717.

Kornblum, H.I., Yanni, D.S., Easterday, M.C., and Seroogy, K.B. (2000). Expression of the EGF Receptor Family Members ErbB2, ErbB3, and ErbB4 in Germinal Zones of the Developing Brain and in Neurosphere Cultures Containing CNS Stem Cells. Dev. Neurosci. *22*, 16–24.

Krebs, D.L., and Hilton, D.J. (2001). SOCS proteins: negative regulators of cytokine signaling. Stem Cells Dayt. Ohio *19*, 378–387.

Kriegstein, A., and Alvarez-Buylla, A. (2009). The glial nature of embryonic and adult neural stem cells. Annu. Rev. Neurosci. *32*, 149–184.

Kubbutat, M.H.G., Jones, S.N., and Vousden, K.H. (1997). Regulation of p53 stability by Mdm2. Nature *387*, 299–303.

Kumamoto, T., Toma, K., Gunadi, null, McKenna, W.L., Kasukawa, T., Katzman, S., Chen, B., and Hanashima, C. (2013). Foxg1 coordinates the switch from nonradially to radially migrating glutamatergic subtypes in the neocortex through spatiotemporal repression. Cell Rep. *3*, 931–945.

Kusaka, M., Katoh-Fukui, Y., Ogawa, H., Miyabayashi, K., Baba, T., Shima, Y., Sugiyama, N., Sugimoto, Y., Okuno, Y., Kodama, R., et al. (2010). Abnormal epithelial cell polarity and ectopic epidermal growth factor receptor (EGFR) expression induced in Emx2 KO embryonic gonads. Endocrinology *151*, 5893–5904.

Kuschel, S., Rüther, U., and Theil, T. (2003). A disrupted balance between Bmp/Wnt and Fgf signaling underlies the ventralization of the Gli3 mutant telencephalon. Dev. Biol. *260*, 484–495.

Kwon, I.-S., Cho, S.-K., Kim, M.-J., Tsai, M.-J., Mitsuda, N., Suh-Kim, H., and Lee, Y.-D. (2009). Expression of Disabled 1 suppresses astroglial differentiation in neural stem cells. Mol. Cell. Neurosci. *40*, 50–61.

Labuhn, M., Jones, G., Speel, E.J., Maier, D., Zweifel, C., Gratzl, O., Van Meir, E.G., Hegi, M.E., and Merlo, A. (2001). Quantitative real-time PCR does not show selective targeting of p14(ARF) but concomitant inactivation of both p16(INK4A) and p14(ARF) in 105 human primary gliomas. Oncogene *20*, 1103–1109.

Lam, P.Y., Di Tomaso, E., Ng, H.K., Pang, J.C., Roussel, M.F., and Hjelm, N.M. (2000). Expression of p19INK4d, CDK4, CDK6 in glioblastoma multiforme. Br. J. Neurosurg. *14*, 28–32.

Lehmann, U., Schmitz, J., Weissenbach, M., Sobota, R.M., Hortner, M., Friederichs, K., Behrmann, I., Tsiaris, W., Sasaki, A., Schneider-Mergener, J., et al. (2003). SHP2 and SOCS3 contribute to Tyr-759-dependent attenuation of interleukin-6 signaling through gp130. J. Biol. Chem. *278*, 661–671.

Levison, S.W., and Goldman, J.E. (1993). Both oligodendrocytes and astrocytes develop from progenitors in the subventricular zone of postnatal rat forebrain. Neuron *10*, 201–212.

Li, Q., Wijesekera, O., Salas, S.J., Wang, J.Y., Zhu, M., Aprhys, C., Chaichana, K.L., Chesler, D.A., Zhang, H., Smith, C.L., et al. (2014). Mesenchymal stem cells from human fat engineered to secrete BMP4 are nononcogenic, suppress brain cancer, and prolong survival. Clin. Cancer Res. Off. J. Am. Assoc. Cancer Res. *20*, 2375–2387.

Lillien, L., and Raphael, H. (2000). BMP and FGF regulate the development of EGF-responsive neural progenitor cells. Dev. Camb. Engl. *127*, 4993–5005.

Lillien, L.E., Sendtner, M., Rohrer, H., Hughes, S.M., and Raff, M.C. (1988). Type-2 astrocyte development in rat brain cultures is initiated by a CNTF-like protein produced by type-1 astrocytes. Neuron *1*, 485–494.

Louis, D.N. (1994). The p53 gene and protein in human brain tumors. J. Neuropathol. Exp. Neurol. *53*, 11–21.

Louvi, A., and Artavanis-Tsakonas, S. (2006). Notch signalling in vertebrate neural development. Nat. Rev. Neurosci. *7*, 93–102.

Lum, M., Turbic, A., Mitrovic, B., and Turnley, A.M. (2009). Fibroblast growth factor-9 inhibits astrocyte differentiation of adult mouse neural progenitor cells. J. Neurosci. Res. *87*, 2201–2210.

Luskin, M.B., and McDermott, K. (1994). Divergent lineages for oligodendrocytes and astrocytes originating in the neonatal forebrain subventricular zone. Glia *11*, 211–226.

Maher, E.A., Furnari, F.B., Bachoo, R.M., Rowitch, D.H., Louis, D.N., Cavenee, W.K., and DePinho, R.A. (2001). Malignant glioma: genetics and biology of a grave matter. Genes Dev. *15*, 1311–1333.

Mallamaci, A. (2013). Developmental control of cortico-cerebral astrogenesis. Int. J. Dev. Biol. *57*, 689–706.

Mallamaci, A., Iannone, R., Briata, P., Pintonello, L., Mercurio, S., Boncinelli, E., and Corte, G. (1998). EMX2 protein in the developing mouse brain and olfactory area. Mech. Dev. *77*, 165–172.

Mallamaci, A., Muzio, L., Chan, C.H., Parnavelas, J., and Boncinelli, E. (2000a). Area identity shifts in the early cerebral cortex of Emx2-/- mutant mice. Nat. Neurosci. *3*, 679–686.

Mallamaci, A., Mercurio, S., Muzio, L., Cecchi, C., Pardini, C.L., Gruss, P., and Boncinelli, E. (2000b). The lack of Emx2 causes impairment of Reelin signaling and defects of neuronal migration in the developing cerebral cortex. J. Neurosci. Off. J. Soc. Neurosci. *20*, 1109–1118.

Mariani, J., Favaro, R., Lancini, C., Vaccari, G., Ferri, A.L., Bertolini, J., Tonoli, D., Latorre, E., Caccia, R., Ronchi, A., et al. (2012). Emx2 is a dose-dependent negative regulator of Sox2 telencephalic enhancers. Nucleic Acids Res. *40*, 6461–6476.

Martynoga, B., Morrison, H., Price, D.J., and Mason, J.O. (2005). Foxg1 is required for specification of ventral telencephalon and region-specific regulation of dorsal telencephalic precursor proliferation and apoptosis. Dev. Biol. *283*, 113–127.

Mayer, S.I., Rössler, O.G., Endo, T., Charnay, P., and Thiel, G. (2009). Epidermal-growth-factor-induced proliferation of astrocytes requires Egr transcription factors. J. Cell Sci. *122*, 3340–3350.

McConnell, S.K. (1995). Strategies for the generation of neuronal diversity in the developing central nervous system. J. Neurosci. Off. J. Soc. Neurosci. *15*, 6987–6998.

McKinnon, R.D., Matsui, T., Dubois-Dalcq, M., and Aaronson, S.A. (1990). FGF modulates the PDGF-driven pathway of oligodendrocyte development. Neuron *5*, 603–614.

Mei, L., and Xiong, W.-C. (2008). Neuregulin 1 in neural development, synaptic plasticity and schizophrenia. Nat. Rev. Neurosci. *9*, 437–452.

Miller, F.D., and Gauthier, A.S. (2007). Timing Is Everything: Making Neurons versus Glia in the Developing Cortex. Neuron *54*, 357–369.

Misson, J.P., Austin, C.P., Takahashi, T., Cepko, C.L., and Caviness, V.S. (1991). The alignment of migrating neural cells in relation to the murine neopallial radial glial fiber system. Cereb. Cortex N. Y. N 1991 *1*, 221–229.

Molofsky, A.V., and Deneen, B. (2015). Astrocyte development: A Guide for the Perplexed. Glia *63*, 1320–1329.

Molofsky, A.V., Krencik, R., Krenick, R., Ullian, E.M., Ullian, E., Tsai, H., Deneen, B., Richardson, W.D., Barres, B.A., and Rowitch, D.H. (2012). Astrocytes and disease: a neurodevelopmental perspective. Genes Dev. *26*, 891–907.

Momand, J., Zambetti, G.P., Olson, D.C., George, D., and Levine, A.J. (1992). The mdm-2 oncogene product forms a complex with the p53 protein and inhibits p53-mediated transactivation. Cell *69*, 1237–1245.

Mondal, S., Ivanchuk, S.M., Rutka, J.T., and Boulianne, G.L. (2007). Sloppy paired 1/2 regulate glial cell fates by inhibiting Gcm function. Glia *55*, 282–293.

Muzio, L., and Mallamaci, A. (2005). Foxg1 confines Cajal-Retzius neuronogenesis and hippocampal morphogenesis to the dorsomedial pallium. J. Neurosci. Off. J. Soc. Neurosci. *25*, 4435–4441.

Muzio, L., Di Benedetto, B., DiBenedetto, B., Stoykova, A., Boncinelli, E., Gruss, P., and Mallamaci, A. (2002). Emx2 and Pax6 control regionalization of the pre-neuronogenic cortical primordium. Cereb. Cortex N. Y. N 1991 *12*, 129–139.

Muzio, L., Soria, J.M., Pannese, M., Piccolo, S., and Mallamaci, A. (2005). A mutually stimulating loop involving emx2 and canonical wnt signalling specifically promotes expansion of occipital cortex and hippocampus. Cereb. Cortex N. Y. N 1991 *15*, 2021–2028.

Nagane, M., Coufal, F., Lin, H., Bögler, O., Cavenee, W.K., and Huang, H.J. (1996). A common mutant epidermal growth factor receptor confers enhanced tumorigenicity on human glioblastoma cells by increasing proliferation and reducing apoptosis. Cancer Res. *56*, 5079–5086.

Nagao, M., Campbell, K., Burns, K., Kuan, C.-Y., Trumpp, A., and Nakafuku, M. (2008). Coordinated control of self-renewal and differentiation of neural stem cells by Myc and the p19ARF-p53 pathway. J. Cell Biol. *183*, 1243–1257.

Naka, H., Nakamura, S., Shimazaki, T., and Okano, H. (2008). Requirement for COUP-TFI and II in the temporal specification of neural stem cells in CNS development. Nat. Neurosci. *11*, 1014–1023.

Nakashima, K., Yanagisawa, M., Arakawa, H., and Taga, T. (1999). Astrocyte differentiation mediated by LIF in cooperation with BMP2. FEBS Lett. *457*, 43–46.

Namihira, M., Nakashima, K., and Taga, T. (2004). Developmental stage dependent regulation of DNA methylation and chromatin modification in a immature astrocyte specific gene promoter. FEBS Lett. *572*, 184–188.

Namihira, M., Kohyama, J., Semi, K., Sanosaka, T., Deneen, B., Taga, T., and Nakashima, K. (2009). Committed Neuronal Precursors Confer Astrocytic Potential on Residual Neural Precursor Cells. Dev. Cell *16*, 245–255.

Nédélec, S., Foucher, I., Brunet, I., Bouillot, C., Prochiantz, A., and Trembleau, A. (2004). Emx2 homeodomain transcription factor interacts with eukaryotic translation initiation factor 4E (eIF4E) in the axons of olfactory sensory neurons. Proc. Natl. Acad. Sci. U. S. A. *101*, 10815–10820.

Neglia, J.P., Meadows, A.T., Robison, L.L., Kim, T.H., Newton, W.A., Ruymann, F.B., Sather, H.N., and Hammond, G.D. (1991). Second neoplasms after acute lymphoblastic leukemia in childhood. N. Engl. J. Med. *325*, 1330–1336.

Nishikawa, R., Ji, X.D., Harmon, R.C., Lazar, C.S., Gill, G.N., Cavenee, W.K., and Huang, H.J. (1994). A mutant epidermal growth factor receptor common in human glioma confers enhanced tumorigenicity. Proc. Natl. Acad. Sci. U. S. A. *91*, 7727–7731.

Nishioka, K., Rice, J.C., Sarma, K., Erdjument-Bromage, H., Werner, J., Wang, Y., Chuikov, S., Valenzuela, P., Tempst, P., Steward, R., et al. (2002). PR-Set7 is a nucleosome-specific methyltransferase that modifies lysine 20 of histone H4 and is associated with silent chromatin. Mol. Cell *9*, 1201–1213.

Nishiyama, A., Komitova, M., Suzuki, R., and Zhu, X. (2009). Polydendrocytes (NG2 cells): multifunctional cells with lineage plasticity. Nat. Rev. Neurosci. *10*, 9–22.

Noctor, S.C., Martínez-Cerdeño, V., Ivic, L., and Kriegstein, A.R. (2004). Cortical neurons arise in symmetric and asymmetric division zones and migrate through specific phases. Nat. Neurosci. *7*, 136–144.

Noctor, S.C., Martínez-Cerdeño, V., and Kriegstein, A.R. (2008). Distinct behaviors of neural stem and progenitor cells underlie cortical neurogenesis. J. Comp. Neurol. *508*, 28–44.

Noonan, F.C., Goodfellow, P.J., Staloch, L.J., Mutch, D.G., and Simon, T.C. (2003). Antisense transcripts at the EMX2 locus in human and mouse. Genomics *81*, 58–66.

Ochiai, W., Yanagisawa, M., Takizawa, T., Nakashima, K., and Taga, T. (2001). Astrocyte differentiation of fetal neuroepithelial cells involving cardiotrophin-1-induced activation of STAT3. Cytokine *14*, 264–271.

Ohgaki, H., and Kleihues, P. (2007). Genetic pathways to primary and secondary glioblastoma. Am. J. Pathol. *170*, 1445–1453.

Ohgaki, H., Dessen, P., Jourde, B., Horstmann, S., Nishikawa, T., Di Patre, P.-L., Burkhard, C., Schüler, D., Probst-Hensch, N.M., Maiorka, P.C., et al. (2004). Genetic pathways to glioblastoma: a population-based study. Cancer Res. *64*, 6892–6899.

O'Leary, D.D. (1989). Do cortical areas emerge from a protocortex? Trends Neurosci. *12*, 400–406.

Onishi, K., Tonge, P.D., Nagy, A., and Zandstra, P.W. (2014). Local BMP-SMAD1 Signaling Increases LIF Receptor-Dependent STAT3 Responsiveness and Primed-to-Naive Mouse Pluripotent Stem Cell Conversion Frequency. Stem Cell Rep. *3*, 156–168.

Oumesmar, B.N., Vignais, L., and Evercooren, A.B.-V. (1997). Developmental Expression of Platelet-Derived Growth Factor α-Receptor in Neurons and Glial Cells of the Mouse CNS. J. Neurosci. *17*, 125–139.

Pancrazi, L., Di Benedetto, G., Colombaioni, L., Della Sala, G., Testa, G., Olimpico, F., Reyes, A., Zeviani, M., Pozzan, T., and Costa, M. (2015). Foxg1 localizes to mitochondria and coordinates cell differentiation and bioenergetics. Proc. Natl. Acad. Sci. U. S. A. *112*, 13910–13915.

Park, D.M., Jung, J., Masjkur, J., Makrogkikas, S., Ebermann, D., Saha, S., Rogliano, R., Paolillo, N., Pacioni, S., McKay, R.D., et al. (2013). Hes3 regulates cell number in cultures from glioblastoma multiforme with stem cell characteristics. Sci. Rep. *3*, 1095.

Pellegrini, M., Mansouri, A., Simeone, A., Boncinelli, E., and Gruss, P. (1996). Dentate gyrus formation requires Emx2. Dev. Camb. Engl. *122*, 3893–3898.

Pellegrini, M., Pantano, S., Fumi, M.P., Lucchini, F., and Forabosco, A. (2001). Agenesis of the scapula in Emx2 homozygous mutants. Dev. Biol. *232*, 149–156.

Piccirillo, S.G.M., Reynolds, B.A., Zanetti, N., Lamorte, G., Binda, E., Broggi, G., Brem, H., Olivi, A., Dimeco, F., and Vescovi, A.L. (2006). Bone morphogenetic proteins inhibit the tumorigenic potential of human brain tumour-initiating cells. Nature *444*, 761–765.

Piper, M., Barry, G., Hawkins, J., Mason, S., Lindwall, C., Little, E., Sarkar, A., Smith, A.G., Moldrich, R.X., Boyle, G.M., et al. (2010). NFIA Controls Telencephalic Progenitor Cell Differentiation through Repression of the Notch Effector Hes1. J. Neurosci. *30*, 9127–9139.

Pruitt, K., Ülkü, A.S., Frantz, K., Rojas, R.J., Muniz-Medina, V.M., Rangnekar, V.M., Der, C.J., and Shields, J.M. (2005). Ras-mediated Loss of the Pro-apoptotic Response Protein Par-4 Is Mediated by DNA Hypermethylation through Raf-independent and Raf-dependent Signaling Cascades in Epithelial Cells. J. Biol. Chem. *280*, 23363–23370.

Rallu, M., Machold, R., Gaiano, N., Corbin, J.G., McMahon, A.P., and Fishell, G. (2002). Dorsoventral patterning is established in the telencephalon of mutants lacking both Gli3 and Hedgehog signaling. Dev. Camb. Engl. *129*, 4963–4974.

Reifenberger, G., Ichimura, K., Reifenberger, J., Elkahloun, A.G., Meltzer, P.S., and Collins, V.P. (1996). Refined mapping of 12q13-q15 amplicons in human malignant gliomas suggests CDK4/SAS and MDM2 as independent amplification targets. Cancer Res. *56*, 5141–5145.

Rodriguez, C., Huang, L.J.-S., Son, J.K., McKee, A., Xiao, Z., and Lodish, H.F. (2001). Functional Cloning of the Proto-oncogene Brain Factor-1 (BF-1) As a Smad-binding Antagonist of Transforming Growth Factor-β Signaling. J. Biol. Chem. *276*, 30224–30230.

Rowitch, D.H., and Kriegstein, A.R. (2010). Developmental genetics of vertebrate glial-cell specification. Nature *468*, 214–222.

de Sampaio e Spohr, T.C.L., Martinez, R., da Silva, E.F., Neto, V.M., and Gomes, F.C.A. (2002). Neuro-glia interaction effects on GFAP gene: a novel role for transforming growth factor-beta1. Eur. J. Neurosci. *16*, 2059–2069.

Santos-Ocampo, S., Colvin, J.S., Chellaiah, A., and Ornitz, D.M. (1996). Expression and biological activity of mouse fibroblast growth factor-9. J. Biol. Chem. *271*, 1726–1731.

Sardi, S.P., Murtie, J., Koirala, S., Patten, B.A., and Corfas, G. (2006). Presenilin-Dependent ErbB4 Nuclear Signaling Regulates the Timing of Astrogenesis in the Developing Brain. Cell *127*, 185–197.

Sasai, Y., and De Robertis, E.M. (1997). Ectodermal patterning in vertebrate embryos. Dev. Biol. *182*, 5–20.

Scheffzek, K., Ahmadian, M.R., Kabsch, W., Wiesmüller, L., Lautwein, A., Schmitz, F., and Wittinghofer, A. (1997). The Ras-RasGAP complex: structural basis for GTPase activation and its loss in oncogenic Ras mutants. Science *277*, 333–338.

Schmitz, J., Weissenbach, M., Haan, S., Heinrich, P.C., and Schaper, F. (2000). SOCS3 exerts its inhibitory function on interleukin-6 signal transduction through the SHP2 recruitment site of gp130. J. Biol. Chem. *275*, 12848–12856.

Schwartzbaum, J.A., Fisher, J.L., Aldape, K.D., and Wrensch, M. (2006). Epidemiology and molecular pathology of glioma. Nat. Clin. Pract. Neurol. *2*, 494–503.

Seoane, J., Le, H.-V., Shen, L., Anderson, S.A., and Massagué, J. (2004). Integration of Smad and forkhead pathways in the control of neuroepithelial and glioblastoma cell proliferation. Cell *117*, 211–223.

Seuntjens, E., Nityanandam, A., Miquelajauregui, A., Debruyn, J., Stryjewska, A., Goebbels, S., Nave, K.-A., Huylebroeck, D., and Tarabykin, V. (2009). Sip1 regulates sequential fate decisions by feedback signaling from postmitotic neurons to progenitors. Nat. Neurosci. *12*, 1373–1380.

Shi, Y., and Massagué, J. (2003). Mechanisms of TGF-beta signaling from cell membrane to the nucleus. Cell *113*, 685–700.

Shimamura, K., and Rubenstein, J.L. (1997). Inductive interactions direct early regionalization of the mouse forebrain. Dev. Camb. Engl. *124*, 2709–2718.

Shimogori, T., Banuchi, V., Ng, H.Y., Strauss, J.B., and Grove, E.A. (2004). Embryonic signaling centers expressing BMP, WNT and FGF proteins interact to pattern the cerebral cortex. Dev. Camb. Engl. *131*, 5639–5647.

Sibilia, M., Steinbach, J.P., Stingl, L., Aguzzi, A., and Wagner, E.F. (1998). A strain-independent postnatal neurodegeneration in mice lacking the EGF receptor. EMBO J. *17*, 719–731.

Simeone, A., Acampora, D., Gulisano, M., Stornaiuolo, A., and Boncinelli, E. (1992). Nested expression domains of four homeobox genes in developing rostral brain. Nature *358*, 687–690.

Sloan, S.A., and Barres, B.A. (2014). Mechanisms of astrocyte development and their contributions to neurodevelopmental disorders. Curr. Opin. Neurobiol. *27*, 75–81.

Sofroniew, M.V. (2009). Molecular dissection of reactive astrogliosis and glial scar formation. Trends Neurosci. *32*, 638–647.

Song, M.-R., and Ghosh, A. (2004). FGF2-induced chromatin remodeling regulates CNTF-mediated gene expression and astrocyte differentiation. Nat. Neurosci. *7*, 229–235.

Spigoni, G., Gedressi, C., and Mallamaci, A. (2010). Regulation of Emx2 expression by antisense transcripts in murine cortico-cerebral precursors. PloS One *5*, e8658.

St Louis, D.C., Woodcock, J.B., Franzoso, G., Blair, P.J., Carlson, L.M., Murillo, M., Wells, M.R., Williams, A.J., Smoot, D.S., Kaushal, S., et al. (1999). Evidence for distinct intracellular signaling pathways in CD34+ progenitor to dendritic cell differentiation from a human cell line model. J. Immunol. Baltim. Md 1950 *162*, 3237–3248.

Stambolic, V., Suzuki, A., de la Pompa, J.L., Brothers, G.M., Mirtsos, C., Sasaki, T., Ruland, J., Penninger, J.M., Siderovski, D.P., and Mak, T.W. (1998). Negative regulation of PKB/Akt-dependent cell survival by the tumor suppressor PTEN. Cell *95*, 29–39.

Steck, P.A., Pershouse, M.A., Jasser, S.A., Yung, W.K.A., Lin, H., Ligon, A.H., Langford, L.A., Baumgard, M.L., Hattier, T., Davis, T., et al. (1997). Identification of a candidate tumour suppressor gene, MMAC1, at chromosome 10q23.3 that is mutated in multiple advanced cancers. Nat. Genet. *15*, 356–362.

Stipursky, J., and Gomes, F.C.A. (2007). TGF-β1/SMAD signaling induces astrocyte fate commitment in vitro: Implications for radial glia development. Glia *55*, 1023–1033.

Stipursky, J., Francis, D., and Gomes, F.C.A. (2012). Activation of MAPK/PI3K/SMAD Pathways by TGF-β1 Controls Differentiation of Radial Glia into Astrocytes in vitro. Dev. Neurosci. *34*, 68–81.

Storm, E.E., Garel, S., Borello, U., Hebert, J.M., Martinez, S., McConnell, S.K., Martin, G.R., and Rubenstein, J.L.R. (2006). Dose-dependent functions of Fgf8 in regulating telencephalic patterning centers. Dev. Camb. Engl. *133*, 1831–1844.

Sturm, D., Bender, S., Jones, D.T.W., Lichter, P., Grill, J., Becher, O., Hawkins, C., Majewski, J., Jones, C., Costello, J.F., et al. (2014). Paediatric and adult glioblastoma: multiform (epi)genomic culprits emerge. Nat. Rev. Cancer *14*, 92–107.

Sun, Y., Nadal-Vicens, M., Misono, S., Lin, M.Z., Zubiaga, A., Hua, X., Fan, G., and Greenberg, M.E. (2001). Neurogenin promotes neurogenesis and inhibits glial differentiation by independent mechanisms. Cell *104*, 365–376.

Takahashi, T., Nowakowski, R.S., and Caviness, V.S. (1995). The cell cycle of the pseudostratified ventricular epithelium of the embryonic murine cerebral wall. J. Neurosci. Off. J. Soc. Neurosci. *15*, 6046–6057.

Thomas, P., and Beddington, R. (1996). Anterior primitive endoderm may be responsible for patterning the anterior neural plate in the mouse embryo. Curr. Biol. CB *6*, 1487–1496.

Toma, K., Kumamoto, T., and Hanashima, C. (2014). The timing of upper-layer neurogenesis is conferred by sequential derepression and negative feedback from deep-layer neurons. J. Neurosci. Off. J. Soc. Neurosci. *34*, 13259–13276.

Tortosa, A., Ino, Y., Odell, N., Swilley, S., Sasaki, H., Louis, D.N., and Henson, J.W. (2000). Molecular genetics of radiographically defined de novo glioblastoma multiforme. Neuropathol. Appl. Neurobiol. *26*, 544–552.

Tsai, H.-H., Li, H., Fuentealba, L.C., Molofsky, A.V., Taveira-Marques, R., Zhuang, H., Tenney, A., Murnen, A.T., Fancy, S.P.J., Merkle, F., et al. (2012). Regional astrocyte allocation regulates CNS synaptogenesis and repair. Science *337*, 358–362.

Veliz, I., Loo, Y., Castillo, O., Karachaliou, N., Nigro, O., and Rosell, R. (2015). Advances and challenges in the molecular biology and treatment of glioblastoma—is there any hope for the future? Ann. Transl. Med. *3*.

Verhaak, R.G.W., Hoadley, K.A., Purdom, E., Wang, V., Qi, Y., Wilkerson, M.D., Miller, C.R., Ding, L., Golub, T., Mesirov, J.P., et al. (2010). An integrated genomic analysis identifies clinically relevant subtypes of glioblastoma characterized by abnormalities in PDGFRA, IDH1, EGFR and NF1. Cancer Cell *17*, 98.

Vezzali, R., Weise, S.C., Hellbach, N., Machado, V., Heidrich, S., Vogel, T., Vezzali, R., Weise, S.C., Hellbach, N., Machado, V., et al. (2016). The FOXG1/FOXO/SMAD network balances proliferation and differentiation of cortical progenitors and activates Kcnh3 expression in mature neurons. Oncotarget *7*, 37436–37455.

Viti, J., Feathers, A., Phillips, J., and Lillien, L. (2003). Epidermal Growth Factor Receptors Control Competence to Interpret Leukemia Inhibitory Factor as an Astrocyte Inducer in Developing Cortex. J. Neurosci. *23*, 3385–3393.

Voigt, T. (1989). Development of glial cells in the cerebral wall of ferrets: direct tracing of their transformation from radial glia into astrocytes. J. Comp. Neurol. *289*, 74–88.

Wang, Y., Kim, E., Wang, X., Novitch, B.G., Yoshikawa, K., Chang, L.-S., and Zhu, Y. (2012). ERK Inhibition Rescues Defects in Fate Specification of Nf1-Deficient Neural Progenitors and Brain Abnormalities. Cell *150*, 816–830.

Xuan, S., Baptista, C.A., Balas, G., Tao, W., Soares, V.C., and Lai, E. (1995). Winged helix transcription factor BF-1 is essential for the development of the cerebral hemispheres. Neuron *14*, 1141–1152.

Yamaguchi, K., Shirakabe, K., Shibuya, H., Irie, K., Oishi, I., Ueno, N., Taniguchi, T., Nishida, E., and Matsumoto, K. (1995). Identification of a member of the MAPKKK family as a potential mediator of TGF-beta signal transduction. Science *270*, 2008–2011.

Yeh, H.J., Silos-Santiago, I., Wang, Y.X., George, R.J., Snider, W.D., and Deuel, T.F. (1993). Developmental expression of the platelet-derived growth factor alpha-receptor gene in mammalian central nervous system. Proc. Natl. Acad. Sci. U. S. A. *90*, 1952–1956.

Yoshida, M., Suda, Y., Matsuo, I., Miyamoto, N., Takeda, N., Kuratani, S., and Aizawa, S. (1997). Emx1 and Emx2 functions in development of dorsal telencephalon. Dev. Camb. Engl. *124*, 101–111.

Zhang, X., Liu, H., Cong, G., Tian, Z., Ren, D., Wilson, J.X., and Huang, G. (2008). Effects of folate on notch signaling and cell proliferation in neural stem cells of neonatal rats in vitro. J. Nutr. Sci. Vitaminol. (Tokyo) *54*, 353–356.

Zhang, Y., Sloan, S.A., Clarke, L.E., Caneda, C., Plaza, C.A., Blumenthal, P.D., Vogel, H., Steinberg, G.K., Edwards, M.S.B., Li, G., et al. (2016). Purification and Characterization of Progenitor and Mature Human Astrocytes Reveals Transcriptional and Functional Differences with Mouse. Neuron *89*, 37–53.